

**AAK1 Regulates Microtubule-Dependent Autophagosome Transport
by Controlling MARK2 Phosphorylation in Neurons**

Inaugural-Dissertation

zur

Erlangung des Doktorgrades

der Mathematisch-Naturwissenschaftlichen Fakultät

der Universität zu Köln

vorgelegt von

Ebru OZER YILDIZ

aus Fatih, Türkei

Köln, 2024

1. Gutachterin: Prof. Dr. Natalia Kononenko

2. Gutachter: Prof. Dr. Marcus Krüger

Tag der mündlichen Prüfung:

Contents

Abbreviations	7
Summary.....	10
Zusammenfassung.....	11
I.Introduction	13
1.Endocytosis.....	13
1.1.Clathrin-mediated endocytosis.....	13
1.1.1. Steps of clathrin-mediated endocytosis	14
1.1.1.1. Nucleation	14
1.1.1.2. Cargo Selection	16
1.1.1.3. Coat formation	17
1.1.1.4. Scission.....	18
1.1.1.5. Uncoating.....	19
1.2. CME in synapse and neurodegenerative diseases.....	19
1.2.1. Synaptic Vesicle Recycling and CME	20
1.2.2. Alzheimer's Disease and CME	22
1.2.3. Parkinson's Disease and CME.....	24
1.2.4. Huntington's Disease and CME.....	25
2. AAK1	25
2.1. Biological Function of AAK1	27
2.2. AAK1 in Central Nervous System Diseases.....	28
3. Microtubule Affinity-Regulating Kinases.....	30
3.1. MARKs in diseases	31
3.1.1. Microtubule affinity regulating kinase 1 (MARK1).....	31
3.3.2. Microtubule affinity regulating kinase 2 (MARK2).....	32
3.3.3. Microtubule affinity regulating kinase 3 (MARK3).....	33
3.3.4. Microtubule affinity regulating kinase 4 (MARK4).....	33
4. Autophagy	34
4.1. Steps of autophagy.....	35
4.1.1. Initiation of the phagophore formation	36
4.1.2. Nucleation	36
4.1.3. Elongation and maturation	37
4.1.3. Fusion of the autophagosome with the lysosome	37
II. Objectives	41
III. Material and Method.....	43

1. Materials	43
2. Methods	49
2.1. Animals	49
2.1.1. Mouse breeding and maintenance	49
2.1.2. Creating AAK1 knockout mice	49
2.2. Genotyping	50
2.2.1. Tissue sample and DNA extraction	50
2.2.2. PCR and gel electrophoresis	50
2.3. Primary neuronal culture	52
2.3.1. PDL-coating	52
2.3.2. Primary cortical culture	52
2.3.3. Transfection of primary neuronal culture	53
2.3.4. Transferrin488 uptake assay in cultured neurons	53
2.3.5. Starvation and BafA1 treatment in cultured neurons	54
2.3.6. Live imaging of cultured neurons	54
2.4. Ex vivo acute slices	54
2.4.1. Starvation and chloroquine treatment in acute slices	55
2.4.2. AAK1 inhibitor SGC-AAK1-1 treatment in acute slices	55
2.4.3. Synaptosome isolation from cortex and acute slices	55
2.4.4. Plasma membrane protein extraction from synaptosomes	55
2.5. Animal behavior	56
2.5.1. Open field	56
2.5.2. Beam walk	57
2.5.3. Rotarod	57
2.5.4. Echo-MRI body composition analysis	57
2.6. Histology methods	57
2.6.1. Perfusion	58
2.6.2. Immunohistochemistry	58
2.6.3. Cresyl-violet (Nissl) staining	59
2.6.4. Electron microscopy	60
2.7. Immunoblot	60
2.7.1. Tissue preparation and lysis	60
2.7.2. SDS-PAGE and immunoblotting	61
2.8. Proteomic and phosphoproteomic	63

2.8.1. Immunoprecipitation and mass spectrometry analysis of AAK1-binding partners.....	63
2.8.2. Proteom and phosphoproteom analysis of AAK1 KO cortex and synaptosomes	63
2.8.3. Proteom analysis of HEK293T TurboID-PM cells	65
2.8.4. Data Acquisition for proteom and phosphoproteom	66
2.8.4.1. Sample Processing.....	67
2.8.5. Data Acquisition for IP and TurboID samples	67
2.8.5.1. Sample Processing.....	68
2.9. Statistical analysis	68
IV. Results.....	69
1. AAK1 expression differs in region and age in mouse brain	69
2. AAK1 KO mice show reduced body weight without changes in body composition	70
3. AAK1 deletion reduces levels of endocytic proteins AP-2 and clathrin in the cortex of AAK1 KO mice and disrupts endocytosis in cultured neurons.....	72
4. AAK1 depletion did not result in anatomical changes in the brain	74
5. Characterization of CamKII α -driven AAK1 KO mice reveals minor anatomical and metabolic differences	75
6. AAK1 KO and AAK1 cKO mice show hyperactivity.....	78
7. Motor coordination deficits in AAK1 KO and AAK1 cKO mice	79
8. Proteomic analysis of AAK1 interactome in the cortex reveals enrichment of endocytic and autophagic pathways.....	82
9. Proteomic and phosphoproteomic analysis reveals autophagy and trafficking pathways associated with AAK1 in the brain	84
10. AAK1 deficiency leads to age-dependent autophagic dysregulation and impaired autophagic flux	87
11. AAK1 depletion results in synaptic accumulation of ATG9A and changes in synaptic vesicular content	90
12. AAK1 depletion in cortical synaptosomes leads to dysregulation of autophagic flux	92

13. Proteomics and phosphoproteomics from AAK1 KO cortical synaptosomes reveal significantly dysregulated vesicular and microtubule related pathways	94
14. HEK cells plasma membrane-tagged TurboID approach reveals potential novel substrates of AAK1.....	97
15. AAK1 depleted primary neurons show decreased microtubule dynamics.....	98
16. AAK1 depletion impairs autophagosome trafficking in neurons	99
17. Inhibition of AAK1 kinase activity results in MARK2 relocalization in synapses	100
18. AAK1 depletion results in changes in microtubule dynamics both in-vivo and in-vitro.....	102
V. Discussion.....	104
1. AAK1 expression in the brain shows regional and temporal diversity	104
2. AAK1 KO and cKO mice display hyperactivity, delayed growth and motor deficit	105
3. AAK1 regulates autophagy	110
4. AAK1 regulates microtubule dynamics and vesicular trafficking via MARK2 phosphorylation.....	112
VI. Closing remarks	116
VII. References.....	118
VIII. Acknowledgments	133

Abbreviations

AAK1	Adaptor associated kinase 1
AP-2	Adaptor protein 2
AD	Alzheimer's disease
ADHD	Attention-deficit hyperactivity disorder
ALS	Amyotrophic lateral sclerosis
ASD	Autism spectrum disorder
ATG	Autophagy-related protein/gene
AVs	Autophagic vacuoles
BafA1	Bafilomycin A1
°C	Celsius
cKO	Conditional knockout
CHC	Clathrin heavy chain
CMA	Chaperone-mediated autophagy
CME	Clathrin-mediated endocytosis
CNS	Central nervous system
CCVs	Clathrin coated vesicles
CCPs	Clathrin coated pits
CQ	Chloroquine
DNA	Deoxyribunucleotic acid
DMEM	Dulbecco's modified eagle medium
EM	Electronmicroscopy
FBS	Fetal bovine serum
FC	Fold change
GFAP	Glial fibrillary acidic protein
GFP	Green fluorescent protein
GO	Gene ontology
h	hours
HEK	Human embryonic kidney cells
HTT	Huntingtin
HD	Huntington's disease

ICC	Immunocytochemistry
IHC	Immunohistochemistry
kDa	Kilodalton
KEGG	Kyoto Encyclopedia of Genes and Genomes
KO	Knockout
LC3	Microtubule-associated protein 1 light chain 3
LC3 I	Non-lipidated LC3
LC3 II	Lipidated LC3
LIR	LC3-interacting region
LRRK2	Leucine-rich repeat kinase
MARKs	Microtubule affinity regulating kinases
MDD	Major depressive disorder
min	Minutes
mm	Millimeter
MS	Mass spectrometry
mTOR	Mammalian target of rapamycin
mTORC1	Mammalian target of rapamycin complex 1
NAK	Numb-associated kinase
OF	Open field
PD	Parkinson's disease
p62	SQSTM1/Sequestosome 1
P/S	Penicillin/streptomycin
PSD	Post synaptic density
RFP	Red fluorescent protein
RPM	Revolution per minute
SDS-PAGE	Sodium dodecyl sulfate-polyacrylamide gel electrophoresis
SNARE	Soluble NSF Attachment Protein Receptor
SOD1	Superoxide dismutase 1
SYT1	Synaptotagmin1
SVs	Synaptic vesicles
SVR	Synaptic vesicle recycling
Tfn	Transferrin

TfnR	Transferrin receptor
+TIP	Microtubule plus-end tracking protein
T (Thr)	Threonine
TMX	Tamoxifen

Summary

Clathrin-mediated endocytosis (CME) is one of the most essential endocytic pathways in eukaryotic cells, playing a crucial role in the uptake of nutrients and substances such as low-density lipoprotein receptor (LDLR) and transferrin receptor (TfnR). In neurons, which are highly polarized, non-mitotic, and possess long axons and dendrites that extend far from the cell soma, CME is of paramount importance. It plays a pivotal role in synaptic vesicle recycling, ensuring the continuity of synaptic function and plasma membrane (PM) renewal, which is vital for neuronal health. Adaptor-associated kinase 1 (AAK1) was originally discovered as a kinase that phosphorylates the adaptor protein complex-2 (AP-2), enhancing its affinity for the PM and facilitating the maturation of endocytic pits. Recent studies have uncovered versatile roles for AAK1 beyond its canonical role in CME, including potential roles in neurodegeneration and autophagy regulation. Our study aimed to elucidate the role of AAK1 in the brain *in vivo*, utilizing both global and conditional knockout (cKO) mouse models of AAK1. Strikingly, these models demonstrated similar phenotypes, including reduced body weight, hyperactivity in open field tests, and impaired motor behavior during beam walk assays. These findings strongly indicate a neuron-specific role for AAK1 that is critical for maintaining neuronal function and health. To understand the molecular basis of these phenotypes, we employed a "narrowing-down" approach, starting from the whole brain and moving down to synaptosomes, combined with biochemical, proteomic, and imaging techniques. Our data revealed that AAK1 plays an essential role in the regulation of microtubule-associated protein kinase-2 (MARK2) in the brain.

Interestingly, AAK1 expression in wildtype (WT) cortices peaks at around 12 weeks of age, coinciding with the peak period of synaptic refinement and plasticity. This temporal pattern aligns with the observed increase in ATG9A expression in AAK1 knockout (KO) mice at 12 weeks, suggesting that AAK1 may play a role in maintaining autophagy homeostasis during this critical developmental window. Indeed, the loss of AAK1 led to dysregulated autophagy, as reflected by an increased number of autophagosomes and a decrease in synaptic vesicles within synapses, indicating impaired autophagosome trafficking. The dysregulation of MARK2 localization due to AAK1 depletion also affected microtubule dynamics, synaptic physiology, and vesicular trafficking. This was reflected by altered microtubule post-translational modifications. These changes ultimately led to an accumulation of autophagosomes in synapses, impaired autophagic flux, and reduced synaptic vesicle availability, further implicating AAK1 as a critical regulator of autophagosome trafficking and synaptic health.

Taken together, these findings demonstrate that AAK1 is a key regulator of neuronal function, linking autophagosome trafficking and microtubule dynamics through the modulation of MARK2 particularly during critical windows of synaptic plasticity and maturation.

Zusammenfassung

Die clathrin-vermittelte Endozytose (CME) ist einer der wichtigsten endozytotischen Wege in eukaryotischen Zellen und spielt eine entscheidende Rolle bei der Aufnahme von Nährstoffen und Substanzen wie dem LDL-Rezeptor (low-density lipoprotein receptor, LDLR) und dem Transferrin-Rezeptor (TfnR). Bei Neuronen, die hochpolarisiert, nicht-mitotisch und mit langen Axonen und Dendriten weit vom Zellkörper entfernt sind, ist CME von größter Bedeutung. CME spielt eine zentrale Rolle beim Recycling von synaptischen Vesikeln und gewährleistet die Kontinuität der synaptischen Funktion sowie die Erneuerung der Plasmamembran (PM), was für die neuronale Gesundheit von entscheidender Bedeutung ist. Die Adaptor-assoziierte Kinase 1 (AAK1) wurde ursprünglich als Kinase entdeckt, die den Adaptor-Protein-Komplex 2 (AP2) phosphoryliert, wodurch dessen Affinität zur PM erhöht und die Reifung der endozytotischen Vesikel gefördert wird. Neuere Studien haben gezeigt, dass AAK1 über ihre kanonische Rolle in der CME hinaus vielseitige Funktionen hat und möglicherweise eine Rolle bei der Neurodegeneration und der Regulation der Autophagie spielt. Unsere Studie zielte darauf ab, die Rolle von AAK1 im Gehirn in vivo zu untersuchen, wobei sowohl globale als auch konditionale Knockout (cKO) Mausmodelle von AAK1 verwendet wurden. Diese Modelle zeigten auffallend ähnliche Phänotypen, darunter reduziertes Körpergewicht, Hyperaktivität und beeinträchtigte motorische Fähigkeiten im Beam-Walk-Test. Diese Ergebnisse deuten stark darauf hin, dass AAK1 eine neuronenspezifische Rolle spielt, die entscheidend für die Aufrechterhaltung der neuronalen Funktion und Gesundheit ist. Um die molekularen Grundlagen dieser Phänotypen zu verstehen, haben wir einen „Narrowing-Down“-Ansatz verwendet, der vom gesamten Gehirn bis hin zu synaptischen Kompartimenten (Synaptosomen) reicht und mit biochemischen, proteomischen und bildgebenden Techniken kombiniert wurde. Unsere Daten zeigten, dass AAK1 eine wesentliche Rolle bei der Regulation der Mikrotubuli-assoziierten Proteinkinase 2 (MARK2) spielt, einem neuartigen Substrat im Gehirn.

Interessanterweise erreicht die AAK1-Expression in Wildtyp-Kortexen (WT) ihren Höhepunkt etwa im Alter von 12 Wochen, was mit der Spitzenphase der synaptischen Verfeinerung und Plastizität übereinstimmt. Dieses zeitliche Muster stimmt mit dem beobachteten Anstieg der ATG9A-Expression in AAK1-Knockout-Mäusen (KO) im Alter von 12 Wochen überein, was darauf hindeutet, dass AAK1 eine Rolle bei der Aufrechterhaltung der Autophagie-Homöostase während dieses kritischen Entwicklungszeitfensters spielen könnte. Tatsächlich führte der Verlust von AAK1 zu einer dysregulierten Autophagie, was sich durch eine erhöhte Anzahl von Autophagosomen und eine verringerte Anzahl von synaptischen Vesikeln in Synapsen widerspiegelte, was auf eine beeinträchtigte Autophagosomen-Trafficking hinweist. Die Dysregulation der MARK2-Lokalisation aufgrund des AAK1-Mangels beeinträchtigte ebenfalls

die Mikrotubuli-Dynamik, die synaptische Physiologie und den vesikulären Transport. Dies spiegelte sich in veränderten posttranslationalen Modifikationen von Mikrotubuli wider. Diese Veränderungen führten letztendlich zur Akkumulation von Autophagosomen in Synapsen, einer beeinträchtigten Autophagie-Flussrate und einer reduzierten Verfügbarkeit von synaptischen Vesikeln, was AAK1 als kritischen Regulator des Autophagosomen-Traffickings und der synaptischen Gesundheit weiter impliziert.

Zusammenfassend zeigen diese Ergebnisse, dass AAK1 ein wichtiger Regulator der neuronalen Funktion ist, der das Autophagosomen-Trafficking und die Mikrotubuli-Dynamik durch die Modulation von MARK2 insbesondere während kritischer Phasen der synaptischen Plastizität und Reifung miteinander verknüpft.

I.Introduction

1.Endocytosis

Endocytosis is recognized as a fundamental process crucial for cellular health. It facilitates the internalization of various substrates and contributes to the maintenance of plasma membrane homeostasis. While essential small molecules like amino acids, sugars, and ions can move through the plasma membrane (PM) via specific protein pumps or membrane channels, the internalization of macromolecules necessitates PM invagination and subsequent internalization, a process referred to as endocytosis (Alberts B 2002).

The field of endocytosis was initially established over a century ago by Ilya Ilyich Mechnikov, whose discovery of phagocytosis in 1884 marked a pivotal moment (Metchnikoff 1884). Phagocytosis, often referred to as the cell's "uptake of macro particles" or "cell eating," demonstrated the capacity of eukaryotic cells to engulf larger particles for various cellular processes. The evolution of this field continued with Warren H. Lewis's discovery of pinocytosis in 1931 (Schmid, Sorkin & Zerial 2014). Pinocytosis, known as the cell's "uptake of fluid or solutes," introduced a new dimension to cellular uptake mechanisms (Schmid, Sorkin & Zerial 2014). Unlike phagocytosis, pinocytosis is not limited to eukaryotic cells; rather, it is carried out by all types of cells through a diverse array of mechanisms. These mechanisms include macropinocytosis, clathrin-mediated endocytosis (CME), caveolae-mediated endocytosis, and clathrin- and caveolae-independent endocytosis. Each of these pathways represents distinct strategies through which cells internalize extracellular material, contributing to fundamental cellular processes and homeostasis.

The complex landscape of endocytosis encompasses various mechanisms, each playing a critical role in cellular physiology. Among these, CME stands out as a cornerstone process. CME, characterized by the formation of clathrin-coated pits on the plasma membrane, orchestrates the internalization of specific cargo molecules, ranging from receptors to nutrients. Understanding the molecular intricacies of CME not only sheds light on fundamental cellular processes but also holds profound implications for numerous physiological and pathological conditions which will be touched on later in the text.

1.1.Clathrin-mediated endocytosis

CME is a well-understood endocytic pathway among others. It constitutively occurs in all mammalian cells and plays role in uptake of crucial nutrients and substances such as low-density lipoprotein receptor (LDLR) and, transferrin receptor (TfnR) (Hopkins, Miller & Beardmore 1985, Trowbridge, Collawn & Hopkins 1993).

It has been described for the first time in oocytes almost 60 years ago (Roth & Porter 1964). Importantly following that Heuser and Reese showed the recycling of the synaptic vesicle membrane during transmitter release at the frog neuromuscular junction (Heuser & Reese 1973). Today it is known that more than 50 proteins are involved in this endocytic pathway, and ongoing research is providing new insights regarding CME and its role in health disease.

In essence, endocytosis follows a series of coordinated, overlapping steps (Mettlen et al 2018). It begins with specialized protein clusters, originating from the cell's interior, gathering on the inner surface of the cell membrane (nucleation). Cargo molecules, the target substances for uptake, then become concentrated within this nucleation area (cargo selection). Cargo molecules on nucleation site attract additional proteins, forming a structured "coat" (coat formation). The coat, in turn, triggers the membrane to bend inwards, forming a pit, much like a small alcove. Finally, the neck of this pit constricts and pinches off, separating a newly formed, coated vesicle containing the cargo from the main membrane (scission). The process is aided by the formation of actin filaments, which help shape the membrane, and the subsequent removal of the protein coat, releasing the vesicle for further transport within the cell (uncoating) (Fig. 1).

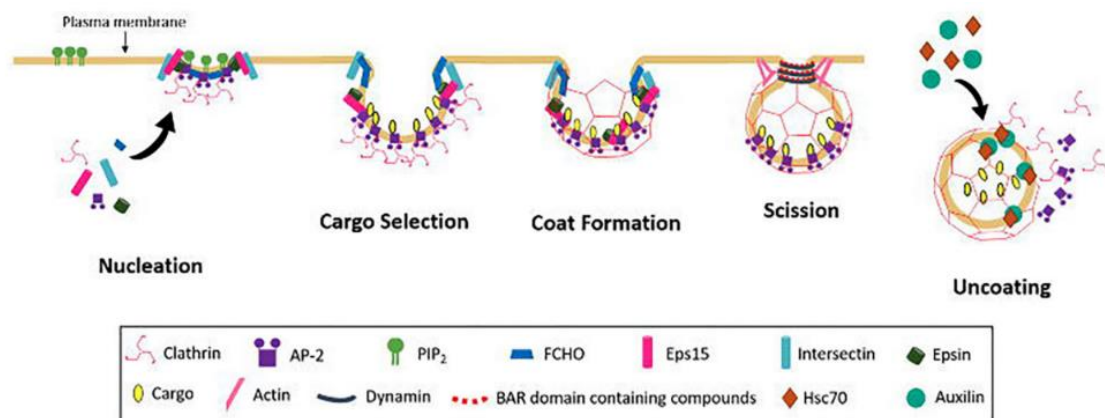


Figure 1: Schematic diagram of clathrin coated vesicle (CCV) formation: CME occurs in the following steps: nucleation, cargo selection, coat formation, vesicle scission and uncoating (Prichard et al 2021).

1.1.1. Steps of clathrin-mediated endocytosis

1.1.1.1. Nucleation

The initiation of CME begins with the formation of clathrin-coated pits (CCP), though the precise mechanisms driving this process are not fully understood. Central to this process is the allosteric regulation of adaptor protein 2 complex (AP-2), which controls the initiation,

growth, and stabilization of CCPs. The heterotetrameric AP-2 complex, composed of α -, β 2-, μ 2-, and σ 2-subunits, binds to the phosphatidylinositol-4,5-bisphosphate (PI(4,5)P₂), enriched at the plasma membrane, and recognizes endocytic sorting motifs on cargo proteins. This binding triggers clathrin assembly and recruits endocytic accessory proteins (EAPs), positioning AP-2 as a crucial regulator of CCP formation (Schmid & McMahon 2007).

Live-cell imaging studies have shown that CCP assembly is initiated when two AP-2 complexes begin recruiting clathrin triskelia (Mettlen et al 2018). The depletion of AP-2 via siRNA significantly reduces the number of CCPs at the membrane, underscoring the importance of AP-2 in CCP nucleation and stabilization (Hinrichsen et al 2003). Structural studies of AP-2 have revealed that it undergoes allosteric conformational changes that regulate CCP initiation, stabilization, and growth. In its cytosolic form, AP-2 remains in a closed conformation, with the clathrin binding site and PI(4,5)P₂/cargo binding sites buried. Upon binding to PI(4,5)P₂ at the membrane, AP-2 undergoes a conformational shift to an open state, exposing these critical sites and stabilizing nascent CCPs (Jackson et al 2010, Kadlecova et al 2017).

EAPs further regulate AP-2 allosterically and redundantly assist in CCP initiation. These EAPs, such as FCHo1/2, Eps15, intersectin, NECAP, and CALM (PICALM), are recruited early in CCP formation and interact with AP-2 and each other through low-affinity, multimeric interactions. Known as endocytic pioneers, these EAPs help initiate and stabilize AP-2 clusters at the membrane, enhancing clathrin recruitment and CCP stabilization and growth. For instance, FCHo1/2 proteins, containing F-BAR domains, stabilize AP-2's open conformation, thereby improving the efficiency of CCP initiation (Henne et al 2010, Holloper et al 2014). CALM and its isoform AP180, which function as adaptors for SNARE proteins, are essential for ensuring proper targeting and fusion along the endocytic pathway. The depletion of CALM leads to increased turnover of abortive CCPs and hinders CCP maturation, highlighting its role in CCP stabilization and maturation (Mettlen et al 2009). NECAP coordinates CCP initiation and growth by interacting near the clathrin binding site on the β 2 hinge and through interactions with FCHo, and CALM, functioning to fine-tune CCP dynamics (Ritter et al 2013).

Beyond protein and lipid interactions, AP-2's open conformation is maintained through phosphorylation which is important for its stabilization. Adaptor-associated kinase 1 (AAK1), part of the Numb-associated kinase (NAK) family—which also includes GAK (cyclin G-associated kinase), BIKE/BMP2K (BMP2-inducible kinase), and the Ark/Prk kinases in yeast—phosphorylates the μ 2 subunit of AP-2, enhancing its membrane-binding capability (Ricotta et al 2002, Smythe & Ayscough 2003). Specifically, AAK1 targets the Thr156 residue (Olusanya et al 2001), situated within a flexible linker that is unstructured when AP-2 is in its closed conformation but becomes structured when AP-2 is open. This phosphorylation event helps to

stabilize the $\mu 2$ subunit in its open form, thereby revealing its PI(4,5)P₂ and cargo binding sites (Conner & Schmid 2002, Kadlecova et al 2017, Ricotta et al 2002). Additionally, AAK1 is known to bind and become activated by assembled clathrin, potentially creating a positive feedback loop that further promotes clathrin assembly driven by AP-2 (Conner, Schröter & Schmid 2003). A detailed discussion of AAK1 will be provided later in the text.

1.1.1.2. Cargo Selection

CME is critical for forming vesicles that transport a wide variety of cellular cargo across the plasma membrane. The specificity of cargo selection in CME relies on numerous adaptor proteins, with AP-2 being one of the most studied and integral to this process. AP-2 initiates CCP formation by binding to both clathrin and PI(4,5)P₂ at the plasma membrane (Cocucci et al 2012, Traub 2009).

The AP protein family, which includes AP-1, AP-2, AP-3, AP-4, and AP-5, comprises heterotetrameric complexes with distinct cellular localizations and functions (Fig. 2). For instance, AP-1 operates at intracellular membranes which is similar to AP-2, whereas AP-3 participates in protein sorting to lysosomes and can function independently of clathrin (Hirst & Robinson 1998, Robinson 2015, Traub 2009, Traub & Bonifacino 2013). AP-4 has no association with clathrin, and AP-5's specific roles remain less defined (Hirst et al 2011, Hirst, Irving & Borner 2013, Hirst et al 2018). Each AP complex formed by four unique subunits: two large subunits with a molecular weight of 90 – 130 kDa ($\gamma/\alpha/\delta/\epsilon/\zeta$ and $\beta 1-5$, respectively), one medium sized subunit of about 50 kDa ($\mu 1-5$), and one small sized subunit of about 20 kDa ($\sigma 1-5$). AP-2 comprises an α subunit (110 kDa), $\beta 2$ subunit (100 kDa), $\mu 2$ subunit (50 kDa), and $\sigma 2$ subunit (17 kDa) and in AP-2, the α and $\beta 2$ subunits play a crucial role in binding clathrin and other adaptors (α and $\beta 2$ subunits) while the core structure recognizes cargo sorting signals and binds PI(4,5)P₂ (Collins et al 2002, Scarmato & Kirchhausen 1990, Traub 2009).

Adaptor proteins in CME are classified as clathrin-associated sorting proteins (CLASPs), which anchor within the clathrin scaffold and identify sorting signals to facilitate cargo recruitment.

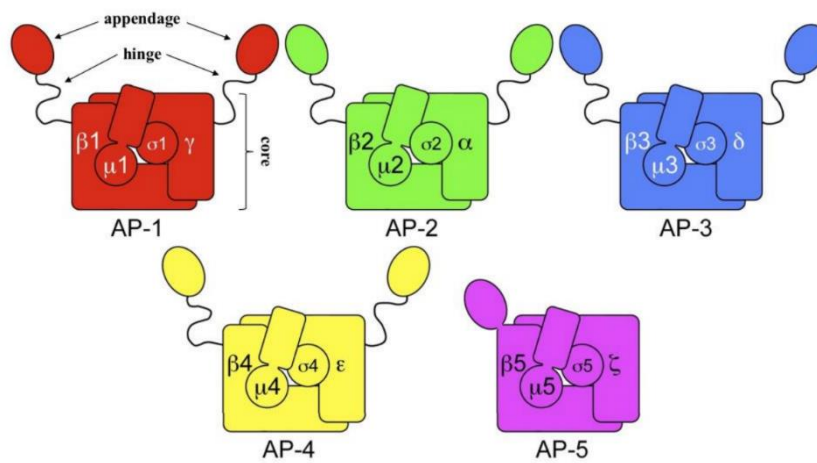


Figure 2: Structure of Adaptor complexes (AP) 1-5. Adaptor protein complexes are heterotetramers made up of two large, one medium, and one small subunit. The N-terminal regions of the large subunits, along with the medium and small subunits, form a core that binds membranes and sorts cargo. Both C-terminal appendage domains, connected to the core by an unstructured hinge (except in AP-5), interact with clathrin and regulatory proteins to facilitate endocytosis. Picture taken and modified from (Hirst et al 2014).

Based on their structural identity, CLASPs are grouped into oligomeric and monomeric categories (Traub & Bonifacino 2013). CLASPs, through their interaction with clathrin, become embedded in the polyhedral clathrin scaffold, where they identify and engage with sorting signals to recruit cargo (Ohno et al 1995).

AP-2 is the primary adaptor for cargo selection, but other AP complexes and CLASPs, such as FCHO1, eps15, Numb, β -arrestin, AP180 (exclusively expressed in neurons), and epsin, contribute to endocytosis through recognition of specific amino acid motifs or post-translational modifications like ubiquitination and phosphorylation (Höning et al 2005, Naudi-Fabra et al 2024, Traub & Bonifacino 2013).

1.1.1.3. Coat formation

Coat assembly or formation in CME begins as clathrin triskelia self-polymerize into a polyhedral cage around the cargo, forming a clathrin-coated vesicle (CCV) still connected to the plasma membrane by a narrow neck (Kaksonen & Roux 2018). During this process, curvature effectors like EPS15 and epsin are displaced to stabilize the coat (McMahon & Boucrot 2011). There are two main models of membrane bending in CCP formation: the constant curvature model (Cocucci et al 2012), where clathrin polymerizes onto a curved membrane, maintaining

constant curvature as the area increases; and the constant area model, where clathrin assembles on a flat membrane before bending occurs (Avinoam et al 2015, Haucke & Kozlov 2018). Evidence suggests that both models may operate simultaneously, as both early and late-stage curvature has been observed. Accessory proteins like epsin and CALM, along with actin filaments, may further aid in inducing membrane curvature during vesicle formation (Carlsson & Bayly 2014, Kaksonen & Roux 2018).

1.1.1.4. Scission

The scission phase is the critical final step in vesicle formation, primarily driven by the large GTPase dynamin. Dynamin assembles into a helical structure at the neck of the clathrin-coated pit, where it facilitates membrane fission. Its role in vesicle scission in mammals is supported by three main findings: dynamin's ability to assemble into dense oligomers helps initiate neck constriction, fission requires GTP hydrolysis, and dynamin oligomers undergo further tightening in the presence of GTP (Kaksonen & Roux 2018, Roux et al 2006). For dynamin to function effectively, it relies on various helper proteins, particularly those containing BAR domains like amphiphysin, endophilin, and sorting nexin 9 (SNX9). BAR domain proteins contribute in several ways, including recruiting other fission proteins (such as dynamin) and actively assisting in membrane shaping and scission (Ringstad et al 1999, Takei et al 1999). Additionally, BAR domain proteins play a role in actin recruitment to the budding site, which supports both membrane shaping and scission processes.

The BAR domain is a dimeric structure with a curved, crescent-like shape that binds to membranes. Remarkably, BAR domains can form membrane tubules upon high-density binding, with their curvature matching that of the BAR crescent (Peter et al 2004). This domain is known as a curvature sensor, and different BAR domains exhibit unique curvatures: for instance, F-BAR domains have a broader curvature (60–80nm radius), while N-BAR domains are more sharply curved (around 10nm). Evidence indicates that the recruitment timing of various BAR proteins aligns with changes in membrane curvature during endocytosis; proteins with F-BAR domains (e.g., FCHO1/2) appear early, while those with N-BAR domains (like endophilin and amphiphysin) arrive later, with intermediate-curvature proteins like SNX9 recruited in between (Kaksonen & Roux 2018, Posor et al 2013, Schöneberg et al 2017, Wu et al 2010). Additionally, specific phosphoinositides (PIPs) produced during clathrin coat assembly are crucial for recruiting these proteins. For instance, SNX9 recruitment is guided by phosphatidylinositol 3,4-bisphosphate (PI(3,4)P₂) production, while PI(4,5)P₂ dephosphorylation by synaptojanin supports dynamin-mediated membrane fission (Posor et al 2013, Wu et al 2010).

1.1.1.5. Uncoating

During the uncoating phase, the disassembly of the vesicle's coat allows the endocytic machinery proteins to be released and recycled for future endocytosis events. This uncoating step also prepares the new vesicle to merge with an early endosome, initiating further intracellular trafficking. Two key proteins, auxilin and heat shock cognate protein 70 (HSC70), play a central role in this disassembly process. Auxilin binds within the clathrin lattice at overlapping “ankle” regions and brings HSC70 to critical points within the lattice, facilitating interaction and uncoating (Newmyer, Christensen & Sever 2003, Schlossman et al 1984, Ungewickell 1985). In vitro studies revealed that the auxilin-HSC70-clathrin complex activates the ATPase function of HSC70, which drives coat disassembly. Remarkably, this clathrin coat breakdown initiates a controlled cycle of polymerization and depolymerization, which could support the remodeling of clathrin coats to encourage membrane curvature in vesicle formation. The disassembly mechanism of HSC70 is influenced by its nucleotide binding state: with ADP bound, HSC70 attaches to clathrin via auxilin. When ATP replaces ADP in HSC70's nucleotide pocket, the complex dissociates, completing the uncoating process (Barouch et al 1994, Kaksonen & Roux 2018).

1.2. CME in synapse and neurodegenerative diseases

Before discussing neurodegenerative diseases and synaptic dysfunction in neurodegenerative diseases, it's essential to briefly review the fundamental role of synaptic physiology and synaptic vesicles (SVs). These components are crucial for effective nervous system communication, with CME playing a vital role in recycling synaptic vesicles after neurotransmitter release.

Neurotransmission, or the process of communication between neurons, is fundamental to cellular interaction within both the sensory and nervous systems, facilitating a range of physiological responses and behaviors. This process relies on the release of neurotransmitters from presynaptic terminal via highly specialized, spherical structures called SVs, which play a critical role in signaling across synapses—the junctions between neurons. Within these vesicles, neurotransmitters are stored and primed for release upon receiving an electrical signal. Once released, they travel across the synaptic cleft to bind to receptors on the neighboring neuron, thus perpetuating the signal and enabling complex communication networks throughout the brain and body (Caire, Reddy & Varacallo 2024, Südhof 2013).

The presynaptic terminal is responsible for the release of neurotransmitters and is where CME plays a critical role by recycling SVs to maintain synaptic transmission efficiency. On the other hand, the postsynaptic terminal contains receptors that bind the released neurotransmitters, leading to downstream signaling and subsequent cellular responses. Together, these coordinated pre- and postsynaptic functions ensure proper synaptic plasticity, which is crucial for learning, memory, and overall neuronal health (Kennedy 2013, Silva et al 1992, Zeng et al 2001).

1.2.1. Synaptic Vesicle Recycling and CME

Although synaptic vesicles are crucial for maintaining neuronal function, their numbers are limited and require constant balance and careful regulation. This balance is achieved through the recycling of both synaptic vesicle membranes and associated proteins, a process essential for continuous neurotransmission (Heuser & Reese 1973, Sudhof 2004). Within the presynaptic terminal, synaptic vesicles (SVs) are categorized into four functional “pools”: the readily releasable pool (RRP), the recycling pool, the reserve pool, and the resting pool (Chanaday et al 2019b). SVs in the RRP, which are positioned close to the plasma membrane, and are primed for immediate fusion upon signal arrival. When an action potential reaches the presynapse, it opens Ca^{2+} channels, causing a local increase in Ca^{2+} concentration that triggers the fusion of RRP vesicles with the membrane. To maintain efficient signaling, the RRP must be consistently refilled either by recruiting vesicles from the reserve pool or rapidly reusing those that have just undergone fusion (Guo et al 2015, Holderith et al 2012, Kononenko & Haucke 2015) (Fig. 3) The process of SVR involves exocytosis from the RRP, followed by endocytic retrieval, which maintains a consistent supply of SVs filled with neurotransmitters for sustained neurotransmission (Denker & Rizzoli 2010, Prichard et al 2021). Once internalized through endocytosis, these new SVs are rapidly refilled with neurotransmitters in preparation for their next fusion event. Two primary components enable this refilling process: vacuolar H^+ ATPase (vATPase) and vesicular neurotransmitter transporters. vATPase generates an electrochemical gradient across the SV membrane, providing the necessary force for transporters to move neurotransmitters into the vesicles. These transporters also determine the specific neurotransmitter type stored within each SV. The recycling of these components is closely coordinated with the SVR process (Blakely & Edwards 2012, Farsi, Jahn & Woehler 2017). Studies across various biological systems highlight the significant role of CME as a primary mechanism for SVR. This connection is supported by high levels of clathrin and dynamin expression—elevated 10- to 50-fold in neurons—possibly enabling the rapid CME activity necessary to meet the demands of synaptic transmission. This increase likely facilitates a greater number of clathrin-coated vesicles carry the right transporters to fill it with the correct

neurotransmitter, allowing for accurate signaling in the nervous system (Chanaday et al 2019a, Silm et al 2019). Furthermore, clathrin is also essential for coordination of the SVs acidification timing, which is highly vital for neurotransmitter loading. Proper acidification requires the dissociation of the clathrin coat, suggesting that the uncoating process might regulate the timing of neurotransmitter filling immediately after the SVs are reformed (Farsi et al 2018). Efficient synaptic vesicle recycling is essential for maintaining normal sensory and nervous system function, as well as for supporting synaptic physiology. Disruptions in SVR and potentially in CME are linked to a variety of neurological disorders, including Parkinson's disease (Vidyadhara, Lee & Chandra 2019), Alzheimer's disease (Jaye, Sandau & Saugstad 2024), epilepsy (Prichard et al 2021), Huntington's disease (Yu et al 2014a), and schizophrenia (Schubert et al 2012). These associations underscore the importance of SVR and CME as critical mechanisms in neuronal health and as potential targets for understanding and treating these conditions efficiently (Heuser & Reese 1973, Maycox et al 1992, Morgan et al 2000, Morgan et al 2001, Morgan et al 1999, Overhoff, De Bruyckere & Kononenko 2021).

Additionally, neurons express specific forms of CME components, including neuron-enriched clathrin light chains and unique inserts within the β -subunit of the AP-2 complex, alongside neuron-specific variants like dynamin 1 and the α -subunit of AP-2 (Brodsky et al 1991, Morris

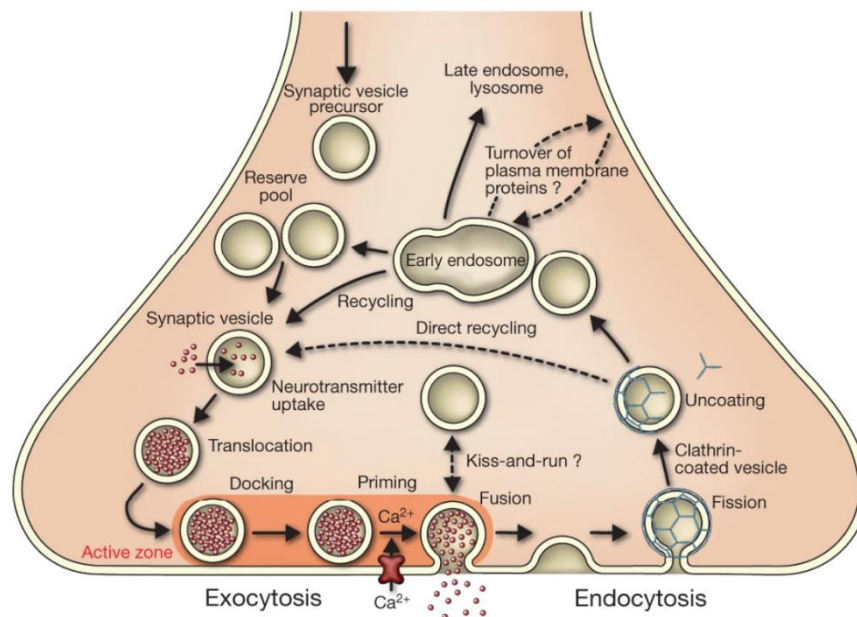


Figure 3: SV recycling SVs, which are filled with neurotransmitters, are stored within the cytoplasm of neurons. When activated, these vesicles are transported to the active zone where they dock in preparation for release. Priming is a crucial process that encompasses all the steps necessary for the exocytotic complex to achieve release readiness; while it is typically thought to occur after docking, it can begin before docking during periods of sustained neuronal activity. This can lead to the rapid fusion of newly arrived vesicles. Following exocytosis, vesicle proteins likely remain clustered and are subsequently retrieved via endocytosis. Retrieval process is primarily mediated by CME. Once clathrin has uncoated the vesicles, they are regenerated within the nerve terminal, potentially involving an endosomal intermediate. The actively recycling vesicles are in slow exchange with a reserve pool, ensuring a constant supply for synaptic transmission (Jahn & Fasshauer 2012).

& Schmid 1995, Prichard et al 2021, Robinson et al 1994).

1.2.2. Alzheimer's Disease and CME

Neurodegenerative diseases are progressive, and incurable conditions result in degeneration and / or death of nerve cells. One prominent example is Alzheimer's disease (AD), a progressive neurodegenerative disorder and the leading cause of dementia, characterized by memory loss, cognitive decline, and behavioral changes. AD pathology is defined by the accumulation of amyloid-beta ($A\beta$) plaques and tau tangles, which disrupt communication between neurons and ultimately lead to cell death (Leng et al 2021). Beyond plaque and tangle formation, AD involves multiple interconnected mechanisms, including vascular dysfunction,

endolysosomal impairment, disrupted autophagy, and oxidative stress (Jaye, Sandau & Saugstad 2024).

Mechanistically, A β aggregates into plaques, initiating a cascade that drives tau pathology and neuronal degeneration (Hardy & Allsop 1991). The amyloid precursor protein (APP), essential for neuronal development and function, undergoes processing through either a non-amyloidogenic pathway (via α - and γ -secretase) or an amyloidogenic pathway (via β - and γ -secretase). The latter pathway produces amyloid- β peptide (A β), which, along with neurofibrillary tangles, is central to AD pathology (Alsaqati, Thomas & Kidd 2018). Notably, A β 1-42 internalization has been shown to alter endolysosomal marker distribution and trigger neuronal degeneration, pointing to disruptions in cellular trafficking and degradation processes in AD (Song et al 2011).

Evidence from postmortem studies reveals altered levels of many proteins associated with CME in the AD brain. For instance, decreased AP-2 complex subunit alpha-1 in the superior frontal gyrus (Yao et al 2000), and reduced AP180 in areas such as the dentate gyrus and temporal cortex (Yao et al 1999) have been observed. In another study it has been shown that AP-2 controls APP processing and A β production. It prevents amyloidogenesis by functioning downstream of BACE1 endocytosis, regulating BACE1 endosomal trafficking and its delivery to lysosomes (Bera et al 2020). Moreover isoform-specific changes of α -adaptins have been shown in patients' brains. IHC studies indicated colocalization of AP2A1 with tau pathology in late-onset Alzheimer's disease (LOAD) brains, whereas AP2A2 was found colocalized with microglial cells (Srinivasan et al 2022). Similarly, levels of Dynamin1 (Cao et al 2010) and Dynamin2 (Aidaraliev et al 2008) decrease in the hippocampus and entorhinal cortex while other proteins, including Intersectin 1 (ITSN1), Clathrin heavy chain (CHC), RAB5A, and Amphiphysin 2, are increased in the frontal cortex (Alsaqati, Thomas & Kidd 2023, De Jesús-Cortés et al 2012, Thomas et al 2011). Intriguingly, the Clathrin light chain (CLTA) has even been identified in neurofibrillary tangles within the hippocampus (Nakamura et al 1994). Genetic studies also link endocytic pathway dysfunction with AD risk, highlighting abnormal A β levels as significantly associated with endocytosis, while tau appears to have a lesser association (Schork & Elman 2023, Tesi et al 2020). These findings underscore the involvement of endocytosis, particularly CME, in AD's etiology and possible resilience mechanisms. However, caution is needed while interpreting these relationships, as each protein plays distinct and often region-specific roles within the brain. Furthermore, age and sex should be considered, as CME regulation is both age- and sex-dependent, adding another layer of complexity to AD pathology (2023).

1.2.3. Parkinson's Disease and CME

Parkinson's disease (PD) is the second most prevalent neurodegenerative disorder following AD. It is characterized by a range of motor symptoms, including resting tremors, masked facial expressions, rigidity, and bradykinesia, which stem from the depletion of dopamine—a critical neurotransmitter (de Lau & Breteler 2006).

The primary pathological feature of PD is the loss of dopaminergic neurons in the substantia nigra pars compacta (SNpc) of the midbrain, although the exact mechanisms driving this neurodegeneration remain poorly understood. A key player in PD pathology is α -synuclein (α -Syn), which forms cytoplasmic inclusions known as Lewy bodies—aggregates that primarily consist of misfolded α -synuclein (Spillantini et al 1998). Notably, the accumulation and aggregation of α -synuclein lead to synaptic dysfunction in dopaminergic neurons within the striatum, often preceding neuronal death (Sossi et al 2004, Zou, Tian & Zhang 2021). Under normal physiological conditions, α -synuclein is predominantly located in presynaptic nerve terminals across various brain regions, such as the cerebral cortex, hippocampus, and striatum. It is primarily found within the synaptic vesicle fraction (Lee et al 2008). Emerging evidence suggests that α -synuclein plays a critical role in stabilizing the curvature of synaptic vesicles, thus influencing membrane remodeling, clustering of synaptic vesicles, and the maintenance of synaptic vesicle pools. Additionally, it promotes the assembly of SNARE complexes and modulates the release cycle of synaptic vesicles (Braun et al 2012, Burré 2015, Burré et al 2010).

Research indicates that CME is impaired in PD, with several genes associated with the disease implicated in vesicular trafficking, particularly in SVR. For instance, mutations in the E3 ubiquitin ligase Parkin are linked to early-onset autosomal recessive PD. The interaction between Parkin and endophilin an endocytic protein that directs dynamin to the necks of CCVs highlights Parkin's potential regulatory role in SVR and PD pathogenesis (Cao et al 2014). Moreover, elevated levels of monomeric α -synuclein correlate with an increase in free CCVs, indicating defects in clathrin uncoating processes (Busch et al 2014, Medeiros et al 2017). Late-onset autosomal dominant PD is frequently associated with mutations in leucine-rich repeat kinase 2 (LRRK2). Notably, LRRK2 interacts with endophilin and is crucial for regulating synaptic vesicle dynamics, with additional connections to dynamin (Singh, Jadhav & Bhatt 2017, Tsuyoshi & Yuzuru 2015). Studies on LRRK2 mutant mice demonstrate an accumulation of CCVs alongside a reduced density of synaptic vesicles in dopaminergic terminals (Xiong et al 2018). Another research shows that LRRK2 may influence AP-2 function by modulating the recruitment and phosphorylation of AP-2 components, a role underscored by the dysregulated AP-2 levels observed in LRRK2 knockout tissues. Notably, the R1441C

LRRK2 mutation impairs both AP-2-dependent CME and synaptic vesicle endocytosis (Heaton et al 2020).

1.2.4. Huntington's Disease and CME

Huntington's Disease (HD) is a hereditary neurodegenerative disorder, primarily characterized by cognitive decline, movement abnormalities such as chorea, and symptoms of dementia. HD results from a mutation in the *huntingtin (HTT)* gene, which disrupts the normal function of the huntingtin protein (HTT), leading to the degeneration of specific medium spiny neurons in striatum and producing psychiatric, motor, and cognitive symptoms. This degeneration also affects the mitochondrial electron transport chain, further contributing to cellular dysfunction (Bates et al 2015). Studies suggest that HTT may play a role in CME, linking the disruption of this pathway to neuronal impairments in HD (Harjes & Wanker 2003, McAdam et al 2020, Singh, Jadhav & Bhatt 2017). The mutated HTT protein aggregates and disrupts CME by inhibiting the internalization and recycling of SVs, which impairs neurotransmitter release and neuronal function (Trushina et al 2006, Yu et al 2014b). HTT also interacts with various clathrin-mediated SVR components, including HSC70, which is essential for vesicle uncoating during endocytosis (Morgan et al 2001). Aggregation of mutated Htt can sequester HSC70, preventing its normal function in uncoating and, thus, blocking efficient endocytosis (Yu et al 2014b). Additionally, HTT interacts directly with the adaptor protein complex AP-2, assisting in AP-2 recruitment to the membrane. Mutation-induced dysfunction in Htt disrupts this docking process, leading to reduced AP-2 recruitment and impaired CME (Borgonovo et al 2013). Collectively, these interactions highlight the central role of Htt in regulating CME and suggest that its dysfunction may contribute to HD pathology through disrupted vesicle recycling.

2. AAK1

AAK1 is a serine/threonine kinase that belongs to the Numb-associated kinase (NAK) family. In mammals, this family includes myristoylated and palmitoylated serine/threonine kinase 1 (MPSK1, also known as STK16/TSF1/PKL12/Krct), cyclin G-associated kinase (GAK), bone morphogenetic protein 2 inducible kinase (BIKE), and AAK1 itself (Manning et al 2002). Structurally, AAK1 consists of three domains: a highly conserved N-terminal serine/threonine kinase domain, an intermediate QPA-rich region, and a C-terminal α -adaptin-interacting domain (AID) (Sorrell et al 2016). While AAK1 shares strong similarities with other members of the NAK family, particularly in its kinase domain, it differs significantly in its other domains. Notably, AAK1 and BIKE share 74% identity in their kinase domains and 50% in their overall sequences (Smythe & Ayscough 2003, Sorrell et al 2016). The key distinguishing features

between AAK1 and BIKE lie in three residues within the ATP-binding pocket: two minor differences in the hinge region (Asp127 in AAK1 vs. Glu131 in BIKE, and Phe127 vs. Tyr132) and one significant variation in the P loop (Ala58 in AAK1 vs. Ser63 in BIKE), which help define the unique characteristics of AAK1 (Xin et al 2023) (Fig. 4)

AAK1 exists in multiple isoforms, each varying in length and domain composition, contributing to its functional versatility. The primary and longest isoform, often referred to as the canonical sequence, is approximately 961 amino acids long. This isoform includes several key domains: an N-terminal kinase domain responsible for its catalytic activity, a central clathrin-binding domain essential for endocytosis, and a C-terminal domain that interacts with the AP-2. Additionally, a longer isoform of AAK1 (AAK1L), containing an extended C-terminal region, has been identified (Henderson & Conner 2007). This extended form encodes an additional clathrin-binding domain (CBD2), which consists of several low-affinity interaction motifs. Despite CBD2's ability to directly bind to clathrin, its overexpression has been shown to impair transferrin endocytosis, suggesting a complex role in CME (Henderson & Conner 2007).

Alternative splicing of the AAK1 gene gives rise to shorter isoforms, approximately 878 amino acids in length, which may lack one or more functional domains, potentially limiting their role in clathrin-mediated endocytosis and other cellular processes. This diversity in isoforms enables the fine-tuning of AAK1's functions across various cellular contexts. AAK1 was originally identified as an interaction partner of α -adaptin, a key component of the AP-2 complex, and was shown to phosphorylate the μ 2 subunit of AP-2 at threonine 156, playing a crucial regulatory role in CME (Conner & Schmid 2002). Over time, research has revealed that AAK1 is involved in numerous other pathways beyond CME, highlighting its broader significance in cellular processes.

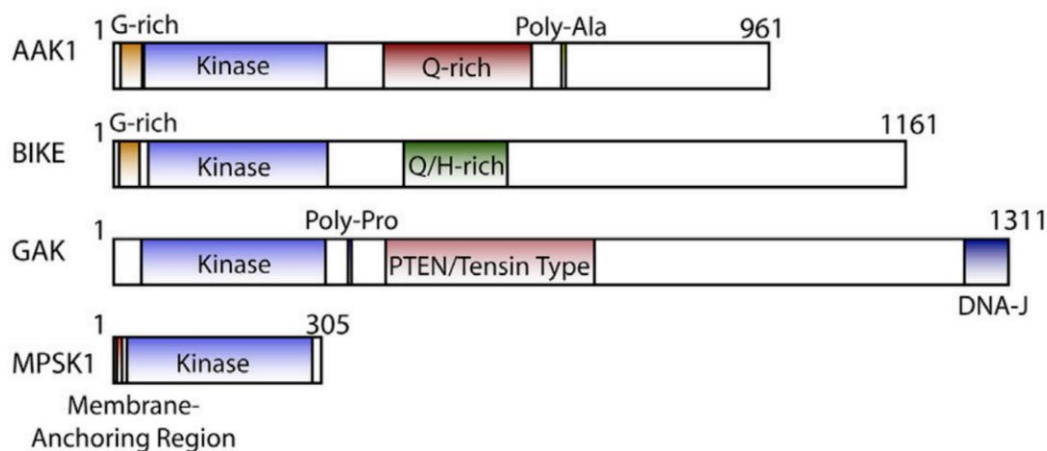


Figure 4: Domain organization of human NAKs. Figure is adapted from (Sorrell et al 2016).

2.1. Biological Function of AAK1

AAK1 has been implicated in multiple biological pathways. For instance, as a substrate of nuclear DBF2-related kinases 1 and 2 (NDR1/2), AAK1 plays a significant role in the development of cultured hippocampal neurons by promoting dendrite branching and dendritic spine growth. Research has shown that these dendritic changes are triggered by phosphorylation at serine 635 (S635) in the C-terminal AP-2 binding domain, a modification mediated by NDR1/2 (Ultanir et al 2012).

In addition to its involvement in neurodevelopment, AAK1 is also a key regulator of the Notch signaling pathway, which is critical for cell-cell communication during both development and adulthood across various species, from invertebrates to higher eukaryotes. The activation of the Notch receptor by its ligands requires a complex multi-step process involving γ -secretase, which is dependent on both monoubiquitination and CME (Gupta-Rossi et al 2011). Gupta Rossi and colleagues demonstrated that AAK1 directly interacts with the membrane-tethered active form of Notch, which is released after metalloprotease cleavage. AAK1 functions upstream of γ -secretase cleavage by stabilizing both the membrane-bound active Notch form and its monoubiquitinated version. Their study further confirmed that AAK1 acts as an adaptor, facilitating the interaction between Notch and components of the CME pathway, such as Eps15b. Additionally, overexpression of AAK1 increases the localization of activated Notch in Rab5-positive endocytic vesicles. In contrast, AAK1 depletion or overexpression of Numb, an inhibitor of the pathway, disrupts this localization. These findings suggest that, following ligand-induced Notch activation, the membrane-bound form of Notch can be directed into different endocytic pathways, ultimately leading to distinct cellular outcomes.

Beyond its involvement in neurodevelopment and Notch signaling, AAK1 has also been shown to play a critical role in the regulation of the WNT pathway. AAK1 activates the WNT signaling cascade by promoting the synthesis and trafficking of Rab5, a key regulator of early and late endosomal processes. This action facilitates the endocytosis of signaling receptors, allowing for proper signal transmission. Furthermore, AAK1 is activated by Numb, a protein that modulates the balance between the WNT and Notch pathways. Through this interaction, AAK1 inhibits Notch receptors, indicating a finely tuned dynamic between AAK1 and the Notch signaling pathway.

In the WNT pathway, AAK1 promotes the endocytosis of the WNT receptor LRP6, which is internalized within a reticulon fiber network. AAK1 phosphorylates the Thr156 site of AP-2 μ , a key event that regulates LRP6's internalization. Notably, LRP6 also acts as a negative

regulator of WNT signaling, establishing a feedback loop that is controlled by AAK1 to maintain signaling balance (Agajanian et al 2019). In addition to receptor endocytosis, AAK1 stabilizes β -catenin, a central mediator of WNT signaling. By activating β -catenin-dependent pathways, AAK1 accelerates the transcription of key WNT target genes, linking its function to critical processes like cellular growth, differentiation, and tissue development (Yang et al 2011). In another important and at the same time the first study for AAK1-LC3B relation it has been shown that LC3 lipidation via the macroautophagy core machinery is required to efficiently localize AAK1 to major histocompatibility complex (MHC) class I molecules for optimal internalization and degradation (Loi et al 2016). Collectively, these findings highlight AAK1's diverse regulatory roles, not only in CME but also in broader signaling networks that influence developmental and cellular fate decisions.

2.2. AAK1 in Central Nervous System Diseases

AAK1, beyond its established role in canonical endocytic pathways, has been increasingly implicated in various neurodegenerative and neuropsychiatric disorders. Genome-wide association studies (GWAS) have identified AAK1 as a gene potentially influencing PD susceptibility and variability in age of onset, suggesting a genetic link between AAK1 and PD risk (Latourelle et al 2009). Additionally, Shi et al demonstrated that AAK1 partially colocalizes with endosomal and presynaptic markers under normal physiological conditions but redistributed into aggregates containing mutant SOD1 and neurofilament proteins in rodent models of amyotrophic lateral sclerosis (ALS). This redistribution suggests that AAK1 mislocalization may disrupt cellular organization and contribute to ALS pathology. Supporting this, Shi and colleagues observed that AAK1 levels were reduced in ALS patients without corresponding changes in SOD1 levels, indicating a unique disease-related decline in AAK1 (Shi, Conner & Liu 2014).

In parallel, a study using mRNA and lncRNA analysis highlighted that AAK1, regulated by the lncRNA MALAT1, may form protein-protein interaction modules that are significant in ALS pathogenesis. These findings propose that AAK1-related mechanisms may be crucial in neurodegenerative progression (Liu et al 2021). In AD, AAK1 expression has also been observed to increase alongside AP-2 and Rab5 in the cortex, hippocampus, and plasma of AD model mice. Fu et al noted a positive correlation between elevated AAK1 levels and cognitive impairment in these models, suggesting AAK1's involvement in cognitive decline potentially through its effects on CME. This relationship points to a possible role for AAK1 in modulating A β production and clearance, linking CME with AD pathology (Fu et al 2018).

Beyond neurodegeneration, AAK1 has also been studied in the context of central nervous system (CNS) disorders like schizophrenia. Kuai et al found that AAK1 depletion through RNAi and small molecule inhibitors altered the trafficking and expression of ErbB4, an essential receptor implicated in neuronal growth and signaling. The mislocalization of ErbB4 to the plasma membrane in AAK1-depleted cells was shown to enhance Nrg1-induced signaling and neurite outgrowth, underscoring AAK1's potential regulatory function in neuronal architecture (Kuai et al 2011). Additionally, AAK1's inhibition has demonstrated therapeutic promise in managing neuropathic pain, which is mechanistically linked to α 2-adrenergic signaling, an antinociceptive pathway in humans (Kostich et al 2016).

The interaction of AAK1 with neurotrophic signaling pathways further implicates it in CNS disorders. Specifically, genetic studies show that deleting ErbB4 in parvalbumin-positive interneurons leads to behaviors in mice that are indicative of schizophrenia, suggesting that AAK1-related signaling pathways may be essential in the etiology of psychotic disorders (Wen et al 2010). Finally, AAK1 has also been identified as a significant upregulated gene in major depressive disorder (MDD) through blood gene expression analysis across multiple neuropsychiatric conditions, including ADHD and autism spectrum disorder (de Jong et al 2016). This discovery points to broader implications for AAK1 in mood regulation and cognitive function.

Despite mounting evidence of AAK1's role in neurodegenerative and psychiatric disease mechanisms, no in vivo studies have thoroughly examined the effects of AAK1 depletion on disease context. Addressing this gap, our study aims to investigate the in vivo impact of AAK1 loss, advancing understanding of its potential as a therapeutic target in CNS disorders.

3. Microtubule Affinity-Regulating Kinases

Microtubule affinity-regulating kinases (MARKs) are a family of kinases closely related to the PAR-1 proteins, playing a key role in establishing cell polarity. They do so by phosphorylating microtubule-associated proteins—such as tau, MAP2, and MAP4—at the KXGS motif within the microtubule-binding domain. This phosphorylation leads to the detachment and

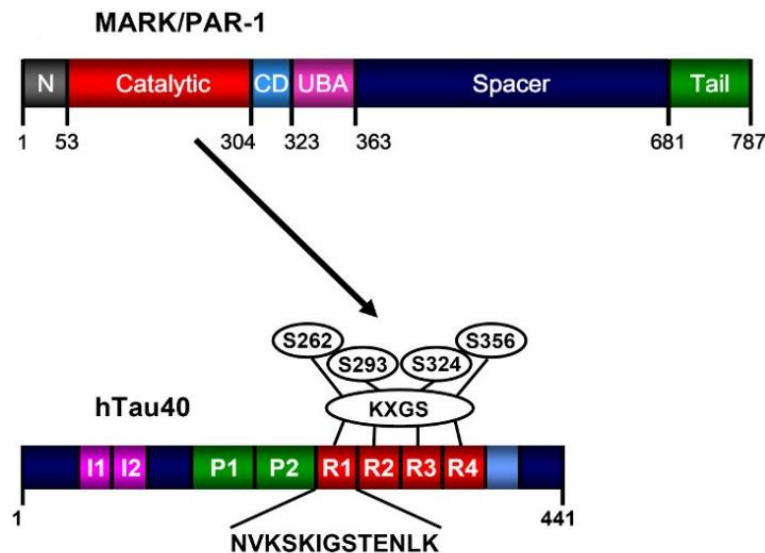


Figure 5: Domain structure of MARK family kinases: The domains include the header domain, the kinase catalytic domain, the common docking (CD) site, the ubiquitin-associated (UBA) domain, the spacer domain, and the tail domain, which contains the 'kinase-associated domain' (KA1). Bottom: bar diagram of tau protein, highlighting the repeat domain and the KXGS motifs that can be phosphorylated by MARK (Timm et al 2008).

destabilization of microtubules (Drewes et al 1997). In humans, the PAR-1/MARK family consists of four proteins: MARK1 (Par-1c), MARK2 (Par-1b), MARK3 (Par-1a), and MARK4 (Par-1d). MARK activity is particularly significant in neurons, where it regulates axonal growth by phosphorylating tau protein. This modification reduces tau's affinity for microtubules, leading to its dissociation and microtubule destabilization, a process implicated in various neurodegenerative conditions. When tau becomes unbound from microtubules, it is prone to pathological aggregation, a hallmark of Alzheimer's disease (AD).

In AD, the tau phosphorylation sites targeted by MARK, particularly the KXGS motifs, are among the earliest to show abnormal phosphorylation. Furthermore, MARK proteins are upregulated in the neurofibrillary tangles characteristic of AD brains (Chin et al 2000), and elevated MARK phosphorylation of tau has been observed early in transgenic mouse models of tauopathies (Eckermann et al 2007, Mocanu et al 2008). Given their critical role in both

microtubule dynamics and tau regulation, MARK proteins have garnered attention as potential therapeutic targets for neurodegenerative diseases and other disorders.

Structurally, the four MARK proteins share a common organization: an N-terminal header (N), a conserved catalytic domain, and a ubiquitin-associated (UBA) domain. These are linked to a more variable spacer region, which leads to the C-terminal kinase-associated domain (KA1). The KA1 domain is particularly important for membrane association, as it binds to acidic phospholipids, such as phosphatidylserine, facilitating membrane interactions (Fig. 5) (Moravcevic et al 2010).

3.1. MARKs in diseases

3.1.1. Microtubule affinity regulating kinase 1 (MARK1)

MARK1 has emerged as a critical player in neurodevelopmental processes, with increasing evidence pointing to its role in cognitive function. Genetic studies suggest that MARK1 underwent accelerated evolution in humans, indicating its importance in brain function and cognitive traits. In neurodevelopmental disorders, dysregulation of MARK1 has been associated with structural and functional changes in neurons. Specifically, research in mice with a forebrain-specific cKO of MARK1 has revealed abnormalities in dendritic spine formation in hippocampal CA1 pyramidal neurons. This includes a marked reduction in spine density, which is significant because dendritic spines are essential for synaptic connectivity and plasticity. The cKO of MARK1 also leads to abnormal accumulation of key synaptic proteins, Guanylate kinase-associated protein (GKAP) and Glutamate Ionotropic Receptor AMPA Type Subunit 2 (GluA2), indicating disruptions in synaptic organization and protein trafficking. These structural deficits are reflected in behavioral impairments, such as spatial learning challenges in the Morris water maze and a reduction in anxiety-like behaviors, linking MARK1 function to both cognitive and emotional regulation (Kelly-Castro et al 2024).

Another study supports the dual role of MARK1 in neuronal morphology and transport. Both overexpression and knockdown of MARK1 in murine neocortical neurons lead to significantly reduced dendrite length, along with altered dendritic transport dynamics. This aligns with MARK1's role as part of the PAR-1 protein kinase family, which is integral to axon-dendrite specification, a process crucial for establishing neuronal polarity. Subtle changes in MARK1 expression or activity could thus influence dendritic function and morphology, potentially contributing to cognitive variations in humans (Maussion et al 2008).

MARK1 also interacts with pathways involved in Alzheimer's disease pathology. Death-associated protein kinase (DAPK), which is implicated in neuronal cell death and cytoskeletal

disruption, can inhibit microtubule assembly by activating MARK1/2. This activation promotes tau phosphorylation, destabilizing microtubules—a hallmark process in neurodegenerative diseases like Alzheimer's (Wu et al 2011). The MARK1's functions in dendritic morphology, synaptic structure, cognitive processes, and neurodegeneration highlights its importance in both brain development and disease.

3.3.2. Microtubule affinity regulating kinase 2 (MARK2)

Research indicates that Par1b (MARK2) is crucial for establishing body axes through the regulation of the cellular cytoskeleton in model organisms like *C. elegans* and *Drosophila* (Marx et al 2010). Particularly, MARK2 is shown to be essential for neurites in vitro as it provides mechanical strength and tracks for intracellular transport (Biernat et al 2002). The dysregulation of MARK2 is closely linked with the occurrence and development of neurodegenerative diseases and cancer. For instance, one study demonstrated that reduced levels of MARK2 or doublecortin (DCX) impair migration, but while MARK2 reduction stabilizes microtubules, DCX reduction increases their dynamics. Interestingly, co-reducing both partially restores normal migration, highlighting the need for balanced polarity and microtubule dynamics for effective neuronal movement (Sapir et al 2008). Moreover, research in primary rat hippocampal cultures revealed that the MARK2 isoform localizes to axonal exclusion zones and exhibits strong enrichment in dendritic spines. Notably, its overexpression in wild-type neurons resulted in decreased maximum dendritic length and generally shorter dendrites (Chudobová & Zempel 2023).

Another important study from 2024 identified MARK2 loss-of-function (LoF) variants as significant in autism spectrum disorder (ASD) and neurodevelopmental disorders. Research on human neuronal cells and Mark2^{+/-} mice showed that MARK2 deficiency disrupts early neuronal development, affects cell polarity, and alters cortical structure, resulting in ASD-like behaviors. Additionally, loss of MARK2 is linked to reduced WNT/ β -catenin signaling, suggesting lithium as a possible treatment for individuals with MARK2-associated ASD (Gong et al 2024).

Taken together, these findings underscore the importance of MARK2 as a candidate gene in understanding not only neurodevelopmental disorders but also the broader implications of its dysregulation in neurodegenerative diseases within the central nervous system. Its critical role in neuronal structure and function highlights the potential for therapeutic interventions targeting MARK2-related pathways.

3.3.3. Microtubule affinity regulating kinase 3 (MARK3)

In four MARK isoforms MARK3 is the first one to be discovered. In one study MARK3 was found in a subset of neurons containing granulovacuolar degeneration bodies (GVDs) and showed weak, general cytoplasmic staining in neurons of both elderly individuals without dementia and those with Alzheimer's disease. These findings suggest a strong association between the expression of MARK3 and Tau phosphorylation at Ser262 within the GVDs in Alzheimer's disease (Lund et al 2014). Additionally, it has been showed that MARK3 interacts with Melanocyte Inducing Transcription Factor (MITF), which is known to cause COMMAD syndrome with severe microphthalmia (George et al 2016, Schwarz et al 2010) and MARK3 deficiency may affect the Wnt signalling pathway (Sun et al 2001). In another study MARK3 overexpression was found to inhibit cell proliferation and angiogenesis in ovarian cancer cells. Metabolic stress activates cell cycle arrest at the G2/M phase by phosphorylating CDC25B and CDC25C, while RNA-seq analyses suggest that MARK3 limits cell cycle progression and angiogenesis, partly by downregulating AP-1 and Hippo signaling targets (Machino et al 2022). Lastly, different studies showed that it related with osteoporosis and dysregulated bone mineral density (BMD) which is line with MITF and COMMAD axis showed previously (Schwarz et al 2010, Zhang et al 2021).

3.3.4. Microtubule affinity regulating kinase 4 (MARK4)

Last isoform of MARKs family is MARK4. A gain-of-function variant in the kinase MARK4 has been identified in two siblings with neurodevelopmental disability and distinct physical features. This variant, a germline missense mutation (c.604T>C, p.Phe202Leu), occurs in the kinase's catalytic domain. While the variant does not affect protein levels, it enhances MARK4's ability to phosphorylate tau isoforms, a key factor in neurodevelopmental disorders, and increases ribosomal protein S6 phosphorylation, indicating heightened mTORC1 pathway activity. This study links the MARK4 variant to developmental and cognitive challenges, as well as behavioral and dysmorphic traits (Samra et al 2024).

MARK4 has two known isoforms: MARK4L and MARK4S. This study on the mouse MARK4 gene shows that while both isoforms are present in the CNS, MARK4S is especially upregulated during neuronal differentiation, making it a potential neuron-specific marker in the brain. The increased expression of MARK4S in early neuronal development suggests a specialized role in supporting neuronal functions (Moroni et al 2006).

It has been demonstrated that MARK4 phosphorylates Tau at specific sites within its microtubule-binding regions, including Ser-262 and Ser-356, which generates a p-tau variant with enhanced seeding potential. A reduction in MARK4 disrupts Tau phosphorylation patterns,

likely causing increased detachment from microtubules and impairing microtubule-based transport (Gong et al 2012, Oba et al 2020). In another study MARK4 identified as an activator of YAP/TAZ in the Hippo pathway, crucial for regulating cell proliferation. MARK4 depletion reduced YAP/TAZ activity and limits breast cancer cell growth and migration, suggesting its potential as a therapeutic target for cancer (Heidary Arash et al 2017).

4. Autophagy

To maintain long-term cellular function and tissue health, especially in the context of aging, efficient mechanisms for cellular maintenance and degradation are crucial. Among these, autophagy is one of the most well-characterized pathways, playing a key role in both degradation and recycling of cellular components. Initially observed in the 1960s, autophagy was described when cytoplasmic components were identified within lysosomes (Ashford & Porter 1962). However, it wasn't until the 1990s, through the pioneering work of Yoshinori Ohsumi, that the molecular players, pathways, and regulatory mechanisms of autophagy were fully elucidated (Baba et al 1994, Mizushima et al 1998, Noda & Ohsumi 1998, Takeshige et al 1992).

Autophagy is an evolutionarily conserved catabolic process that contributes to cellular homeostasis by recycling nutrients. It is broadly classified into two forms: basal and induced autophagy. Basal autophagy occurs continuously, even in nutrient-rich conditions, acting as a quality control system through the turnover of cytoplasmic components. Several studies have shown that when autophagy is impaired, ubiquitinated proteins accumulate within cells (Hara et al 2006, Komatsu et al 2005). Conversely, under nutrient-deprived conditions, such as during starvation, autophagy is upregulated to maintain amino acid levels essential for survival (Hara et al 2006, Komatsu et al 2006).

There are three primary types of autophagy: macroautophagy, microautophagy, and chaperone-mediated autophagy (CMA), all of which involve delivering cellular components to the lysosome for degradation. In CMA, proteins containing a specific KFERQ motif are recognized and targeted by chaperones, then transported into the lysosome for degradation (Dice 1990, Kaushik & Cuervo 2012, Terlecky et al 1992). Microautophagy involves the direct engulfment of cytoplasmic material by the lysosomal membrane. Macroautophagy, the most prominent form, differs from the other types by the formation of an autophagosome—a double-membraned vesicle that captures cytoplasmic material. This autophagosome then fuses with a lysosome to form an autolysosome, where degradation occurs. Macroautophagy can target bulk cytoplasmic material or specific organelles thanks to specific receptors, including mitochondria (mitophagy), lipids (lipophagy), the endoplasmic reticulum (ER-phagy),

pathogens (xenophagy), the nucleus (nucleophagy), and lysosomes (lysophagy) (Aman et al 2021) (Fig. 6).

Although autophagy appears straightforward, the canonical process is highly complex and involves numerous proteins. It progresses through four key stages: the initiation of phagophore formation, nucleation, elongation and the maturation and fusion of the autophagosome with

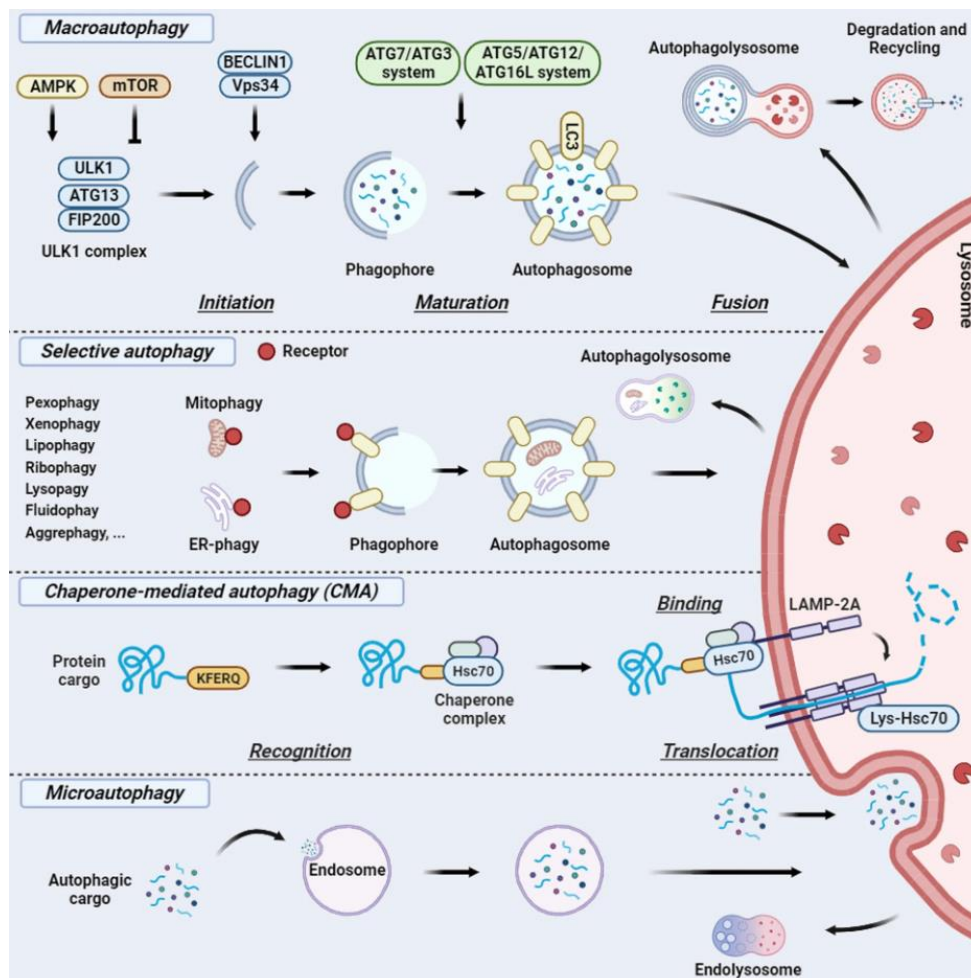


Figure 6: Primary type of autophagy, a schematic overview: Macroautophagy is regulated by the ULK1 complex, controlled by AMPK and mTOR, initiating double-membrane formation around cargo via the Beclin1-Vps34 complex. During elongation, lipidated LC3 family proteins (LC3II) are conjugated by ATG7-ATG3 and ATG5-ATG12-ATG6L1 complexes. Mature autophagosomes fuse with lysosomes to form autophagolysosomes, where degradation and recycling occur. Selective autophagy degrades damaged organelles or specific substrates via selective receptors (e.g., LC3B, GABARAP). Chaperone-mediated autophagy (CMA) targets KFERQ motif proteins, while microautophagy involves non-selective cytoplasmic uptake through lysosomal membrane invagination (Giansanti et al 2023).

the lysosome.

4.1. Steps of autophagy

4.1.1. Initiation of the phagophore formation

Autophagosomes form rapidly and spontaneously within the cell in response to various signals, requiring a continuous lipid source to support this dynamic process. These lipid sources are derived from multiple cellular membranes, including the endoplasmic reticulum (ER), ER-mitochondria contact sites (known as MAMs), recycling endosomes, the Golgi apparatus, and the plasma membrane (Axe et al 2008, Ge & Schekman 2014, Puri et al 2013).

Autophagy initiation is regulated by specific cellular triggers, such as amino acid deprivation, decreased insulin levels, and lower ATP availability, which signal nutrient scarcity and reduced energy (defined as AMP/ATP levels). Nutrient and energy status are sensed primarily by two signaling pathways: the mammalian target of rapamycin complex 1 (mTORC1) and AMP-activated protein kinase (AMPK). These two regulators have opposite roles; mTORC1, activated by adequate amino acid and growth factor levels, inhibits autophagy under nutrient-rich conditions. In contrast, AMPK activates autophagy when ATP levels are low, thus acting as an energy sensor that signals the need for cellular recycling to restore energy (Cheong et al 2008, Hawkins & Klionsky 2020, Kawamata et al 2008).

Both mTORC1 and AMPK converge to regulate the autophagy initiation machinery by signaling to the Atg1 complex in yeast (or its mammalian equivalent, unc-51 like autophagy-activating kinase 1 (ULK1 complex)), which plays a pivotal role in autophagosome formation. In mammals, this ULK1 complex comprises several essential components, including ULK1 (the mammalian Atg1 homolog), ATG13, FIP200, and ATG101, which collectively act as a scaffold to initiate the formation of the phagophore assembly site (PAS) (Cheong et al 2008, Hawkins & Klionsky 2020, Kawamata et al 2008). The phosphorylation status of these proteins determines their activity: under dephosphorylated conditions, ATG13 binds to ATG17-31-29 dimers, forming a complex essential for the proper localization and function of PAS, thereby enabling the autophagic process to proceed.

4.1.2. Nucleation

As mentioned before autophagosome formation initiates on ER (more specifically on omegasomes) and ER-mitochondrion contact sites in mammals. After PAS formation ATG1/ULK1 complex recruits ATG14-containing class III phosphatidylinositol 3-kinase (PtdIns3K/PI3K) complex, that includes the vacuolar protein sorting 34 (VPS34), 15 (VPS15), and Beclin-1 (BECN1) (Furuya et al 2005, Itakura et al 2008, Itakura & Mizushima 2010). Here VPS34 generates phosphatidylinositol 3-phosphate (PI3P), a phospholipid found in cell membranes that helps to recruit proteins. Importantly, presence of PI3P also allows recruitment of tryptophan-aspartic acid (WD) repeat domain phosphoinositide-interacting (WIPI) proteins

which play role in different stages of autophagosome formation and recruitment of ATG12-ATG5-ATG16L1 E3-like complex through a direct interaction with ATG16L1 for later stages (Dooley et al 2014).

4.1.3. Elongation and maturation

The expansion of the isolation membrane includes two ubiquitin-like conjugation systems. The first one is formation of ATG12-ATG5-ATG16L (E3) complex which is essential for the formation of pre-autophagosomes. ATG12 is activated by E1-like Atg7 in an ATP-dependent manner (Kim et al 1999, Mizushima et al 1998, Shintani et al 1999, Tanida et al 2001). ATG12 is then transferred to E2-like ATG10 and finally attached to acceptor lysine residue of ATG5 (Mizushima et al 1998, Shintani et al 1999). Two sets of ATG12-ATG5 conjugates further interacts with Atg16L dimer (Kuma et al 2002). The second ubiquitin-like conjugation system is microtubule associated protein 1 light chain 3 (LC3 - also known as ATG8) modification. This conjugation pathway starts with LC3I cleavage by cysteine protease ATG4 and then this processes LC3 conjugated with phospholipid phosphatidylethanolamine (PE) (LC3-PE / LC3II) by E1-like ATG7 and transferred to E2-like ATG3 (Hemelaar et al 2003, Ichimura et al 2000, Kim et al 1999, Tanida et al 2001). Afterwards, this lipidated LC3-II associates with newly forming autophagosome membranes. LC3-II remains on mature autophagosomes until its fusion with lysosomes. The conversion of LC3I to LC3II is a well-known marker of autophagy and under starvation and stress conditions the amount of lipidated LC3 increased (Kabeya et al 2000). One thing to emphasize unlike yeast, mammals have several Atg8-like proteins which are divided into LC3 and GABARAP subfamilies (Hemelaar et al 2003, Weidberg et al 2010). Even though they are quite similar to each other in the concept of autophagy latest studies have been indicated their distinct roles in or out of autophagy (Chen et al 2024, Jatana et al 2020).

Another important protein in elongation and maturation is a lipid scramblase protein ATG9. ATG9 localizes to the Golgi complex under normal conditions but translocates to recycling endosomes and small vesicles referred to as the ATG9 compartment upon induction of autophagy in an ULK1-dependent manner (Mari et al 2010, Young et al 2006, Zhou et al 2017a). Phospholipids delivered by ATG2 are translocated from the cytoplasmic to the luminal leaflet by ATG9, thereby driving autophagosomal membrane expansion (Maeda, Otomo & Otomo 2019, Osawa et al 2019, Valverde et al 2019).

4.1.3. Fusion of the autophagosome with the lysosome

Autophagosomes, cellular structures responsible for degrading and recycling cellular material, must fuse with lysosomes to form autolysosomes and complete the degradation process. This fusion requires the autophagosomes to be actively transported to lysosomes along microtubules. During transport, some autophagosomes can also fuse with early endosomes, creating an intermediate structure known as an amphisome. For these fusion processes, a coordinated group of proteins is essential, particularly the small GTPase families, such as Rab (Ras-associated binding) and Arf (ADP-ribosylation factor), along with tethering factors and SNARE proteins (Tian, Teng & Chen 2021).

Rab GTPases are crucial regulators of membrane trafficking in eukaryotic cells, acting as molecular switches that alternate between an active (GTP-bound) and inactive (GDP-bound) state. This switching mechanism is controlled by Guanine Exchange Factors (GEFs), which promote GTP binding, and GTPase-activating proteins (GAPs), which stimulate GTP hydrolysis (Stenmark 2009). During autophagosome maturation, specific Rab proteins like RAB2, RAB7, and the ARF-like GTPase ARL8 are recruited to the autophagosome membrane. These GTPases, in conjunction with the HOPS complex, help tether the autophagosome to the lysosome, bringing their membranes into close proximity and promoting fusion (Pu et al 2015).

The actual fusion event is driven by SNARE proteins, which provide the mechanical force necessary to merge the membranes. In this step, specific SNARE components—including VAMP7, VAMP8, Syntaxin 17, and SNAP29—assemble into a complex that catalyzes membrane fusion (Jiang et al 2014, Mao et al 2019, Pu et al 2015, Wang & Diao 2022). This fusion is further regulated by phosphoinositide enzymes: Inositol polyphosphate-5 phosphatase converts lysosomal membrane phospholipid PI(3,5)P₂ back to PI3P, while PI4K-II α generates PI4P, which is required for membrane organization and fusion (Hasegawa et al 2016).

Microtubule-based motor proteins, including kinesins and dyneins, play a pivotal role in transporting autophagosomes and lysosomes toward each other along the microtubules. Specifically, the dynein-dynactin complex supports the movement of autophagosomes and amphisomes toward lysosomes (Cason & Holzbaur 2022, Jordens et al 2001, Kimura, Noda & Yoshimori 2008, Wijdeven et al 2016). These motor proteins interact with small GTPases such as RAB7 and ARL8, linking the autophagosomes/amphisomes to their transport pathways and supporting the fusion process. (Langemeyer, Fröhlich & Ungermann 2018, Mohan et al 2018).

Finally, once the autophagosome and lysosome membranes have fused, the cytoplasmic cargo within the autolysosome is degraded by lysosomal hydrolases. This degradation process

relies on the proper acidification and enzymatic activity of the lysosome. Loss of key lysosomal enzymes, like Cathepsin B and D, can halt degradation within the autophagic pathway, leading to an accumulation of undegraded material (Yadati et al 2020).

Emerging evidence suggests a link between AAK1 and the autophagy pathway, although direct evidence remains scarce. AAK1, primarily known for its role in CME, may also be involved in autophagic processes, particularly given its functions in regulating vesicular trafficking. One study demonstrated that AAK1 associates with LC3 to facilitate internalization of MHC class I molecule (Loi et al 2016). In another study indirectly suggest that AAK1 is involved in regulating autophagy by mediating the phosphorylation and activation of AP-2 μ , which facilitates the internalization and autophagy induced degradation of Claudin-2 (CLDN2) in epithelial cells (Ganapathy et al 2022). These findings indicate a potential, albeit still largely unexplored, involvement of AAK1 in the regulation of autophagy, warranting further investigation, especially in neuronal contexts where vesicular trafficking is crucial for cellular homeostasis and synaptic function.

In this context it is pivotal to mention microtubule dynamics in AVs trafficking in neurons, as AVs need to travel long distances along axons and dendrites to reach lysosomes for degradation. AV movement within neurons relies heavily on microtubules, which serve as tracks for these vesicles. Specifically, the fusion of AVs with endosomes, and ultimately lysosomes, depends on intact microtubule networks (Köchler et al 2006). Studies have shown that AVs utilize motor proteins, such as dynein, to move along these microtubule tracks, and impairments in dynein function leads to a reduced ability of autophagosomes to fuse with lysosomes. This impairment is marked by an accumulation of LC3-II and a decrease in the clearance of aggregate-prone proteins, reflecting defects in autophagic flux (Ravikumar et al 2005, Rubinsztein et al 2005).

Proper AV trafficking requires well-regulated microtubule stability, which ensures efficient binding and movement. Due to their inherently unstable nature, microtubules need regulators to stabilize and control their structure. Plus-end tracking proteins (+TIPs), including EB1 and CLIP-170, regulate microtubule dynamics by binding to the plus ends of growing microtubules (Tirnauer & Bierer 2000). Also, severing proteins, such as katanin and spastin, further refine the microtubule network by cutting microtubules to control their length and organization (McNally & Vale 1993). Importantly, microtubule-associated proteins (MAPs), such as MAP2, MAP4, and tau, are key regulators that stabilize microtubules and promote their polymerization and they are critical for controlling the rigidity of individual microtubules, which is pivotal for neurons with long projections (Bulinski & Borisy 1979, KOTANI et al 1986, Nishida et al 2023, Sloboda, Dentler & Rosenbaum 1976). MARK2 is a key player in regulating microtubule

dynamics through the phosphorylation of these MAPs. MAP2, MAP4, and tau can be phosphorylated by MARK2, which leads to changes in their ability to bind and stabilize microtubules, thus regulating microtubule assembly and disassembly (Drewes et al 1997). This modulation of microtubule dynamics by MARK2 is essential not only for stabilizing microtubules but also for regulating intracellular trafficking (Ebner et al 1999), including the movement of AVs. By influencing MAP phosphorylation, MARK2 impacts the binding of microtubule-associated motor proteins, such as dynein and kinesin, which are responsible for transporting vesicles, including AVs, along microtubule tracks (Anjur-Dietrich et al 2023, Han et al 2024b, Yoshimura, Terabayashi & Miki 2010).

II. Objectives

The inclusive aim of this project is to elucidate the multifaceted role of AAK1 in the CNS, particularly in relation to neurodegenerative disorders. AAK1 has emerged as a critical player in endocytosis and intracellular trafficking, impacting various signaling pathways essential to neuronal health and function (Agajanian et al 2019, Gupta-Rossi et al 2011, Kuai et al 2011, Ultanir et al 2012, Xin et al 2023). By employing two distinct transgenic mouse models using *CMV* and *CamKII α* promoters, this study aims to provide an in-depth investigation into the cellular and molecular functions of AAK1 in the brain. Given the current gaps in knowledge regarding the outcomes of AAK1 depletion in in vivo contexts, this project will explore the following key questions:

1. What is the role of AAK1 in the brain?

This aim seeks to clarify the roles of AAK1 and its potential contributions to neuropathology. Given AAK1's established involvement in CME, understanding its specific functions within the brain may shed light on its influence on synaptic transmission and plasticity—processes that are essential for cognitive functions such as learning and memory (Kostich et al., 2016). To explore this, a *CMV*-promoter-driven mouse model that facilitates widespread AAK1 expression across various neural cell types was used. This broad expression pattern enabled an assessment of the systemic effects of AAK1 depletion on neuronal network dynamics and behavior in vivo. This approach provided a broader understanding of AAK1's role and yielded insights into its potential implications in CNS diseases (Fu et al 2018, Latourelle et al 2009).

2. Does AAK1 have cell-type specific role?

The second aim focused on the cell-type specific roles of AAK1, particularly in neurons. Using the *CaMKII α* promoter, which directs expression specifically in excitatory neurons, we investigated whether AAK1's functions are differential in a neuron specific manner. This approach allows us to determine if AAK1 plays specialized roles in synaptic regulation and neuroplasticity in excitatory neurons. Understanding these nuances is essential as dysregulation of AAK1 in specific neuronal population may contribute to the pathophysiology of CNS disorders (Fu et al 2018, Latourelle et al 2009, Xin et al 2023).

3. Does AAK1 have novel neuronal substrates, and what roles do these substrates play in neurodegenerative disorders?

The third aim is to identify and characterize the neuronal substrates of AAK1, exploring how these interactions may contribute to the pathogenesis of neurodegenerative diseases. By elucidating the signaling pathways and protein interactions mediated by AAK1, the study aimed to clarify its contribution to the progression of neurodegeneration and neuronal health (Liu et

al 2021, Shi, Conner & Liu 2014). Identifying these substrates is critical for pinpointing how AAK1 modulation might serve as a therapeutic target in mitigating neurodegenerative processes.

In conclusion, this project seeks to fill significant gaps in our understanding of AAK1's role in CNS function and pathology. By employing two genetically modified mouse models, we aim to dissect the complex interplay of AAK1 within neuronal systems and its broader implications for neurodegenerative disorders. To do that we used quantitative proteomics, live imaging of primary neuronal cells, and the analysis of different subcellular fractions such as synaptosomes and plasma membranes which provide a comprehensive understanding of AAK1's functions. The findings might provide insights into potential therapeutic strategies for conditions associated with AAK1 dysregulation.

III. Material and Method

1. Materials

Table 1: Instruments used for this study.

Instrument	Manufacturer	Catalogue number
BioRupter, Picorupter	Diagenode	B01060010
Cabinet, Horizontal laminar flow	Thermo Fisher Scientific	Heraguard ECO
Cabinet, vertical laminar flow (primary cells)	Thermo Fisher Scientific	Safe 2020
Centrifuges	Eppendorf Hettich VWR	5702R 320R MicroSTAR 17R
Double Edge Coated Blades (Washed version)	Electron Microscopy Science	#72000-WA
EASY-nLCTM 1200 System	Thermo Scientific	LC140
Electrophoresis Power Source	VWR	300V
Electrophoresis chamber (PCR)	VWR	700-0569
Electrophoresis chamber (WB)	Bio-Rad	Mini-Protean Tetra Cell
VOSEP ONE	Evosep	EV-1000
Dissection tools Forceps Scissors Scalpel	FST	11253-27 1 6020-14 11270-20 14090-09 13002-10 14002-13 10073-14
Freezer (-20°C)	LIEBHERR	9988187-12
Fridge (4°C)	LIEBHERR	9983491-10
Gel imager system (PCRs)	Bio-Rad	Gel Doc™ XR+
Incubator CO2 (cell lines)	Binder	C170
Incubator Shaker	Eppendorf	Galaxy 1705
Incubator CO2 (primary neurons)	Eppendorf	M1335-0002

Mcllwain Tissue Chopper	Cavey laboratory engineering Co. LTD	MTC/5E
Microscope, inverted (cell culture)	Leica	Leica DMi1
Microscope, inverted fluorescence Camera	Zeiss Hamamatsu	Axiovert 200M C11440
Temperature module LED Light source Software Objectives: 40x/1.4 oil DIC 63x/1.4 oil 10x/0.3	Zeiss CoolLED Micro-Manager Zeiss Zeiss Zeiss	TempMoudleS pE-4000 MicroManager1.4 420762-9900 420780-9900 420304-9901
Microtom	Thermo Fisher Scientific	Microm HM 430
Microwaver	Inverter	Sharp
Osmometer	Gonotec	Osmomat 3000
pH-meter	Mettler Toledo	Seven Easy
Perfusion pump	WPI	Peri-Star Pro
Photometer	Eppendorf	Bio Photomer plus
Real-time PCR Thermocycler	Applied Biosciences	7500 RealTimePCR System
Sonicator	BRANSON	Sonifier 250
Scales	OHAUS VWR	EX225D T1502746
SpeedVac Eppendorf Concentrator plus	Eppendorf	5305000509
Thermocycler	VWR	peqSTAR
Thermoschaker	CellMedia	
Water bath	VWR	VWB6
Vortex	Scientific Industries	Vortex-Genie 2
Vibratom	Leica	VT1200S
Sep-Pak columns C18 50mg	Waters	WAT036935
Super-frost plus microscope slides	Thermo scientific	193515000

Table 2: Chemicals used for solutions and buffers.

Chemical	Manufacturer	Identifier
2-β-Mercaptoethanol	Roth	4227.1
2-Propanol	Roth	CP41.3
Acetic acid 100%	Roth	3738.4

Acetone	Roth	5052.1
Aceton (Proteomics)	Merck	1.00020.2500
Acetonitrile hypergrade for LC-MS LiChrosolv	Merck	1.00029.2500
Antimycin	Sigma	A8674
Ammonium chloride	Roth	K298.2
Ammonium peroxodisulfate (APS)	Merck	1.012.001.000
Ampicillin sodium salt	Roth	K029.2
Ascorbic acid	Roth	3525.1
Boric acid	VWR	J67202
Bovine Serum Albumin	Sigma	A7906
Bromophenol blue	Sigma	B5525
Bafilomycin1A	Sigma	5.08409
2-Chloracetamid (CAA)	Merck	CAS 79-07-2
Calcium chloride dihydrate	Roth	5239.2
Calcium chloride hexahydrate	Roth	T886.1
Chloroquine disphosphate salt	Sigma	C6628
Cresyl violet acetate	Sigma	C5042
1,4-Dithioerythritol (DTT)	Applichem	CAS 3483-12-3
D-(+)-Glucose	Sigma	G5767
D-mannitol	Roth	M4125
Dimethyl sulfoxide (DMSO)	Roth	A994.2
di-Potassium hydrogenphosphate	Roth	6875.1
di-Sodium hydrogen phosphate dihydrate	Roth	4984.1
di-Sodium hydrogen phosphate anhydrous	Merck	106559
EDTA	Applichem	A1104.1000
Entellan®	Merck	107960
Ethanol	Omnilabs	A1613.2500PE
Formic Acid	Honeywell/FLUKA	607-001-00-0
Gelatin from porcine skin	Sigma	G2500
Glycerol	Roth	7530.1
Glycine	Roth	3908.3
HEPES	Sigma	H4034
Hydrochloric acide 32%	Roth	X896.2
IGEPAL	Sigma	I8896
Luminol	Roth	4203.1
Lysyl Endopeptidase (LysC)	WAKO	129-02541
Magnesium chloride hexahydrate	Roth	2189.1

Methanol	Roth	4627.5
Methanol LC-MS grade	VWR	83638.32
Milk powder	Roth	T145.2
Paraformaldehyde (PFA)	Merck	104.005.100
p-coumaric acid	Sigma	C9008
Ponceau S	Roth	5938.1
Potassium chloride	Roth	6781.1
Potassium dihydrogen phosphate	Roth	3904.1
Potassium disulfite	Sigma	60508
Sodium Chloride	Roth	3957.1
Sodium hydrogen carbonate	Roth	6885.1
Sodium dodecyl sulfate (SDS) ultra-pure	Roth	2326.2
SGC-AAK1-1	Sigma	SML2219
SGC-AAK1-1N	Sigma	SML2220
Tetramethylethylenediamine (TEMED)	Applichem	A1148.0028
Tris (hydrogenmethyl) aminomethane (Tris-base)	VWR	28.808.294
Trizma hydrochloride (Tris-HCl)	Sigma	T3253
Trypan Blue	Roth	CN76.1
Tween 20	VWR	663684B
Urea	Sigma	U1250
Xylene	VWR	28975.291
(Z)-4-Hydroxytamoxifen (Tamoxifen)	Sigma	H7904

Table 3: Reagents used in this study.

Reagent	Manufacturer	Identifier
Acryl/BisTM solution (30%) 37.5:1	VWR	E347
Bradford Reagent	Sigma	B6916
Bovine Serum Albumin	Sigma	A7906
Bovine Serum Albumin (fatty acid free)	Sigma	A6003
Complete Mini Protease Inhibitor	Roche	11836153001
DNA ladder (100 bp/ 1 kb)	Thermo Fisher Sci	SM0323/SM0311
DNA Gel Loading Dye (6X)	Thermo Fisher Sci	R0611

DreamTaq DNA polymerase	Thermo Fisher Sci	EP0703
Dynabeads™ Protein G	Invitrogen	10003D
ECL™ WB detection reagents	GE Healthcare	RPN2106
Isoflurane	Piramal	B73E16A
Ketamin hydrochloride	Sigma	K2753
LongAmp Taq DNA polymerase	BioLabs	M03235
Normal Goat Serum	Gibco	16210064
Nuclease-free water	Ambion	AM9938
PageRuler Plus Prestained Prot. Ladder	Thermo Fisher Sci	26619
Pierce™ High Capacity Streptavidin Agarose	Thermo Fisher Sci	20359
Pierce™ Protease and phosphatase inhibitor mini tablets	Thermo Fisher Sci	A32959
Proteinase K	Sigma	AM2546
ProFection Mammalian Transfection System-Calcium Phosphate	Promega	E1200
Rompun 2% (Xylazin)	Bayer	KP0BZPE
SuperSignal™ West Femto	Thermo Fisher Sci	34094
High Select™ Phosphopeptide Enrichment Kits & Reagents	Thermo Fisher Sci	A32993

Table 4: Cell culture ingredients and reagents used for media preparation.

Reagent	Manufacturer	Identifier
B-27 Supplement (50X)	Thermo Fisher Sci	17504-044
DMEM without glucose	Thermo Fisher Sci	A14430
Deoxyribonuclease I from bovine pancreas	Sigma	D5025
EBSS	Thermo Fisher Sci	14155-048
Fetal Bovine Serum	Merck	S0115
Fetal Bovine Serum	Sigma	F7524
GlutaMAXX™	Thermo Fisher Sci	35050-061
HBSS (1X) [-] CaCl ₂ , [-] MgCl ₂	Thermo Fisher Sci	14175-053
HEPES (1M)	Thermo Fisher Sci	15630-080
Horse serum (heat-inactivated)	Gibco	26050088
Insulin, human recombinant zinc	Thermo Fisher Sci	12585-014
MEM	Sigma	7278
Penicillin/Streptomycin (P/S)	Thermo Fisher Sci	15140-122

Poly-D-lysine (1mg/mL)	Merck	A-003-E
Soybean Trypsin Inhibitor	Merck	10109886001
Sodium Pyruvate	Thermo Fisher Sci	11360-039
Transferrin, Holo, Bovine Plasma	Merck	616420
Trypsin from bovine pancreas	Sigma	T1005
Neurobasal®-A Medium	Gibco	12349-015
Transferrin From Human Serum, Alexa Fluor™ 488 Conjugate	Thermo Fisher Sci	T13342

Table 5: Plasmid DNA used for transfection of cells in-vitro.

Plasmid (source gene)	Manufacturer/Provider
<i>EB3-tdTomato</i>	#50708 addgene
<i>ptagRFP-LC3B</i>	#21075 addgene

Table 6: Data acquisition and analysis.

Computing	Software	Manufacturer
Image processing	Fiji version 1.53	Wayne Rasband, National Institute of Health
Statistical analysis	GraphPad Prism version 9.5.1	GraphPad Software
Image acquisition	LAS X	Leica

Table 7: Microscopes.

Microscope	Manufacturer	Identifier
Transmission electron microscope	JEOL	JEOL JEM2100PLUSCameraGATAN
Slidescanner	Hamamatsu	S360
Confocal microscope LSM 980 with Airyscan 2 2.5x objective 10x objective 40x objective	ZEN, ZEN Connect Modul	EC Plan-Neofluar 2,5x/0,085 Plan-Apochromat 10x/0,45 C-Apochromat 40x/1,2 W Korr FCS Plan-Apochromat 63x/1,4 Oil DIC

63x objective		
Confocal microscope SP8	Leica Microsystems	TCS SP8
10x objective		PL Apo 10x/0.40 CS2
40x objective		PL Apo 40x/0.85 CORR CS
63 x objective		PL Apo 63x/1.40 Oil CS2

2. Methods

2.1. Animals

2.1.1. Mouse breeding and maintenance

All animal experiments were approved and performed according to the regulations of LANUV (Landesamt für Natur, Umwelt und Verbraucherschutz Nordrhein-Westfalen) guidelines. Mice were maintained in a pathogen-free environment in ventilated polycarbonate cages. Animals were housed in groups of five animals per cage with constant temperature and humidity at 12h/12h light/dark cycles. Food and water were provided ad libitum. Breedings were set up with males at least eight weeks old and females at least 6 weeks old. Pups were weaned at the age of 21 days.

2.1.2. Creating AAK1 knockout mice

Animals used in this study are displayed in Table 8 AAK1 KO mice generated using the well-validated 'KO-first allele' strategy. This strategy relies on the identification of an exon common to all transcript variants, upstream of which a LacZ cassette is inserted to make a constitutive KO/gene-trap known as a tm1a allele. In contrast to the tm1a allele, tm1b creates a frameshift mutation after Cre-mediated deletion of the *loxP*-flanked exon. Other allele types are also possible and have been described previously (Skarnes et al 2011).

Fore brain confined *Aak1^{flox/flox}:CamKII α -Cre* mice were created by driving Cre recombinase expression of the endogenous calcium/calmodulin-dependent protein kinase II gene (*CaMKII α*). Exon 2 of the *Aak1* gene was flanked by *loxP* sites thereby creating *AAK1^{flox}* animals.

To further investigate the molecular and cellular consequences of AAK1 depletion, an *in vitro* model was also established. *AAK1^{flox/flox}* mice were crossed with a tamoxifen-inducible CAG-Cre line (*Aak1^{flox/flox}: B6.Cg-Tg(CAG Cre/Esr1^{*}) 5Amc/J*) as previously described (Negrete-Hurtado et al 2020). The CAG promoter is a synthetic construct that combines elements from the cytomegalovirus immediate-early enhancer, the chicken β -actin promoter, and the splice acceptor of the rabbit β -globin gene. The tamoxifen-inducible CAG-Cre system consists of Cre recombinase fused to a mutant form of the mouse estrogen receptor that does

not bind to the natural ligand but is specifically activated by 4-hydroxytamoxifen (tamoxifen, Tmx). In the absence of tamoxifen, the Cre recombinase remains restricted to the cytoplasm; however, it translocates to the nucleus upon tamoxifen binding, allowing recombination to occur (Hayashi & McMahon 2002). To initiate homologous recombination in neurons from floxed animals expressing tamoxifen-inducible Cre recombinase, cultured neurons were treated with 0.2 μ M (Z)-4-hydroxytamoxifen immediately after plating. After 24 hours, cells were further treated with 0.4 μ M of tamoxifen during medium exchange. Control neurons (WT) were treated with an equivalent volume of ethanol, serving as a vehicle control for tamoxifen treatment.

Table 8: Mouse lines used in this study.

Mouse model	Manufacturer
<i>Aak1CMV:Cre</i>	Kononenko lab
<i>Aak1flox:CamKiiα-Cre</i>	Kononenko lab
<i>Aak1CAG:Cre</i>	Kononenko lab

2.2. Genotyping

2.2.1. Tissue sample and DNA extraction

For genotyping, tissue probes were taken from newborn pups at postnatal day 1-3 (tail tip) or from 3 weeks old mice (ear punches). For DNA extraction, tissue samples were incubated in 300 μ l of extraction solution (Table 9) including proteinase K overnight at 55°C on a shaker. Afterwards samples were quickly spinned down, supernatant was transferred into fresh tubes and overlaid with 400 μ l of isopropanol. After 15 minutes (min) incubation at room temperature samples were centrifuged at 13 000 rpm for 10 min. Supernatant was discarded and 300 μ l of 70% ethanol was added before another 10 min centrifugation at 13 000 rpm. Afterwards supernatant was discarded and samples were dried for at least 30-45 min at 55°C on a shaker. The pellet was then dissolved in 75 μ l of autoclaved water.

Table 9: Buffers used for genomic DNA extraction.

Buffers	Ingredients
Extraction solution	100 mM Tris-HCl pH 8.8 5 mM EDTA 0.2% SDS 200 mM NaCl 200 μ g Proteinase K

2.2.2. PCR and gel electrophoresis

To determine allele inheritance, genotyping for single genes was performed by polymerase chain. Sample DNA and mastermix were mixed according to displayed protocols (Table 11). PCR program specifications are displayed in Table 13.

Afterwards PCR samples were run on 2% agarose gels containing (Table 14) SYBR safe for 1h at constant voltage (120V). A 100 bp DNA ladder was used as a marker. Results were visualized via gel imaging system (BioRad).

Table 10: Primer sequences for genotyping.

Gene	Sequence (5' - 3')
<i>Aak1</i> WT allele	
forward	GGA GGT GAG GTA GAA GTT AGG AGC
reverse	GGA CTC TCC TTT TCC TTT CTT CTT CC
<i>Aak1</i> KO allele	
forward	GCA CAT GGC TGA ATA TCG ACG GT
reverse	ACT GAT GGC GAG CTC AGA CCA TAA C
<i>Cre</i>	
Cre_1	GAA CCT GAT GGA CAT GTT CAG G
Cre_2	AGT GCG TTC GAA CGC TAG AGC CTG T
Cre_3	TTA CGT CCA TCG TGG ACA
Cre_4	TGG GCT GGG TGT TAG CC

Table 11: PCR protocol for AAK1, Cre.

Ingredient	Volume
Sample	2 µl
DreamTaq Buffer	2 µl
25 mM MgCl ₂	2 µl
2 mM dNTPs	1.5 µl
Primer (10 mol/ µl)	0.75 µl
DreamTaq Polymerase	0.2 µl
Autoclaved water	12.55 µl

Table 12: Band size of PCR products.

Gene	Band size in base pairs (bp)	
	WT	KO
<i>Aak1</i>	415	471
<i>Cre</i>	235	326

Table 13: PCR Programs.

		<i>Aak1</i>		<i>Cre</i>	
Cycle number		36		35	
		T (°C)	Time (min)	T (°C)	Time (min)
Initial denaturation		95	4	95	5
Cyle	Denaturation	94	0.5	95	0.5
	Annealing	63.5	0.5	62	0.5
	Elongation	72	1	72	0.5
Final extension		72	7	72	5
Hold		4	∞	4	∞

Table 14: Solutions and buffers used for PCR and gel electrophoresis.

Buffers	Ingredients
2% SDS agarose gel	2% (w/v) agarose in 1x TBE
10x TBE	108g Tris-Base; 55g Boric acid; 7.4 g EDTA in 1l dH ₂ O

2.3. Primary neuronal culture

2.3.1. PDL-coating

Coverslips for imaging, dishes and plates were coated with 0.1 M poly-D-lysine (PDL) diluted in PBS by covering surface with PDL solution for 4h at 37°C. Plates and dishes were then washed 3 times with autoclaved water and dried at 37°C until no solution was left.

2.3.2. Primary cortical culture

Postnatal pups (P1-4) were decapitated, and brains were collected in Hank's + 20% fetal bovine serum (Hank's + FBS). Cortex was isolated, meninges were removed and then chopped into 600 µm small pieces (McIlwain tissue chopper, Cavey Laboratory Engineering Co. LTD). Brain tissue was washed twice with Hank's + FBS and then digested in digestion solution containing 10 mg trypsin and 1 µl DNase for 15 min at 37°C. Trypsinization was stopped by two washes with Hank's + FBS followed by two washed with Hank's. Tissue was then transferred into a dissociation solution containing 10 µl DNase, mechanically dissociated using fire-polished glass pipettes and centrifuged at 0.3 rcf for 8 min at 4°C. Supernatant was discarded, cells were dissolved in plating medium (500 µl per brain) and cell density was determined using Neubauer counting chamber. Cells were then plated at a concentration of 110000 cells per well. Cells were fed with a plating medium after 1h, when cells were attached to the PDL-coated surface. After 24 h half of the medium was replaced by

growth medium containing 2 μ M cytosine β -D-arabinofuranoside hydrochloride (AraC) and after 48 h the same volume of growth medium containing 4 μ M AraC was added to the wells. Cortical neurons were kept for 14-16 days (DIV14-16) under constant conditions at 37°C / 5% CO₂.

2.3.3. Transfection of primary neuronal culture

Neurons were transfected at DIV 7–9 days using an optimized calcium phosphate protocol with Calcium Phosphate transfection kit (Promega ProFectin® Mammalian Transfection System). For this 6 μ g plasmid DNA, 250 mM CaCl₂ and water (for each well of a 6-well plate) were mixed with equal volume of 2 \times HEPES buffered saline (100 ml) and incubated for 20 min allowing for precipitate formation, while neurons were starved in NBA medium for the same time at 37 °C, 5% CO₂. Precipitates were added to neurons and incubated at 37 °C, 5% CO₂ for 25-30 min. Finally, neurons were washed twice with HBSS medium and transferred back into their conditioned medium. Transfected neurons were analyzed 5-7 days post transfection.

Table 15: Solutions used for primary cortical culture.

Name	Composition
Basic media	1 l DMEM; 5 g glucose; 200 mg NaHCO ₃ ; 100 mg transferrin
Digestion solution	dH ₂ O; 137 mM NaCl; 5 mM KCl; 7 mM Na ₂ HPO ₄ ; 25 mM HEPES (pH=7.2)
Dissociation solution	Hank's; 12 mM MgSO ₄ .x7H ₂ O
Growth medium	100 ml basic medium; 5 ml FBS; 10 mM glucose; 0.25 ml GlutaMAX; 2 ml B27; 1 mM sodium pyruvate; 1 ml Penicillin/ Streptomycin (P/S)
Hank's	500 ml HBSS; 5 ml sodium pyruvate; 5ml HEPES; 5 ml P/S (pH=7.4)
Hank's + FBS	Hank's; 20% (v/v) fetal bovine serum (FBS)
Plating medium	100 ml basic medium; 10 ml FBS; 10 mM glucose; 1 ml GlutaMAX; 625 μ l insulin, 1.1 ml P/S

2.3.4. Transferrin488 uptake assay in cultured neurons

Neuronal media removed from the wells and replaced by osmolarity adjusted, warm neurobasal media (NBA) (1mL/well for 6 well plate). Neurons were starved in 37°C 5% CO₂ for an hour.

15 μ g/mL Alexa 488 Transferrin from 5mg/mL stock was added to the wells and incubated in 37°C 5% CO₂ for 25 minutes. After incubation cells washed with warm osmolarity adjusted NBA 3 times and fixed with 4% PFA + Sucrose in RT for 15 min. Immunocytochemistry protocol followed after fixation.

2.3.5. Starvation and BafA1 treatment in cultured neurons

Cultured neurons were incubated with Earle's Balanced Salt Solution (EBSS) as starvation media, BafA1 (10 nM), and EBSS + BafA1 (10 nM) for 4 hours at 37°C and 5% CO₂. Neuronal media was used as the control (basal condition). After incubation, cells were harvested for protein extraction and immunoblotting.

2.3.6. Live imaging of cultured neurons

Neurons were imaged on DIV 16-19 (or at DIV 6 in Supplementary Fig. 2x) at 37 °C in imaging buffer (170 mM NaCl, 3.5 mM KCl, 0.4 mM KH₂PO₄, 20 mM N-Tris[hydroxyl-methyl]-methyl-2-aminoethane-sulphonicacid (TES), 5 mM NaHCO₃, 5 mM glucose, 1.2 mM Na₂SO₄, 1.2 mM MgCl₂, 1.3 mM CaCl₂, pH 7.4) using Zeiss Axiovert 200 M microscope (Observer. Z1, Zeiss, USA) equipped with 63x/1.40 Oil DIC objective, a pE-4000 LED light source (CoolLED) and a Hamamatsu Orca-Flash4.0 V2 CMOS digital camera. Time-lapse images of neurons expressing EB3-Tdtomato and LC3B-RFP were acquired every second using Micro-Manager software (Micro-Manager1.4, USA) for 40 s. Kymographs were generated using the software KymoMaker and analyzed by ImageJ. To analyze the number and velocity of EB3 comets and autophagosomes (LC3B-RFP), neurites were selected from individual neurons and the number of comets/μm was quantified manually from the kymographs.

2.4. Ex vivo acute slices

Mice were sacrificed at the age of three months via cervical dislocation and brains were isolated. Cortex was separated and cut with a vibratome (Leica) into 100 μm horizontal sections in ice-cold, carbogen-saturated (95% O₂ and 5% CO₂) high-Ca²⁺artificial cerebrospinal fluid (ACSF).

Table 16: Composition of artificial cerebrospinal fluid (ACSF).

	High-Ca²⁺ ACSF
osmolarity adjusted between 310 and 330 milliosmoles, pH = 7,4	
NaCl (58,44 g/mol)	125 mM
KCl (74,56 g/mol)	2.5 mM
Sodium phosphate buffer (0,4 M)	1.25 mM
NaHCO ₃ (84,01 g/mol)	25 Mm
Glucose (180,16 g/mol)	25 mM
CaCl ₂ (219,09 g/mol)	1 mM

MgCl ₂ (203,3 g/mol)	2 mM
---------------------------------	------

2.4.1. Starvation and chloroquine treatment in acute slices

Cortical ex vivo acute slices were incubated in control/basal medium, control medium with 400 μ M chloroquine, ACSF or ACSF with chloroquine for 6h at 37°C and 5% CO₂. Afterwards samples were shock frozen in liquid nitrogen and stored at -80°C until further processing via immunoblotting.

Table 17: Control/basal medium for acute slices.

Name	Composition
Control/basal medium	MEM; 0.00125% ascorbic acid; 10 mM D-glucose; 1 mM GlutaMAXX; 20% (v/v) horse serum; 0.01 mg/ml insulin; 14.4 mM NaCl; 1% P/S

2.4.2. AAK1 inhibitor SGC-AAK1-1 treatment in acute slices

Cortical acute slices were incubated with an ATP-competitive kinase inhibitor (SGC-AAK1-1) against AP2-associated protein kinase 1/AAK1 and BMP-2-inducible protein kinase/BIKE/BMP2K. SGC-AAK1-1 downregulates cellular AP-2 μ Thr156 phosphorylation level in a dose-dependent manner (EC_{max} ~12.5 μ M). Acute slices were treated 12.5 μ M SGC-AAK1-1 (catalog number, Sigma SML2219) or SGC-AAK1-1N (catalog number, Sigma SML2220) for 4 hours as kinase inhibitor and negative control respectively.

2.4.3. Synaptosome isolation from cortex and acute slices

Synaptosomes were isolated from cortical tissue following the manufacturer's protocol (Thermo Scientific™ Syn-PER™ Synaptic Protein Extraction Reagent, Catalog number 87793). Briefly, cortical tissue (150-200 mg) was homogenized on ice in Syn-PER reagent supplemented with protease/phosphatase inhibitors using a Dounce tissue grinder (15 slow strokes). The homogenate was centrifuged at 1200 x g for 10 minutes at 4°C. The supernatant was transferred to a new tube, and a portion was saved for analysis if necessary. The supernatant was then centrifuged at 15,000 x g for 20 minutes at 4°C. The supernatant was retained as the cytosolic fraction, and the pellet was resuspended in 500 μ L of freshly prepared Syn-PER reagent. Protein concentrations were determined using the Bradford assay (Sigma) for downstream analyses.

2.4.4. Plasma membrane protein extraction from synaptosomes

Plasma membrane proteins were extracted from synaptosomes using the Abcam Plasma Membrane Protein Extraction Kit (Catalog number ab65400), following the manufacturer's protocol. Briefly, synaptosomes were homogenized in homogenization buffer supplemented with a protease/phosphatase inhibitor mix (1.5 mL mix per 30-50 mg of synaptosomes). To ensure consistent homogenization and minimize sample variability, syringes with a 26G opening were used, and the homogenate was passed through three times. The homogenate was then transferred to multiple 1.5 mL microcentrifuge tubes and centrifuged at 700 x g for 10 minutes at 4°C. The supernatant was collected, and the pellet discarded. The collected supernatant was further centrifuged at 10,000 x g for 30 minutes at 4°C. After this step, the supernatant was designated as the cytosolic fraction, while the pellet was retained as the total cellular membrane (TCM) fraction, which contains proteins from both the plasma membrane and the membranes of cellular organelles.

The TCM pellet was resuspended in 200 µL of the upper phase solution, and an additional 200 µL of the lower phase solution was added on top. The mixture was vortexed thoroughly and incubated on ice for 5 minutes. After incubation, the tubes were centrifuged at 3500 rpm (approximately 1100 x g) for 5 minutes at 4°C, and the upper phase was carefully transferred to a new tube. To maximize protein yield, 100 µL of the upper phase solution was added back to the lower phase of the original tube, mixed well, and centrifuged again at 3500 rpm (1100 x g) for 5 minutes at 4°C. The upper phase from this step was carefully collected and combined with the previously collected upper phase.

The combined upper phase was further extracted by adding 100 µL of the lower phase solution, mixed thoroughly, and centrifuged at 1100 x g for 5 minutes at 4°C. The resulting upper phase was carefully collected, diluted in five volumes of water, and incubated on ice for 5 minutes. Following this incubation step, the tube was spun at maximum speed for 10 minutes at 4°C. The supernatant was removed, and the pellet, containing the plasma membrane proteins, was stored at -80°C for further analysis.

2.5. Animal behavior

2.5.1. Open field

The open field (OF) test was developed to assess general locomotor activity levels, anxiety and willingness to explore an unknown environment (Denenberg 1969, Stanford 2007). The OF experiment was performed in a white painted square box (50 x 50 x 40 cm), illuminated with >20lux. Mice were monitored by a digital camera placed above the arena, connected to a video tracking system (EthoVision®XT, Noldus). The animals were taken into the behavioral room at least 30min before test session to minimize the stress. Animals were placed

individually in the box and recorded for 5 min in a quiet environment. Before and after the testing, the box was always cleaned with water and 70% ethanol, followed by a waiting period of at least 10 min. Males were always tested first.

2.5.2. Beam walk

To assess motor coordination and balance alterations animals were subjected to beams of different widths to determine how limbs are coordinated during self-paced locomotion in 1) unperturbed (25 mm beam), 2) mildly challenging (12 mm beam) and 3) stability-perturbed (5 mm beam) conditions. In three consecutive days animals were subjected to one of the beams starting with the widest one at 25 mm. Animals were instructed to cross each beam three times and their performance was recorded. The number of slips per run for each beam was quantified. Step cycles were defined as initiation of swing to end of stance, and manually annotated.

2.5.3. Rotarod

In order to analyze motor coordination animals were subjected to the Rotarod test. First animals were acclimated to the behavioral room for some minutes prior to the test. The first two consecutive days animals were trained to balance themselves on top of the rotating rod (TSE system) for 5 minutes at a constant speed of 4 rpm. The actual experiment was performed on day three. Animals had to walk on the rod with a starting speed of 4 rpm and a constant acceleration up 40 rpm to a maximum of 300 seconds. Three individual runs per mouse were performed. For each mouse and run, the latency to fall from the rod was recorded and used as a readout.

2.5.4. Echo-MRI body composition analysis

The body composition of 3-month-old AAK1 KO and AAK1 cKO mice and control littermates was measured using an EchoMRI-100H Body Composition Analyzer (EchoMRI®). The whole-body masses of fat, lean, free water and total water were measured. Mice were placed in an animal holder and measures were taken 3 times per mouse, for a duration of 0.5-3.2 min each. The measurements were then averaged between the 3 runs and shown as percentage of body weight.

2.6. Histology methods

2.6.1. Perfusion

Adult mice were anesthetized (i.p., 10 µl per 10 g body weight) before transcardial perfusion with prewarmed saline solution (0.85% NaCl, 0.025% KCl, 0.02% NaHCO₃, pH 6.9, 0.01% heparin) to 37°C, followed by fixative of choice. Brains were isolated and post-fixed in the same fixative solution for 24 hours at 4°C. For long-term storage brains were stored in a mixture of 20% (v/v) glycerol and 2% (v/v) dimethylsulfoxide (DMSO) in 0.4 M PB phosphate buffer for cryoprotection. Horizontal free-floating sections (40 µm) were obtained at a microtome and stored at -80°C until further use. For stainings corresponding sections from littermates were used.

Table 18: Solutions and reagents used for perfusion.

Buffer	Ingredients
Anesthetic	PBS; 100 mg/ml Ketamine hydrochloride; 20 mg/ml Rompun (Xylazin)
DMSO for brain	46.75 ml H ₂ O; 2 ml DMSO; 25.5 ml glycerol; 31.25 ml 0.4M PB
PFA	PBS; 4% (w/v) PFA; pH=7.4
Glutaraldehyde/ PFA	0.1M Cacodylate buffer; 2.5% (w/v) Glutaraldehyde; 2% (w/v) PFA

2.6.2. Immunohistochemistry

For immunohistochemistry (IHC) 3- and 12-weeks old animals were perfused, and brains were post-fixed in ice-cold freshly depolymerized 4% (w/v) PFA in PBS. 40 µm horizontal free-floating sections were used for this purpose. All the following steps were performed with constant shaking. Sections were rinsed twice in PBS for 5 min and afterwards permeabilized and blocked in 10% normal goat serum (NGS) or 10% normal donkey serum (NDS) in 0.5 % Triton-X in PBS (PB-T) for 1 h at room temperature (RT). Primary antibodies were incubated in 3 % NGS or NDS in 0.3% PB-T for 48 hours at 4°C followed by three washes in 0.3% PB-T for 10 min at RT. Secondary fluorescently labeled antibodies and DAPI were incubated in 3% NGS or NDS in 0.3% PB-T for 2h at RT protected from light. Sections were then washed twice in PBS and mounted on gelatin-coated glass slides.

Images were acquired at the Leica SP8 and Zeiss Airy Scan confocal at a resolution of 1024x1024 pixels and visualized using Fiji (ImageJ). Mean gray values were used as fluorescence readout of protein levels after background subtraction. If otherwise stated, fluorescence levels were normalized to WT levels and used for statistical analysis.

Table 19: Primary antibodies used for immunohistochemistry.

Antibody	Concentration	Manufacturer	Catalog number
ATG9A	1:500	Abcam	ab108338

Calbindin	1:500	Novus Biologicals	NBP2-50028
GFAP	1:500	Sigma	G3893
GFP	1:1000	Abcam	ab13970
Tbr1	1:300	Novus Biologicals	NB110-39113SS
Doublecortin	1:500	Abcam	ab18723
Nestin	1:500	Novus Biologicals	NB100-16074
VGLUT1	1:300	SySy	135304
GabarapL1	1:300	Abcam	ab86497
α -Tubulin	1:1000	Synaptic Systems	302 211
Delta-2 Tubulin	1:300	Abcam	302213
Acetylated tubulin	1:300	Cell signalling	5335
NeuN	1:500	Abcam	ab104224
AP-2 α	1:1000	BD	610502
MAP2	1:500	SySy	188-004
Neurofilament H	1:500	SySy	171106

Table 20: Secondary antibodies used for immunohistochemistry.

Antibody target	Dilution	Manufacturer	Catalog number
Alexa Fluor 488 Goat Anti-Chicken IgG	1:500	Life Technologies GmbH	A11039
Alexa Fluor 488 Goat Anti-Rabbit IgG	1:500	Life Technologies GmbH	A11034
Alexa Fluor 488 Goat Anti-Guinea Pig IgG	1:500	Life Technologies GmbH	A11073
Alexa Fluor 488 Goat Anti-Mouse IgG	1:500	Life Technologies GmbH	A11029
Alexa Fluor 568 Goat anti-rabbit IgG	1:500	Life Technologies GmbH	A11011
Alexa Fluor 647 Goat Anti-Guinea Pig IgG	1:500	Life Technologies GmbH	A21450
Alexa Fluor 647 Goat Anti-Rabbit IgG	1:500	Life Technologies GmbH	A21245
Alexa Fluor 647 Goat Anti-Mouse IgG	1:500	Life Technologies GmbH	A21236

2.6.3. Cresyl-violet (Nissl) staining

For cresyl-violet staining 40 μ m horizontal sections were mounted on “super-frost plus” glass slides and dried overnight. Sections were hydrophilized in water for 1 min before incubation in cresyl-violet solution for 7 min. Sections were then washed three times in water for 2 min before being dehydrated in ascending ethanol solutions (70%, 80%, 90%, 96%, 100%) for 2 min in each solution. Afterwards, sections were incubated in xylene for at least 2 min and then covered with mounting solution Entellan [®] (Merck). Images were acquired at a S360

Hamamatsu slide scanner using a 40x objective. Aperio Scope image viewing software was used to analyze the volume of cortex and thickness of corpus callosum.

2.6.4. Electron microscopy

For electron microscopy (EM) perfused animals with 2% Formaldehyde (Science Services, München, Germany) and 2.5% Glutaraldehyde (Merck, Darmstadt, Germany) in 0.1M Cacodylate buffer, at the age of 8-9 weeks were used. Brain was removed and fixed overnight in the same fixative. 50 µm horizontal vibratome sections were prepared and the region of interest was extracted using a biopsy punch (2mm diameter). Post fixation was applied using 1% Osmiumtetroxid (Science Services, München, Germany) and 1% Potassium hexacyanoferrat (Merck, Darmstadt, Germany) for 30 min at 4°C. After 3x5min wash with ddH₂O, samples were dehydrated using ascending ethanol series (50%, 70%, 90%, 100%) for 10 min each. Infiltration was carried out with a mixture of 50% Epon/ethanol for 1h, 70% Epon/ethanol for 2h and overnight with pure Epon (Merck, Darmstadt, Germany). After fresh Epon for 4h, vibratome sections were mounted onto empty epon blocks and covered with Aclar foil. After 48h hardening at 60°C, Aclar foil was removed and samples were trimmed to the region of interest. Ultrathin sections (70nm) were cut using a diamond knife (Science Service, München, Germany) on an UC6 ultramicrotome (Leica, Wetzlar, Germany) and collected onto pioloform coated slot grids. Post staining was performed with 1.5 % uranyl acetate (Agar Scientific, Stansted, United Kingdom) for 15 min and Reynolds lead citrate (Roth, Karlsruhe, Germany) solution for 3 min.

Images were acquired using a JEM-2100 Plus Transmission Electron Microscope (JEOL, Tokio, Japan) operating at 80kV equipped with a OneView 4K camera (Gatan, Pleasanton, USA). EM quantifications were carried out manually on acquired images with 20000K magnification of synapses. Number of synaptic vesicles, autophagosomes, clathrin coated vesicles and mitochondria were counted and normalized to the total area of the synapse. Additionally, the total area of single mitochondria and the total length (perimeter) of the corresponding cristae was analyzed. Cristae length was then normalized to the total area of mitochondria.

2.7. Immunoblot

2.7.1. Tissue preparation and lysis

Mice were sacrificed at the age of one, three and 12 months via cervical dislocation. Brains were isolated, individual brain regions were separated, shock frozen in liquid nitrogen and stored at -80°C until further use.

Samples were homogenized in RIPA buffer containing protease inhibitor (Roche) and phosphatase inhibitor (ThermoScientific) using a Wheaton otter-Elvehjem Tissue Grinder. Afterwards samples were sonicated (10 pulses), incubated on ice for 45 min and centrifuged at 13 000 rpm for 15 min at 4°C. Supernatants were transferred into fresh tubes and protein concentrations were assessed using Bradford assay (Sigma). Samples were then mixed with Lämmli buffer and boiled for 95°C for 5 min.

2.7.2. SDS-PAGE and immunoblotting

Depending on the assay, 10-20 µg protein per sample were loaded onto SDS-page gels for protein separation and then transferred onto nitrocellulose or methanol-activated PVDF membranes via full-wet transfer assay (BioRad) or semi-wet transfer. Protein transfer was confirmed by Ponceau S staining. Membranes were blocked in 5% milk or bovine serum albumin (BSA) in TBS containing 1% Tween (TBS-T) for 1h at RT followed by primary antibody incubation in TBS overnight at 4°C. Afterwards, membranes were washed three times with TBS-T for 10 min and then incubated with HRP-tagged secondary antibodies for 1h at RT followed by three washes in TBS-T for 10 min at RT. Protein levels were visualized using ECL-based autoradiography film system (Super RX-N, Fujifilm) and analyzed using Gel Analyzer plugin from ImageJ (Fiji). Protein levels were always first normalized to loading control and to WT control.

Table 21: Settings for protein transfer onto membranes.

	Full-wet transfer	Semi-wet transfer
Constant Current	75 V	280 mA
Time for run	90 min	35 min

Table 22: List of buffers used in SDS-PAGE and western blot analysis.

Buffer	Ingredients
1.5 M Tris pH=8.8	181.65g Tris Base; 0.4% (w/v) SDS; 1L ddH ₂ O
0.5 M Tris pH=6.8	6g Tris Base; 0.4% (w/v) SDS; 100 mL ddH ₂ O; pH 6.8
Ponceau S	200 ml dH ₂ O; 0.6 g Ponceau S; 6 ml acetic acid
Resolving gel	dH ₂ O; 1.5 M Tris; 30% Acrylamide; 10% APS; TEMED
Running buffer	H ₂ O; 192mM Glycine ; 25mM Tris-Base; 0.1% (w/v) SDS
Stacking gel	dH ₂ O; 0.5 M Tris; 30% Acrylamide; 10% APS; TEMED

Buffer	Ingredients
1.5 M Tris pH=8.8	181.65g Tris Base; 0.4% (w/v) SDS; 1L ddH ₂ O
0.5 M Tris pH=6.8	6g Tris Base; 0.4% (w/v) SDS; 100 mL ddH ₂ O; pH 6.8
Ponceau S	200 ml dH ₂ O; 0.6 g Ponceau S; 6 ml acetic acid
Resolving gel	dH ₂ O; 1.5 M Tris; 30% Acrylamide; 10% APS; TEMED
TBS 10x	1l dH ₂ O; 88g NaCl; 24 g Tris Base
Transfer buffer	H ₂ O; 192mM Glycine ; 25mM Tris-Base; 0.025% (w/v) SDS

Table 23: List of antibodies used for western blot analysis.

Antibody target	Dilution	Manufacturer	Catalog number
AAK1	1:1000	Cell Signalling	798325
α -Tubulin	1:5000	Synaptic Systems	302 211
β -Actin	1:3000	Sigma	A-5441
AP-2 α	1:1000	BD	610502
AP-2 μ	1:1000	BD	611350
AP-2 μ pT156	1:1000	Abcam	ab109397
ATG9A	1:1000	Abcam	ab108338
ATG5	1:1000	Abcam	ab108327
CHC	1:1000	Homobrew	
MARK2	1:1000	Proteintech	15492-1-AP
Vinculin	1:1000	Abcam	ab129002
LC3B	1:1000	Novus Biologicals	NB600-1384
ATG13	1:1000	Arigo (Biomol GmbH)	ARG55122
GABARAPL1	1:1000	Abcam	ab86497
p62	1:1000	Progen	GP62-C
CDH1	1:1000	BD	
SYT1	1:1000	SySy	105011
ATG16L	1:1000	Cell Signaling	8089
PSD95	1:1000	Synaptic systems	124011
Calbindin	1:1000	Novus Biologicals	NBP2-50028
NBR1	1:1000	Santa Cruz Biotechnology	sc-130380

Table 24: Secondary antibodies used for western blot analysis.

Antibody target	Dilution	Manufacturer	Catalog number
Rabbit anti-Mouse IgG (H+L) peroxidase-conjugated	1:10 000	Sigma	A9044

Goat anti-Rabbit IgG (H+L) peroxidase-conjugated	1:10 000	Sigma	A0545
Goat anti-Guinea Pig IgG (H+L) peroxidase-conjugated	1:5 000	Jackson Immuno Research	106-035-003
Rabbit anti-Chicken IgG (H+L) peroxidase-conjugated	1:5 000	Millipore	AP162P

2.8. Proteomic and phosphoproteomic

2.8.1. Immunoprecipitation and mass spectrometry analysis of AAK1-binding partners

For immunoprecipitation experiments, 20 µl of Dynabeads Protein G (Thermo Fisher Scientific) were coated with 2 µg of an antibody targeting the protein of interest, with the corresponding IgG used as a negative control. To prepare the beads, the storage solution was replaced with 100 µl of PBS, followed by the addition of 2 µg of the antibody. The beads were incubated with the antibody for 2–3 hours at 4°C on a shaker, and then washed once with 200 µl of PBS to remove any unbound antibodies. Wild-type brain cortices were dissected and homogenized using a Wheaton Potter-Elvehjem Tissue Grinder in Co-Immunoprecipitation (Co-IP) buffer (50 mM Tris-HCl, pH 7.4, 1% NP-40/Igepal, 100 mM NaCl, 2 mM MgCl₂), supplemented with a Protease Inhibitor Cocktail (Complete Mini, Roche) and Phosphatase Inhibitor (ThermoScientific). Lysates were sonicated, incubated on ice for 45 minutes, and then centrifuged at 13,000 x g for 20 minutes at 4°C. Protein concentrations were determined using the Bradford assay (Sigma). Equal amounts of protein were incubated overnight at 4°C with beads coated with antibodies specific to the protein of interest and control IgG.

The following day, the lysates were removed, and the beads were washed three times with Co-IP buffer. The beads were then resuspended in 20 µl of Co-IP buffer and 20 µl of 4x SDS buffer and boiled at 95°C for 5 minutes. Subsequently, the gel digestion method was applied. Samples were loaded onto SDS-PAGE gels, followed by reduction with dithiothreitol (DTT) and alkylation with chloroacetamide (CAA). Proteins were digested overnight at 37°C using trypsin. The resulting peptides were extracted and purified using Stagetips (see detailed protocol below).

2.8.2. Proteom and phosphoproteom analysis of AAK1 KO cortex and synaptosomes

Experiments were performed with AAK1 WT/KO age of 3-week-old cortex tissue and 3-month-old cortical synaptosome fraction separately. Cortices / synaptosomes were homogenized in 8M UREA buffer supplemented with protease/phosphatase inhibitors by using a Wheaton Potter-Elvehjem Tissue Grinder (VWR). The lysates were sonicated and centrifuged at 13000 rpm for 10 min. Protein concentration was assessed using Pierce™ 660nm Protein Assay Reagent (Thermo Scientific™) and 1 mg protein of each sample taken for the experiment. The samples were pre-digested in 5 mM TCEP, 27.5 mM CAA and LysC, in an enzyme:substrate ratio of 1:200 for 4 hours at RT after vortexing. Afterwards, the samples were diluted to a concentration of 2 M Urea using 50 mM ABC buffer. Trypsin was added to an enzyme:substrate ratio of 1:100 for overnight digestion at RT. The next day, desalting and phosphopeptide enrichment were performed.

Desalting and phosphopeptide enrichment

The next day, after Trypsin digestion, the samples were acidified with TFA (1:100 [v/v]) before 10 min centrifugation. Desalting of the samples was performed with 50 mg C18 SepPak®Vac cartridges (Waters™). Therefore, the columns were activated with 2 mL 100% CAN and washed three times with 1 mL 0.1% TFA before loading samples. Samples were washed three times with 1 mL 0.1% TFA prior to elution with 0.6 mL elution buffer (60% ACN, 0.1% TFA). 30µg of the sample were taken, desalted and stored in -20 for total proteome analysis before the remaining sample was dried in a vacuum concentrator. TiO₂ Phosphopeptide extraction was performed using the High-Select™ TiO₂ Phosphopeptide Enrichment Kit (Thermo Scientific™) following the manufacturers' instructions. In brief, a lyophilized peptide sample was resuspended in 150 µL Binding/Equilibration Buffer, columns prepared using 20 µL Wash Buffer followed by 20 µL Binding/ Equilibration Buffer. The samples were run twice through the column before the column was washed with 20 µL Binding/ Equilibration Buffer followed by 20 µL Wash Buffer. Afterwards, the columns were washed with 20 µL of LC-MS grade water before the phosphopeptides were eluted from the column in 50 µL Phosphopeptide Elution Buffer. Samples were dried immediately using a vacuum concentrator and subsequently resuspended in 15 µL resuspension buffer (5% FA and 2% ACN). Phosphopeptide samples were stored at -20°C until measurement.

Table 25: Reagents and solutions used for protein extraction for proteomics analysis.

Buffer	Ingredients
Buffer A	dH ₂ O; 0.1% (v/v) formic acid
Buffer B	80% acetonitril; 0.1% (v/v) formic acid
Chloroacetamide (CAA)	550 mM stock CAA
Dithiothreitol (DTT)	100 mM DTT stock

Formic acid (FA)	dH ₂ O; 10%; (v/v) formic acid
Lysyl Endopeptidase (LysC)	0.5 µg/µl LysC
Methanol	100%
Triethylammoniumbicarbonate	50 mM TEAB
Trypsin protease	1 µg/µl Trypsin
Urea buffer	50 mM TEAB; 8M Urea; 50x Protease inhibitor

2.8.3. Proteom analysis of HEK293T TurboID-PM cells

For both Western blotting and proteomic analysis, HEK293T cells stably expressing the TurboID-PM (N-terminal Lyn11 tag – GCIKSKGKDSA (Inoue et al 2005)) fusion construct (*generous gift from Jan Riemer Lab, cell line prepared by Sarah Gerlich*) were cultured in 15-cm dishes for 18-24 hours, reaching approximately 90% confluency. The next day, the cells were washed once with PBS. TurboID expression was induced by supplementing 10 mL of complete media (DMEM + 10% dialyzed FBS + 1% P/S) with 30 µg/mL Cumate for 17 hours. Two hours before biotin labeling, an AAK1 inhibitor or a control analog was applied at a final concentration of 12.5 µM to inhibit AAK1 kinase function. For biotin labeling, the media was replaced with fresh media containing 50 µM biotin, and the cells were incubated for 10 minutes.

After incubation, the plates were placed on ice and washed twice with cold PBS to remove unbound biotin. The cells were then scraped off in 5 mL of PBS and transferred into fresh tubes. The tubes were centrifuged at 700 x g for 3 minutes at 4°C, and the supernatant was discarded. The resulting pellet was resuspended in 200 µL of denaturing IP lysis buffer without Triton X-100 (30 mM Tris-HCl pH 8.1, 100 mM NaCl, 5 mM EDTA) and transferred into a 2 mL safe-lock tube. Fifty microliters of 8% SDS was added, and the tube was inverted. The tubes were boiled for 15 minutes at 95°C and sonicated at maximum amplitude ~15 times (until the samples were no longer viscous). Subsequently, 350 µL of denaturing IP lysis buffer containing 2.5% Triton X-100 was added, and the mixture was incubated on ice for 1 hour.

Bead Preparation:

While the samples were incubating, streptavidin beads were prepared. For each 15-cm dish, 40 µL of streptavidin bead slurry (Thermo Scientific Pierce High-Capacity Streptavidin Agarose, catalog number #20359) was used. The bead slurry was washed three times with NaPO₄ buffer and centrifuged for 1 minute at 2000 x g at 4°C. The beads were divided into fresh tubes in NaPO₄ buffer after washing.

After the 1-hour incubation of the cell lysates, the tubes were centrifuged at 22,000 x g for 1 hour at 4°C. The supernatant was transferred into a fresh tube and mixed with 400 µL of NaPO₄

buffer. The lysates were added to the prepared beads and incubated overnight at 4°C with gentle tumbling.

The following day, the beads were washed five times with NaPO₄ buffer. After washing, the standard proteomics protocol was applied, as detailed below. Briefly, 50 µL of 8 M urea was added to the beads, followed by 2.5 µL of DTT (from a 100 mM stock solution), and incubated for 30 minutes at room temperature (RT). Next, 5 µL of CAA (from a 550 mM stock) was added, and the mixture was incubated for 20 minutes at RT in the dark. For enzymatic digestion, 1 µL of LysC (0.5 µg/µL) was added, and the samples were incubated for 3 hours at RT. The samples were then diluted with 150 µL of 50 mM TEAB buffer to bring the urea concentration down to 2 M. Finally, 0.5 µL of trypsin (1 µg/µL) was added, and the samples were incubated overnight at RT.

Stage-Tip Protocol:

The next day, the stage-tip protocol was applied as described in detail below, with specific steps adjusted for bead handling. The digestion was stopped by acidifying the samples with 100% formic acid (FA) to a final concentration of 1% (2 µL). The samples were centrifuged for 10 minutes at 500 x g, and the supernatant was transferred into a fresh tube and centrifuged again for 5 minutes at 500 x g. The final supernatant was transferred into a new tube. Before loading the samples into stage tips, SDB-RPS stage tips were equilibrated with washes once in methanol, buffer B and twice buffer A, each time followed by centrifugations at 2 600 rpm for 1-2 min. Afterwards, samples were loaded onto StageTips. Samples were centrifuged at 2 600 rpm for 5 min, StageTips were washed with buffer A and centrifuged at 2 600 for 3 min. Then StageTips were washed twice with buffer B and each time centrifuged at 2 600 for 3 min. After the last centrifuge and washing stage tips completely dried with syringe and were submitted to CECAD proteomics facility for further processing.

2.8.4. Data Acquisition for proteom and phosphoproteom

All samples were analyzed by the CECAD proteomics facility on a Q Exactive Plus Orbitrap mass spectrometer that was coupled to an EASY nLC (both Thermo Scientific). Peptides were loaded with solvent A (0.1% formic acid in water) onto an in-house packed analytical column (50 cm, 75 µm inner diameter, filled with 2.7 µm Poroshell EC120 C18, Agilent). Peptides were chromatographically separated at a constant flow rate of 250 nL/min using the following gradient: 3-5% solvent B (0.1% formic acid in 80 % acetonitrile) within 1.0 min, 5-30% solvent B within 121.0 min, 30-40% solvent B within 19.0 min, 40-95% solvent B within 1.0 min, followed by washing and column equilibration. The mass spectrometer was operated in data-dependent acquisition mode. The MS1 survey scan was acquired from 300-1750 m/z at a

resolution of 70,000. The top 10 most abundant peptides were isolated within a 1.8 Th window and subjected to HCD fragmentation at a normalized collision energy of 27%. The AGC target was set to 5e5 charges, allowing a maximum injection time of 55 ms (whole proteome) or 110 ms (phospho proteome), respectively. Product ions were detected in the Orbitrap at a resolution of 17,500 (whole proteome) or 35,000 (phospho proteome). Precursors were dynamically excluded for 25.0 s.

2.8.4.1. Sample Processing

All mass spectrometric raw data were processed with Maxquant (version 2.4.0.0,) (Tyanova, Temu & Cox 2016) using default parameters against the murine canonical database (UP0589, downloaded 04.01.2023) with the match-between-runs option enabled between replicates. For the phospho proteome dataset, phosphorylation (STY) was added as a variable modification. Follow-up analysis was done in Perseus 1.6.15 (Tyanova et al 2016). Hits from the decoy database, the contaminant list and those only identified by modified peptides were removed. Afterwards, results were filtered for data completeness in replicates groups and LFQ values imputed using sigma downshift with standard settings. Finally, FDR-controlled T-tests between sample groups were performed with $s_0 = 0.2$.

2.8.5. Data Acquisition for IP and Turboid samples

All samples were analyzed by the CECAD proteomics facility on a Q Exactive Plus Orbitrap mass spectrometer that was coupled to an EASY nLC (both Thermo Scientific). Peptides were loaded with solvent A (0.1% formic acid in water) onto an in-house packed analytical column (50 cm length, 75 μm inner diameter, filled with 2.7 μm Poroshell EC120 C18, Agilent). Peptides were chromatographically separated at a constant flow rate of 250 nL/min using the following gradient: initial 3 % solvent B (0.1% formic acid in 80 % acetonitrile), 3-5% B within 1.0 min, 5-30% solvent B within 65.0 min, 30-50% solvent B within 13.0 min, 50-95% solvent B within 1.0 min, followed by washing and column equilibration. The mass spectrometer was operated in data-dependent acquisition mode. The MS1 survey scan was acquired from 300-1750 m/z at a resolution of 70,000 and 20 ms maximum injection time. The top 10 most abundant peptides were isolated within a 1.8 Th window and subjected to HCD fragmentation at a normalized collision energy of 27%. The AGC target was set to 5e5 charges, allowing a maximum injection time of 110 ms. Product ions were detected in the Orbitrap at a resolution of 35,000. Precursors were dynamically excluded for 10.0 s.

2.8.5.1. Sample Processing

All mass spectrometric raw data were processed with Maxquant (version 2.0.3.0.) (Tyanova, Temu & Cox 2016) using default parameters against the Uniprot canonical murine database (UP0589, downloaded 04.01.2023) with the match-between-runs option enabled between replicates. Follow-up analysis was done in Perseus 1.6.15 (Tyanova et al 2016). Protein groups were filtered for potential contaminants and insecure identifications. Remaining IDs were filtered for data completeness in at least one group and missing values imputed by sigma downshift (0.3 σ width, 1.8 σ downshift). Afterwards, FDR-controlled two-sided t-tests were performed.

2.9. Statistical analysis

Statistical analysis was carried out using GraphPad Prism (9.5.1). Unpaired Student's t-test analysis was performed for two group comparisons. One-tailed Student's t-test analysis was performed for two group comparisons, after values were normalized to WT levels.

For comparisons with more than two groups, one-way ANOVA followed by a Holm-Sidak post hoc test was applied. Two-way ANOVA was used for comparison of two groups and two independent variables followed by Holm-Sidak post hoc test for multiple comparisons.

P values of less than 0.05 were considered statistically significant. Data are reported as mean values \pm standard error of the mean (SEM).

Pathway analysis of proteomic approaches was performed using ShinyGO 0.81 (South Dakota State University; Ge, Jung and Yao, 2020).

IV. Results

1. AAK1 expression differs in region and age in mouse brain

To investigate whether AAK1 expression varies across brain regions, we performed immunoblot analysis in 6-week-old WT mice. Understanding regional expression patterns of AAK1 is essential, as differential expression may indicate region-specific functions, particularly relevant to neural processes involved in cognition and neuroplasticity. Western blot results (Fig. 7A) showed that AAK1 protein levels are significantly elevated in the cortex (CX) compared to other regions, including the hippocampus (HP), striatum (ST), cerebellum (CB), hindbrain (HB), and midbrain (MB). Quantification of immunoblot (Fig. 7C) confirmed that AAK1 is most abundantly expressed in the cortex, with statistically significant differences between the cortex and all other regions analyzed. This cortical enrichment suggests that AAK1 may play a pivotal role in cortical-specific processes, potentially influencing synaptic regulation and plasticity, which are critical for higher-order cognitive functions.

The expression level of AAK1 in the cortex also showed a clear developmental trend. Immunoblot analysis across different ages (Fig. 7B) reveals that AAK1 levels increase from postnatal day 7 (p7) to 3 months, reaching a peak at 3 months. After this peak, there is a decline in AAK1 expression at 12 months, indicating an age-dependent modulation of AAK1 levels. Quantification of western blot (Fig. 7D) corroborates this trend, with significantly lower AAK1 expression at p7 and a peak at 3 months, followed by a reduction at 12 months.

This pattern is paralleled by the expression of Synaptotagmin 1 (SYT1), a synaptic marker, which follows a similar trajectory of increasing with age up to 3 months and then declining at 12 months. The synchronized expression of AAK1 and SYT1 suggests that AAK1 may play a role in synaptic maturation and maintenance during early adulthood, potentially contributing to optimal synaptic function and plasticity during this critical period for cognitive development.

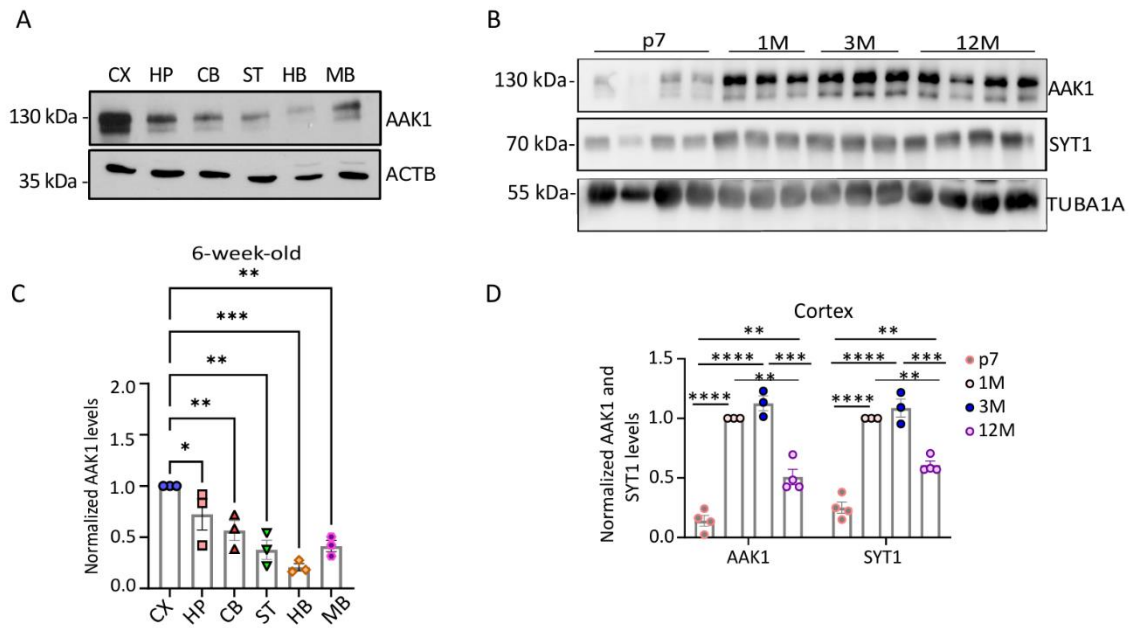


Figure 7: AAK1 expression differs in region and age in mouse brain. (A) Representative immunoblot of AAK1 from age of 6-week-old WT mouse in six brain regions (CX: cortex, HP: hippocampus, CB: cerebellum, ST: striatum, HB: hindbrain, MB: midbrain) (C) Immunoblot analysis of AAK1 levels in 6-week-old CX, HP, CB, ST, HB and MB of WT animals. ACTB was used normalization of protein levels. Each dot represents one animal (N=3) One-way ANOVA with Holm-Sidak's multiple comparison test was performed for comparison of cortex to different brain regions. (B) Representative immunoblot of AAK1 and SYT1 age of p7, 1-month-old (1M), 3-month-old (3M) and 12-month-old (12M) in WT cortex. (D) Immunoblot analysis of AAK1 and SYT1 in the cortex of p7, 1M, 3M and 12M old WT mice. Each dot represents one animal (N=4 for p7 and 12-month-old animals, N=3 for 1 and 3-month-old animals) Two-way ANOVA was used for comparison of AAK1 and SYT1 levels in different ages. All Data are shown as mean \pm SEM. Significant differences are indicated by asterisks (* $p < 0.05$; ** $p < 0.01$; *** $p < 0.001$; **** $p < 0.0001$).

2. AAK1 KO mice show reduced body weight without changes in body composition

To generate the AAK1 KO mouse model, we utilized the European Conditional Mouse Mutagenesis Program (EUCOMM) "knockout-first" gene targeting approach. This approach uses the targeted mutation 1a (*tm1a*) allele, a "knockout-first" construct that allows for conditional gene disruption (Skarnes et al 2011). By crossing *tm1a* mice with a *CMV-Cre* line (mouse expressing Cre recombinase ubiquitously under the control of a human cytomegalovirus (CMV) promoter), we achieved recombination at the *loxP* sites, effectively excising both the neomycin cassette and exon 2 of the *Aak1* gene, leading to the generation of *tm1b*, *lacZ* reporter mice that express β -galactosidase in cells where the gene of interest would typically be expressed (Fig. 8A).

Immunoblot results and analysis confirmed the successful depletion of AAK1 in the brains of KO mice, showing almost complete absence of the protein in comparison to WT (Fig. 8B and C). These findings verify the effective knockout of AAK1, which is crucial for evaluating the in vivo consequences of its loss. Phenotypic assessment revealed a significant reduction in body weight in KO mice compared to WT controls (Fig. 8D and E), suggesting a potential role of AAK1 in growth or metabolic regulation. Importantly, femur length measurements indicated no difference KO and WT mice (Fig. 8F and G) suggesting that the observed weight reduction in KO mice is not due to skeletal abnormalities, but rather may involve other aspects of body composition or energy balance. To investigate this further, we analyzed the body composition of KO and WT animals by using EchoMRI-100H Body Composition Analyzer (EchoMRI®). Measurements of lean mass (Fig. 8H), fat mass (Fig. 8I) and total body water (Fig. 8J) revealed no significant differences between the two groups. This suggests that while AAK1 depletion leads to an overall reduction in body weight, it does not appear to affect the relative distribution of body tissues.

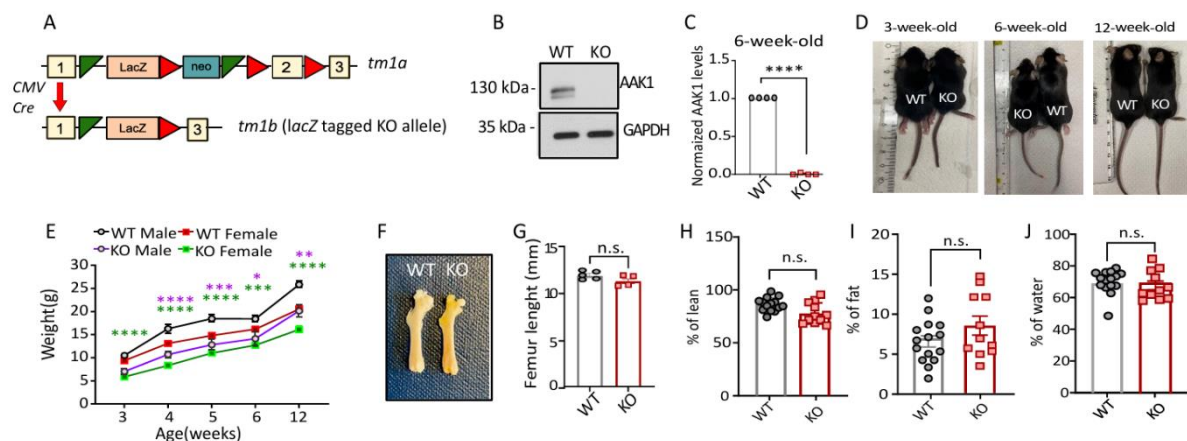


Figure 8: AAK1 KO mice show reduced body weight compared to WT littermates. (A) Schematic representation of the gene-targeting strategy used to create the AAK1 KO mouse. (B) Representative immunoblot of AAK1 in cortex from 6-week-old WT and KO mice, confirming the absence of AAK1 protein in KO brains. GAPDH was used as loading control for normalization of protein levels. (C) Quantification of AAK1 protein levels in WT and KO mice. Each dot represents one animal (N=3). One-tailed unpaired t-test was performed for comparison of WT and KO. (D) Representative images of WT and KO mice at 3, 6, and 12 weeks of age, illustrating the smaller body size in KO mice. (E) Growth curve of WT and KO mice from 3 to 12 weeks, showing significantly reduced body weights in both male and female KO mice across all time points. (N=7 for WT and KO male, N=15 for WT female and N=14 for KO female) Two-Way ANOVA with Holm-Sidak's multiple comparison test was performed. (F-J) Morphological and metabolic characterization of KO and WT mice at 12 weeks. (F) Representative femur images from 12-week-old WT and KO mice. (G) Quantification of femur length in WT and KO mice (N=5 for WT and N=4 for KO), indicating no significant difference (n.s., not significant). Each dot represents one animal. Two-tailed unpaired t-test was performed for comparison of WT and KO. (H-J) Body composition analysis of 12-week-old WT and KO mice, comparing lean mass (H), fat percentage (I), and water percentage (J), with no significant differences observed between genotypes (n.s., not significant). Each dot represents one animal. (N=14 for WT, N=11 for KO) Two-tailed unpaired t-test was performed.

was performed for comparison of WT and KO. All Data are shown as mean \pm SEM. Significant differences are indicated by asterisks (* $p < 0.05$; ** $p < 0.01$; *** $p < 0.001$; **** $p < 0.0001$).

3. AAK1 deletion reduces levels of endocytic proteins AP-2 and clathrin in the cortex of AAK1 KO mice and disrupts endocytosis in cultured neurons.

AAK1 deletion disrupts endocytic processes in the brain cortex and primary neurons. Western blot analysis of cortex from AAK1 KO mice demonstrated that loss of AAK1 significantly reduces the levels of key endocytic proteins, specifically the AP-2 complex subunits AP-2 α and AP-2 μ , in both 6-week-old (Fig. 9A-D) and 12-week-old animals (Fig. 9G-J). This reduction in AP-2 subunits, which are critical for CME, suggests a direct role of AAK1 in regulating the stability or expression of these adaptor proteins. This finding aligns with previous literature that establishes AAK1 as an endocytic kinase. AAK1 is known to interact with α -adaptin, a subunit of the AP-2 complex, and phosphorylates the μ 2 subunit at threonine 156, thereby playing a crucial regulatory role in CME (Conner & Schmid 2002, Conner, Schröter & Schmid 2003, Olusanya et al 2001, Ricotta et al 2002). Interestingly, while AP-2 α levels are significantly decreased, CHC levels remain unaffected in the 6-week-old cortex (Fig. 9E and F), indicating that AAK1's influence on endocytosis may be more selective for AP-2 components rather than clathrin itself.

Further, immunofluorescence staining of primary cortical neurons shows reduced AP-2 α level in KO neurons compared to WT (Fig. 9K). This reduction is accompanied by a marked decrease in transferrin uptake in KO neurons (Fig. 9M), demonstrating impaired endocytic function. Transferrin uptake is commonly used as a measure of receptor-mediated endocytosis, so this finding underscores that AAK1 is essential for efficient endocytosis in neuronal cells. Given that endocytosis is a key process in synaptic vesicle recycling and signaling receptor internalization, these disruptions could impact neuronal communication and synaptic plasticity.

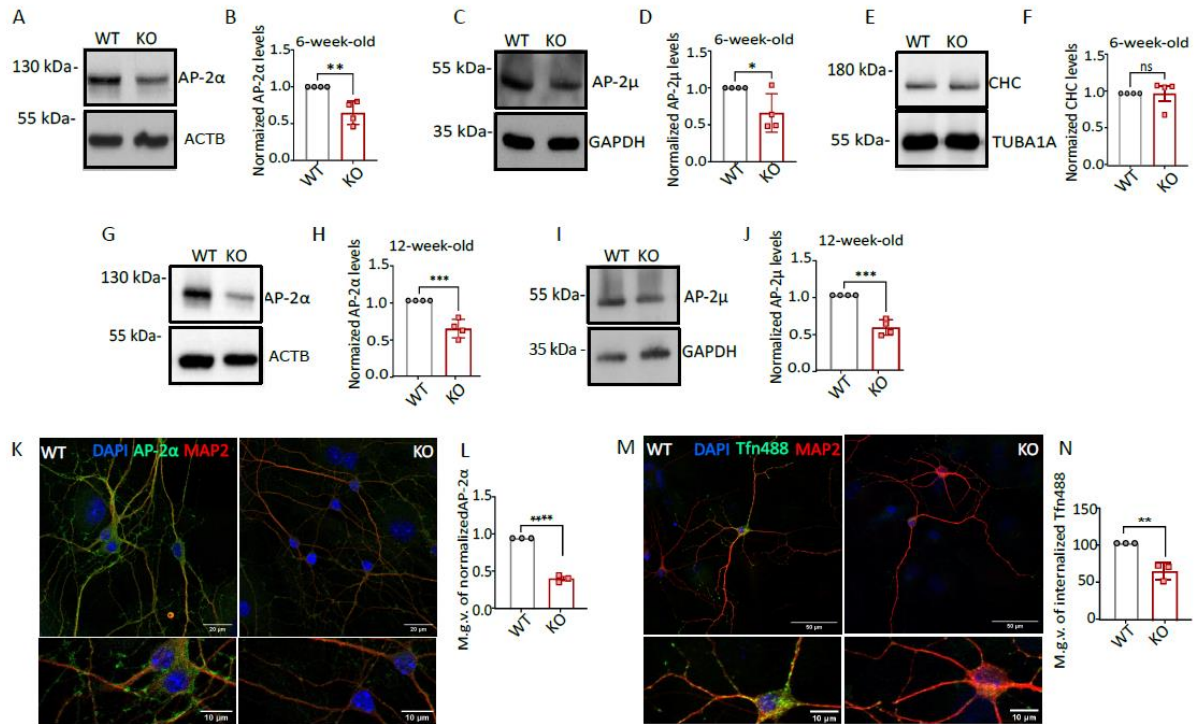


Figure 9: AAK1 depletion results in impaired endocytosis in-vivo and in-vitro (A) Representative immunoblot of AP-2 α in cortex from 6-week-old WT and KO mice, confirming the reduced level of AP-2 α protein in KO brains. ACTB was used as loading control for normalization of protein levels. (B) Quantification of AP-2 α protein levels in WT and KO mice. Each dot represents one animal (N=3). One-tailed unpaired t-test was performed for comparison of WT and KO. (C) Representative immunoblot of AP-2 μ in cortex from 6-week-old WT and KO mice, confirming the reduced level of AP-2 μ protein in KO brains. GAPDH was used as loading control for normalization of protein levels. (D) Quantification of AP-2 μ protein levels in WT and KO mice. Each dot represents one animal (N=3). One-tailed unpaired t-test was performed for comparison of WT and KO. (E) Representative immunoblot of CHC in cortex from 6-week-old WT and KO mice, confirming the reduced level of CHC protein in KO brains. TUBA1A was used as loading control for normalization of protein levels. (F) Quantification of CHC protein levels in WT and KO mice. Each dot represents one animal (N=3). One-tailed unpaired t-test was performed for comparison of WT and KO. (G) Representative immunoblot of AP-2 α in cortex from 12-week-old WT and KO mice, confirming the reduced level of AP-2 α protein in KO brains. ACTB was used as loading control for normalization of protein levels. (H) Quantification of AP-2 α protein levels in WT and KO mice. Each dot represents one animal (N=3). One-tailed unpaired t-test was performed for comparison of WT and KO. (I) Representative immunoblot of AP-2 μ in cortex from 12-week-old WT and KO mice, confirming the reduced level of AP-2 μ protein in KO brains. GAPDH was used as loading control for normalization of protein levels. (J) Quantification of AP-2 μ protein levels in WT and KO mice. Each dot represents one animal (N=3). One-tailed unpaired t-test was performed for comparison of WT and KO. (K) Representative immunofluorescence images of WT and KO neurons stained for AP-2 α (green), MAP2 (red, dendritic marker), and DAPI (blue, nuclear marker). (L) Quantification of mean gray value (m.g.v.) of AP-2 α , indicating significantly lower levels in KO neurons. Each dot represents one animal (N=3). Two-tailed unpaired t-test was performed for comparison of WT and KO. (M) Transferrin uptake assay in WT and KO neurons. Neurons were incubated with fluorescently labeled transferrin (Tfn488, green) to assess endocytosis, with MAP2 (red) and DAPI (blue) staining. (N) Quantification of internalized Tfn488 shows reduced transferrin uptake in KO neurons, indicating impaired endocytic function. Each dot represents one animal (N=3). Two-tailed unpaired t-test was performed for

comparison of WT and KO. All Data are shown as mean \pm SEM. Significant differences are indicated by asterisks (* $p < 0.05$; ** $p < 0.01$; *** $p < 0.001$; **** $p < 0.0001$).

4. AAK1 depletion did not result in anatomical changes in the brain

To investigate the effects of AAK1 depletion on brain anatomy, we performed Nissl staining (Cresyl-violet) (Fig. 10A) and immunofluorescent labelling (Fig. 10K) in both WT and KO mice. In 3-week-old mice, a mild reduction in cortex volume was observed in KO animals compared to WT (Fig. 10C). However, no significant differences were detected in corpus callosum (cc) thickness (Fig. 10B), nor were there any changes in overall brain anatomy (Fig. 10A). In 12-week-old mice, we observed a significant reduction in corpus callosum thickness in KO mice compared to WT (Fig. 10E), while cortex area remained unchanged (Fig. 10F). Representative Nissl-stained sections of the brains from both age groups confirmed that overall brain structure appeared normal, with no gross anatomical abnormalities in either WT or KO (Fig. 10D).

Further, gross morphological examination of the brain from WT and KO mice at 3 weeks (Fig. 10G), 6 weeks (Fig. 10H), and 12 weeks (Fig. 10J) revealed no apparent differences in brain size or shape between the genotypes across these developmental stages.

Immunofluorescent staining was also conducted to assess neuronal and glial cell populations. In 3-week-old WT and KO mice, the cortex was stained for a cortical neuron marker T-Box Brain Transcription Factor 1 (Tbr1) and an astrocytic marker Glial fibrillary acidic protein (GFAP) while the hippocampus was stained for a marker for neural stem cells Nestin and a marker for immature neurons doublecortin (DCX) (Fig. 10K). No structural differences were detected in either cortical or hippocampal regions between WT and KO, suggesting that AAK1 depletion does not significantly impact neuronal or astrocytic organization at this age.

These results suggest that while AAK1 depletion has minor anatomical effects, such as a slight reduction in cortical area at 3 weeks and a reduction in corpus callosum thickness at 12 weeks, it does not lead to major structural changes in the brain. The slight differences observed might indicate that AAK1 plays a subtle role in maintaining certain brain structures, particularly the cortex and corpus callosum. However, its absence does not appear to affect gross brain morphology or cellular organization, at least at the ages examined. Further studies may be required to explore if these changes have functional consequences.

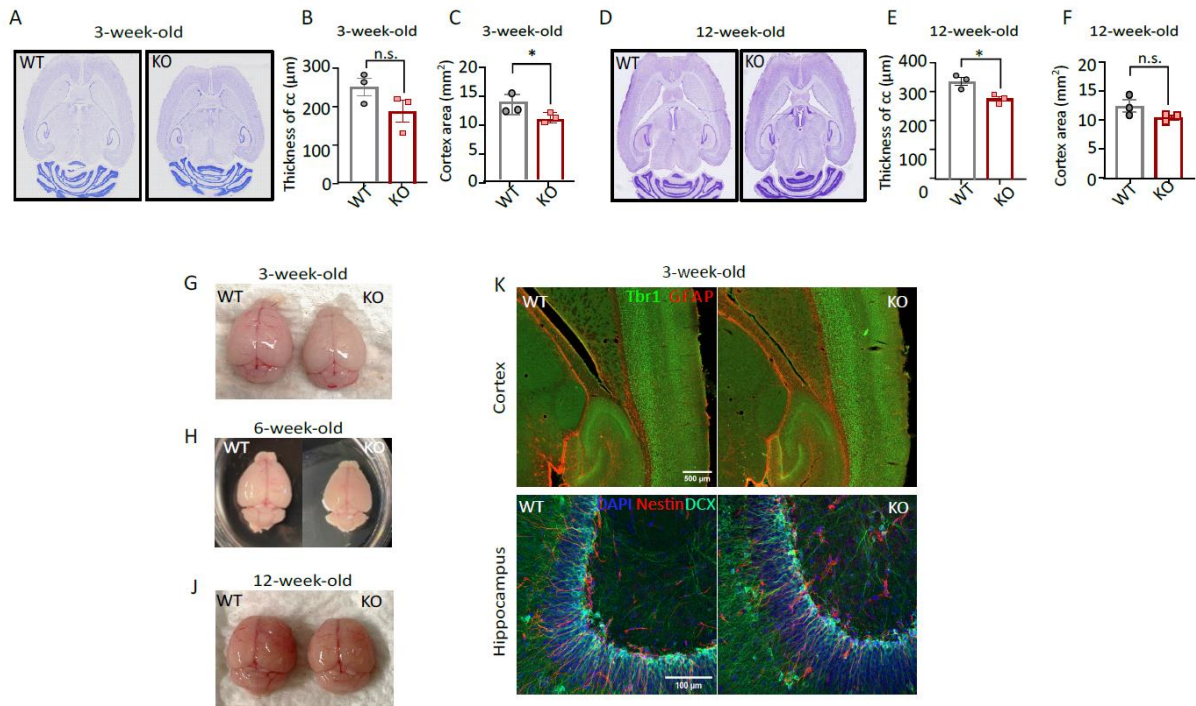


Figure 10: Assessment of anatomical and neurodevelopmental changes in the AAK1 depleted brains. (A) Representative Cresyl-violet stained coronal brain sections and (B) quantification of corpus callosum (cc) thickness and (C) cortex area in 3-week-old WT and KO mice. Each dot represents one animal (N=3). Two-tailed unpaired t-test was performed for comparison of WT and KO. (D) Representative Cresyl-violet stained coronal brain sections and (E) quantification of corpus callosum (cc) thickness and (F) cortex area in 12-week-old WT and KO mice. Each dot represents one animal (N=3). Two-tailed unpaired t-test was performed for comparison of WT and KO. (G-J) Gross brain morphology images from WT and KO mice at different ages: (G) 3-week-old, (H) 6-week-old, and (J) 12-week-old. (K) Representative immunofluorescence images of 3-week-old WT and KO brains to examine cortical and hippocampal structure. Tbr1 (green) labels cortical neurons, and GFAP (red) marks astrocytes in the cortex (top). In the hippocampus (bottom), Nestin (green) highlights neural stem cells, and DCX (red) marks immature neurons. DAPI (blue) stains nuclei. No structural differences are observed between WT and KO in these regions. Scale bars, 500 µm for cortex, 100 µm for hippocampus. All Data are shown as mean ± SEM. Significant differences are indicated by asterisks (* p<0.05; ** p<0.01; *** p<0.001; **** p<0.0001).

5. Characterization of CamKIIα-driven AAK1 KO mice reveals minor anatomical and metabolic differences

Given that previous results (Fig. 8, 9 and 10) were obtained using a global KO model, it remains unclear whether AAK1 has a cell-type specific impact, particularly in neurons where it is known to play a role in endocytic processes. To explore this further, we generated a conditional AAK1 knockout (AAK1 cKO) model under the *CamKIIα* promoter to specifically target AAK1 deletion in excitatory neurons (Dragatsis & Zeitlin 2000). To do so, we again used allele conversion technology. Flp converts the 'knockout-first' allele (tm1a) to a conditional allele (tm1c), restoring gene activity. Cre deletes the promoter-driven selection cassette and deletes the floxed exon

of the tm1c allele to generate a frameshift mutation (tm1d), triggering nonsense mediated decay of the deleted transcript (Skarnes et al 2011) (Fig. 11A). This neuron-specific model allows us to investigate whether AAK1 depletion within neuronal populations, as opposed to the whole organism, leads to distinct phenotypic outcomes. Here, we examined whether this neuron-specific knockout affects body weight, endocytic processes, and anatomical changes in the brain, as observed in the global knockout model.

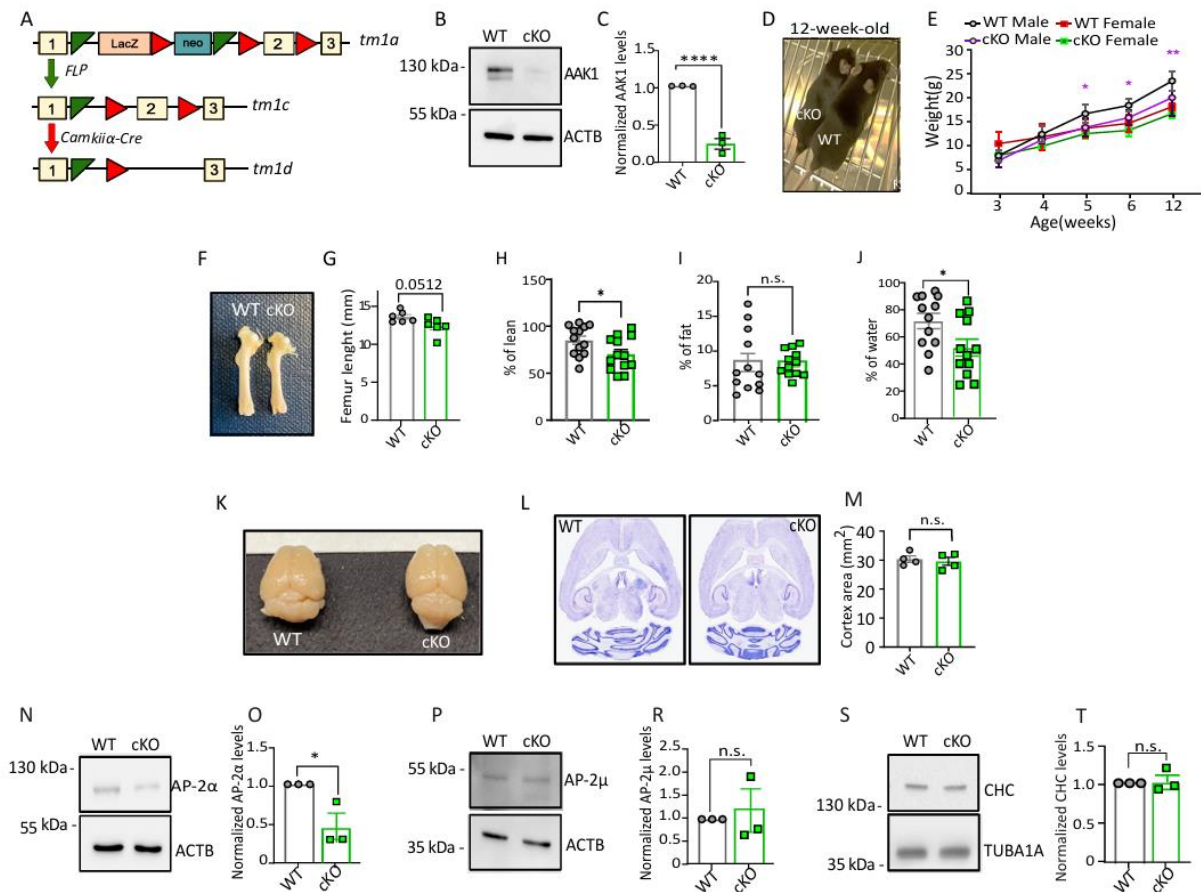
The immunoblot analysis (Fig. 11B, C) shows a substantial reduction in AAK1 protein levels in the brain cortex of AAK1 cKO mice compared to WT, which strongly suggests that AAK1 expression in the cortex is predominantly neuronal. This neuron-specific presence underlines the importance of AAK1 within neuronal populations, making it a key regulator of neuronal functions.

Morphologically, cKO mice exhibit slight but significant differences, such as a reduced body weight. Our measurements revealed a significant reduction in body weight in cKO mice compared to WT controls (Fig. 11E), suggesting a potential role of neuronal AAK1 in growth or metabolic regulation. Although the weight graph does not look that dramatic compared to global AAK1 KO mice, it should be noted that the current analysis included only three WT females; increasing the number of animals may reveal more pronounced effects on body weight or other physiological measures, thus giving a clearer picture of the role of AAK1 in neuronal populations. Surprisingly, we observed reduction in lean body mass and water content (Fig. 11H, J), whereas bone size (femur length) (Fig. 11F, G) and gross brain anatomy (cortex area and structural integrity) remain comparable between cKO and WT mice (Fig. 11K-M). The body composition results indicate a neuron-specific effect of AAK1 depletion on metabolic characteristics, since these changes were not observed in the global AAK1 KO model. This is a promising indication that AAK1 plays a specific role in the metabolic regulation of neurons, affecting lean mass composition and water balance.

The immunoblot analysis of endocytic proteins also provides insight into the specific molecular impact of AAK1 deletion. A selective reduction in AP-2 α is observed in KO mice (Fig. 11N, O), while levels of other endocytic proteins, such as AP-2 μ and CHC, remain unchanged (Fig. 11P-T). This suggests that AAK1 may play a role in regulating the stability or expression of specific subunits of the AP-2 complex rather than broadly affecting the endocytic machinery. The neuron-specific reduction in AP-2 α is particularly intriguing, as it implies that AAK1 may have a more specialized role in the maintenance of synaptic function and receptor recycling in neurons which indicates a clathrin independent role of it.

Taken together, these findings suggest that AAK1 depletion under the *CamKII α* promoter results in a nuanced phenotype, with neuron-specific consequences for metabolic composition

and selective alterations in the endocytic pathway. These data point to a critical role for AAK1 in the regulation of neuronal health and function that may not be fully captured by global knockout models, emphasizing the importance of context-specific analysis to uncover the subtle contributions of AAK1 in brain physiology.



integrity at 12 weeks. (M) Quantification of cortex area showing no significant difference between WT and AAK1 cKO mice. Each dot represents one animal (N=4 for each genotype). Two-tailed unpaired t-test was performed for comparison of WT and AAK1 cKO. (N) Representative immunoblot of AP-2 complex subunit AP-2 α in cortex from 12-week-old WT and AAK1 cKO mice, confirming the reduced level of AP-2 α protein in KO brains. ACTB was used as loading control for normalization of protein levels. (O) Quantification of AP-2 α protein levels in WT and KO mice. Each dot represents one animal (N=3). One-tailed unpaired t-test was performed for comparison of WT and KO. (P) Representative immunoblot of AP-2 complex subunit AP-2 μ in cortex from 12-week-old WT and AAK1 cKO mice. ACTB was used as loading control for normalization of protein levels. (R) Quantification of AP-2 μ protein levels in WT and AAK1 cKO mice. Each dot represents one animal (N=3). One-tailed unpaired t-test was performed for comparison of WT and KO. (S) Representative immunoblot of CHC in cortex from 12-week-old WT and AAK1 cKO mice, confirming the reduced level of CHC protein in KO brains. TUBA1A was used as loading control for normalization of protein levels. (T) Quantification of CHC protein levels in WT and KO mice. Each dot represents one animal (N=3). One-tailed unpaired t-test was performed for comparison of WT and KO. All Data are shown as mean \pm SEM. Significant differences are indicated by asterisks (* p<0.05; ** p<0.01; *** p<0.001; ****p<0.0001).

6. AAK1 KO and AAK1 cKO mice show hyperactivity

To assess behavioral changes resulting from AAK1 depletion, we conducted an open field (OF) test to examine activity levels and movement patterns. Total distance traveled by WT and KO mice was quantified across the entire arena, as well as specifically within the center and border zones (Fig. 12B and E). In both the global and CamKII α -specific AAK1 KO models, KO animals exhibited a significantly greater distance traveled in the arena and border zones compared to WT animals, indicating heightened activity levels (Fig. 12B and E). However, no significant difference was observed in distance traveled within the center zone. This increase in overall activity suggests a potential hyperactive phenotype in AAK1 KO mice. Furthermore, KO animals displayed significantly higher velocity in the center zone, while no significant differences in speed were observed in the arena or border zones. The increased velocity in the center zone may reflect a tendency toward more dynamic, exploratory behavior, supporting the hyperactivity observed in KO groups. Together, these results suggest that AAK1 depletion may lead to altered locomotion patterns and increased exploratory drive, particularly within areas associated with risk, such as the center zone.

The fact that both AAK1 KO models exhibit similar behavioral alterations underscores that this activity is likely a neuron-specific effect. The *CamKII α* promoter targets AAK1 depletion specifically within excitatory neurons, and observing the same hyperactive and exploratory behavior in this model suggests that AAK1 plays a critical role within neurons in modulating movement and exploratory drive. This neuron-specific effect is particularly significant, as it implies that AAK1 function in the brain is central to the regulation of locomotor activity and anxiety-like behavior. The AAK1 cKO model, therefore, serves as a valuable tool for dissecting

AAK1's role in neurobehavioral regulation, providing insights into how AAK1-related pathways may influence hyperactivity and exploration in the brain.

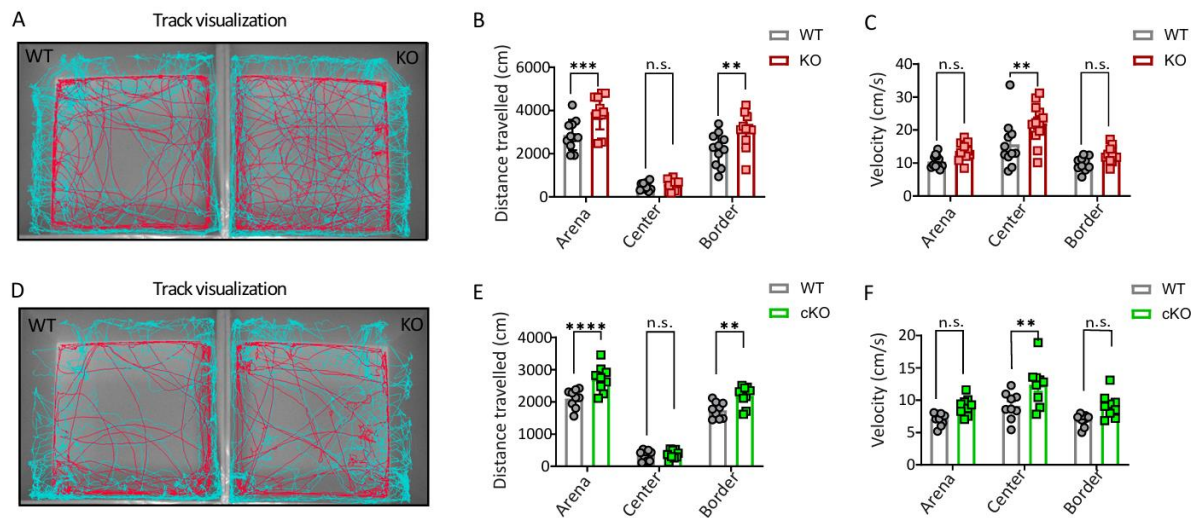


Figure 12: Behavioral assessment of AAK1 KO and AAK1 cKO mice. (A) Representative image for track visualization, showing movement patterns of AAK1 KO and WT mice in open field. Turquoise stands for nose, red stands for center of the body. (B) Quantification of total distance traveled in the arena, center and border regions. Each dot represents one animal (N=11). Two-Way ANOVA with Holm-Sidak's multiple comparison test was performed. (C) Quantification of Velocity measurements in the arena, center, and border regions. Each dot represents one animal (N=11). Two-Way ANOVA with Holm-Sidak's multiple comparison test was performed. (D) Representative image for track visualization, showing movement patterns of AAK1c KO and WT mice in open field. Turquoise stands for nose, red stands for center of the body. (E) Quantification of total distance traveled in the arena, center and border regions. Each dot represents one animal (N=9). Two-Way ANOVA with Holm-Sidak's multiple comparison test was performed. (F) Quantification of Velocity measurements in the arena, center, and border regions. Each dot represents one animal (N=9). Two-Way ANOVA with Holm-Sidak's multiple comparison test was performed. All Data are shown as mean \pm SEM. Significant differences are indicated by asterisks (* $p < 0.05$; ** $p < 0.01$; *** $p < 0.001$; **** $p < 0.0001$).

7. Motor coordination deficits in AAK1 KO and AAK1 cKO mice

To assess motor coordination and balance, a beam walking test was conducted on both AAK1 KO and AAK1 cKO mice. This test involved quantifying slips and step cycles as animals walked on beams of different thicknesses, with thinner beams posing a great challenge.

AAK1 KO mice showed significantly more slips on both the 12 mm and 5 mm beams compared to WT controls (Fig. 13B). In contrast, AAK1 cKO mice exhibited a significant increase in slips only on the 5 mm beam (Fig. 13F). The pronounced effect observed in AAK1 KO mice suggests that AAK1's role in motor coordination extends beyond neurons, potentially involving other cell types or systemic effects. However, the similar trend in the AAK1 cKO, though less pronounced, highlights a neuron-specific contribution to motor impairment.

To measure gait rhythm, the number of step cycles was quantified across beams of different width (Fig. 13C and G). In the AAK1 KO mice (Fig. 13C), there was a significant reduction in step cycles on the 5 mm beam compared to WT mice, indicating a disrupted gait pattern under the most challenging conditions. Interestingly, the AAK1 cKO model (Fig. 13G) did not show significant differences in step cycles across any beam thickness, suggesting that AAK1's influence on step cycle rhythm may depend on not excitatory CamKII α expressing neurons. Additionally, to evaluate different aspects of motor performance the motor we also employed rotarod test. The rotarod test is specifically designed to evaluate general motor coordination, balance, and motor learning, as mice must remain on a rotating rod, which requires them to coordinate their movements in response to an accelerating speed. Surprisingly, the AAK1 KO mice did not display any deficits in the rotarod test, suggesting that their general balance and motor coordination are not significantly impaired by the absence of AAK1.

These findings reveal that AAK1 deficiency impairs motor coordination and balance, particularly under challenging conditions, as evidenced by the increased number of slips and altered step cycles on the narrowest beam. The global AAK1 KO model shows a more severe phenotype, affecting both slips and step cycles, suggesting that AAK1 function in multiple cell types may be required for precise motor coordination. Meanwhile, the CamKII α -specific AAK1 KO model demonstrates similar, though less pronounced, impairments in slips but not in step cycles, underscoring a neuron-specific role of AAK1 in balance and coordination. Together, these results highlight the importance of AAK1 in motor function and suggest that its depletion may lead to specific deficits in neuronal motor coordination, as well as broader impacts on motor control when AAK1 is absent throughout the body.

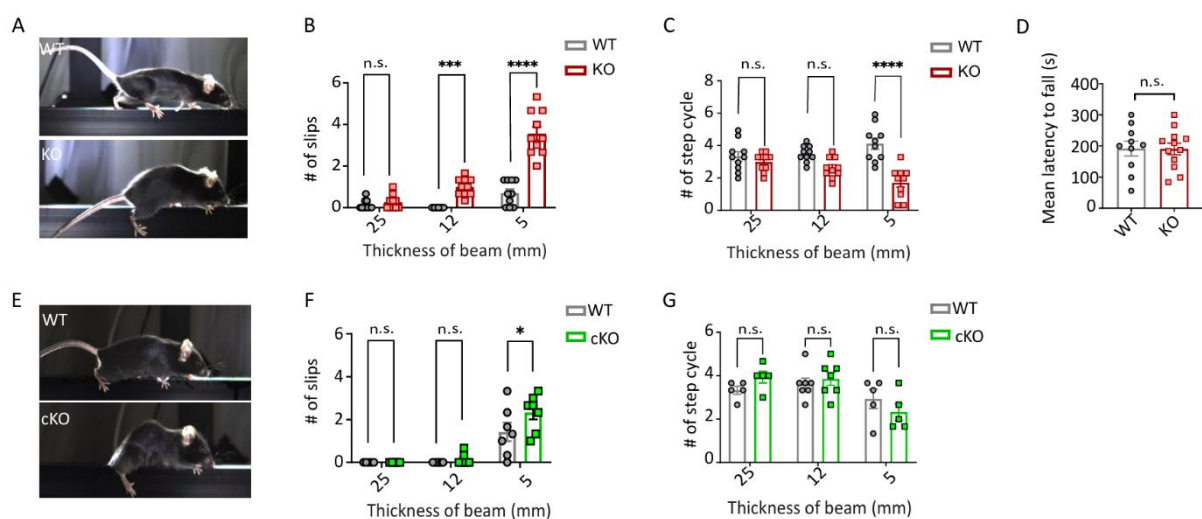


Figure 13: Beam walking performance in AAK1 KO and cKO mice. (A) Representative image of WT and AAK1 KO mice on the 12mm beam. (B-C) Quantification of the number of slips and step cycles for

WT and KO animals on beams of varying thickness (25 mm, 12 mm, and 5 mm). Each dot represents one animal (N=10 for WT and N=8 for AAK1 KO). Two-Way ANOVA with Holm-Sidak's multiple comparison test was performed. (D) Mean latency to fall on rotarod. Each dot represents one animal. (N=10 for WT, N=12 for KO) Two-tailed t-test was performed to compare WT and KO mice. (E) Representative image of WT and AAK1 cKO mice on the 12mm beam. (F-G) Quantification of the number of slips for WT and KO animals on beams of varying thickness (25 mm, 12 mm, and 5 mm). Each dot represents one animal (N=7 for WT and N=7 for AAK1 KO). Two-Way ANOVA with Holm-Sidak's multiple comparison test was performed. All Data are shown as mean \pm SEM. Significant differences are indicated by asterisks (* $p < 0.05$; ** $p < 0.01$; *** $p < 0.001$; **** $p < 0.0001$).

After impaired motor coordination on beam walk we aimed to assess cerebellar changes to explore potential underlying neuropathological features that could contribute to observed motor phenotype in KO mice. First, we checked calbindin-1 (CALB1) in Purkinje cells, a key cell type within the cerebellum that plays a critical role in coordinating motor function (Fig. 14A-C). CALB1 staining and immunoblot analysis (Fig. 14A-C) revealed that Purkinje cell structure and general organization appear without any difference between WT and KO mice, suggesting that AAK1 deficiency does not visibly alter the structural integrity of Purkinje cells in the cerebellum at 12 weeks of age. NBR1, a protein involved in autophagy, was also analyzed to evaluate whether AAK1 depletion might disrupt protein turnover processes. Fig. 14D and E show that NBR1 levels are similar in WT and KO mice, indicating no significant alteration in autophagy pathways involving NBR1 in the cerebellum. This suggests that AAK1 deficiency does not affect all aspects of cellular homeostasis or autophagy in this region. Unlike CALB1 and NBR1, the autophagy-related protein p62/SQSTM1 is significantly elevated in the KO cerebellum (Fig. 14F and G). This increase in p62, a protein that accumulates when autophagic flux is impaired, may indicate a subtle disruption in autophagy or cellular clearance mechanisms within the cerebellum of KO animals. Elevated p62 is often associated with impaired protein turnover, which could contribute to the observed motor deficits by affecting cellular health in cerebellar neurons involved in motor coordination. Overall, these results suggest that AAK1 knockout does not overtly alter Purkinje cell structure or the expression of certain proteins (e.g., CALB1, NBR1) in the cerebellum. However, the significant increase in p62 levels points to potential autophagic dysregulation, which may underlie or contribute to the motor coordination issues observed in AAK1 KO mice. This finding highlights the importance of p62 as a marker of cellular homeostasis disruption and suggests a possible link between AAK1 depletion and impaired autophagy-related processes in the cerebellum.

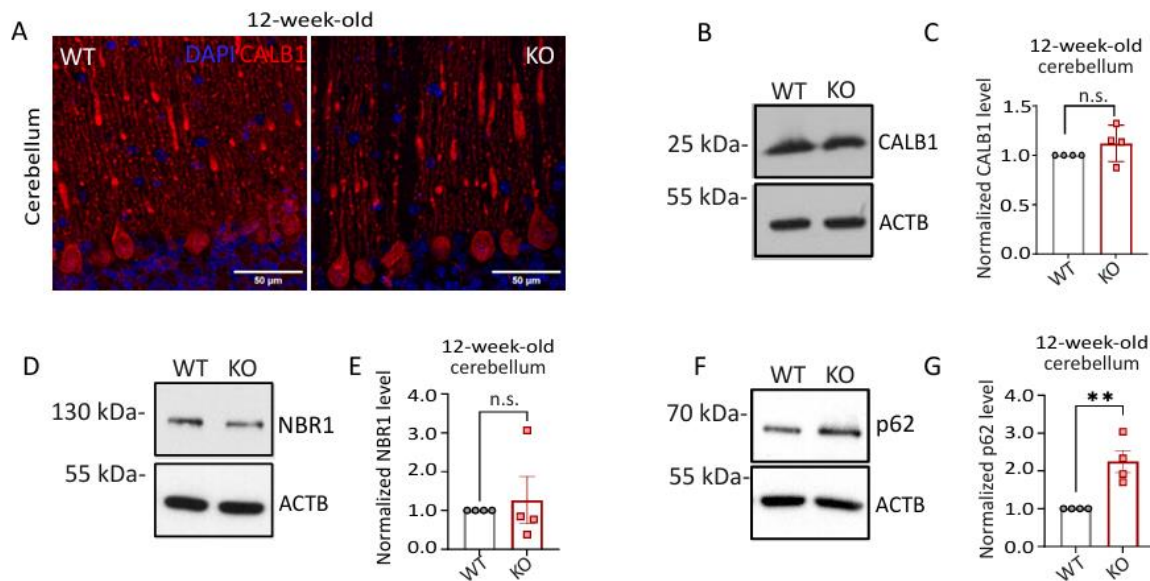


Figure 14: Assessment of cerebellar pathology in AAK1 KO mice. (A) Representative immunofluorescent images of cerebellum show calbindin-1 (CALB1, red) and DAPI (blue) labeling in Purkinje cells from WT and KO mice. Scale bar, 50 μ m. (B) Representative immunoblot of CALB1 in cerebellum from 12-week-old WT and KO mice. ACTB was used as loading control for normalization of protein levels. (C) Quantification of CALB1 expression level. Each dot represents one animal (N=4). One-tailed unpaired t-test was performed for comparison of WT and KO. (D) Representative immunoblot of NBR1 in cerebellum from 12-week-old WT and KO mice. ACTB was used as loading control for normalization of protein levels. (E) Quantification of NBR1 expression level. Each dot represents one animal (N=4). One-tailed unpaired t-test was performed for comparison of WT and KO. (F) Representative immunoblot of p62 in cerebellum from 12-week-old WT and KO mice. ACTB was used as loading control for normalization of protein levels. (G) Quantification of p62 expression level. Each dot represents one animal (N=4). One-tailed unpaired t-test was performed for comparison of WT and KO. All Data are shown as mean \pm SEM. Significant differences are indicated by asterisks (* $p < 0.05$; ** $p < 0.01$; *** $p < 0.001$; **** $p < 0.0001$; n.s. not significant).

8. Proteomic analysis of AAK1 interactome in the cortex reveals enrichment of endocytic and autophagic pathways

To further investigate and comprehend the potential mechanisms of AAK1 in the brain, we performed immunoprecipitation (IP) of AAK1 from cortical tissue followed by proteomic analysis to identify AAK1-interacting proteins.

Volcano plot illustrates the proteins significantly enriched in the AAK1 IP compared to the IgG control (Fig. 15A), with several prominent proteins highlighted. These proteins include components of the CME machinery (e.g., AP2B1, AP2A2, CLTC) and other trafficking-related proteins. This interaction suggests that AAK1 may play a regulatory role in vesicle trafficking within neurons, potentially influencing processes critical for synaptic function. Gene ontology (GO) analysis of biological processes (Fig. 15B) shows that AAK1-associated proteins are

enriched in pathways related to lysosomal membrane permeability, chaperone-mediated and macroautophagy, and endosomal transport. Notably, the enrichment of autophagy-related pathways suggests that AAK1 may influence or be included in autophagic flux, a critical mechanism for cellular cleanup and protein degradation. This finding may provide a potential link to the motor deficits observed in KO animals, as impaired autophagy is often associated with neurodegenerative changes and cellular dysfunction. The cellular component analysis in reveals that AAK1-associated proteins are primarily localized to structures involved in endocytosis and synaptic vesicle cycling, such as CCVs, endocytic zones, and dendritic compartments (Fig. 15C). This localization suggests that AAK1's role extends into synaptic regions, where efficient trafficking is essential for synaptic maintenance and plasticity. KEGG pathway analysis (Fig. 15D) further supports the involvement of AAK1 in endocytic and lysosomal pathways, as well as in the synaptic vesicle cycle and autophagy. The significant enrichment in pathways like lysosome and endocytosis suggests that AAK1 may be essential for regulating cellular homeostasis in neurons by modulating endocytic trafficking and autophagic clearance.

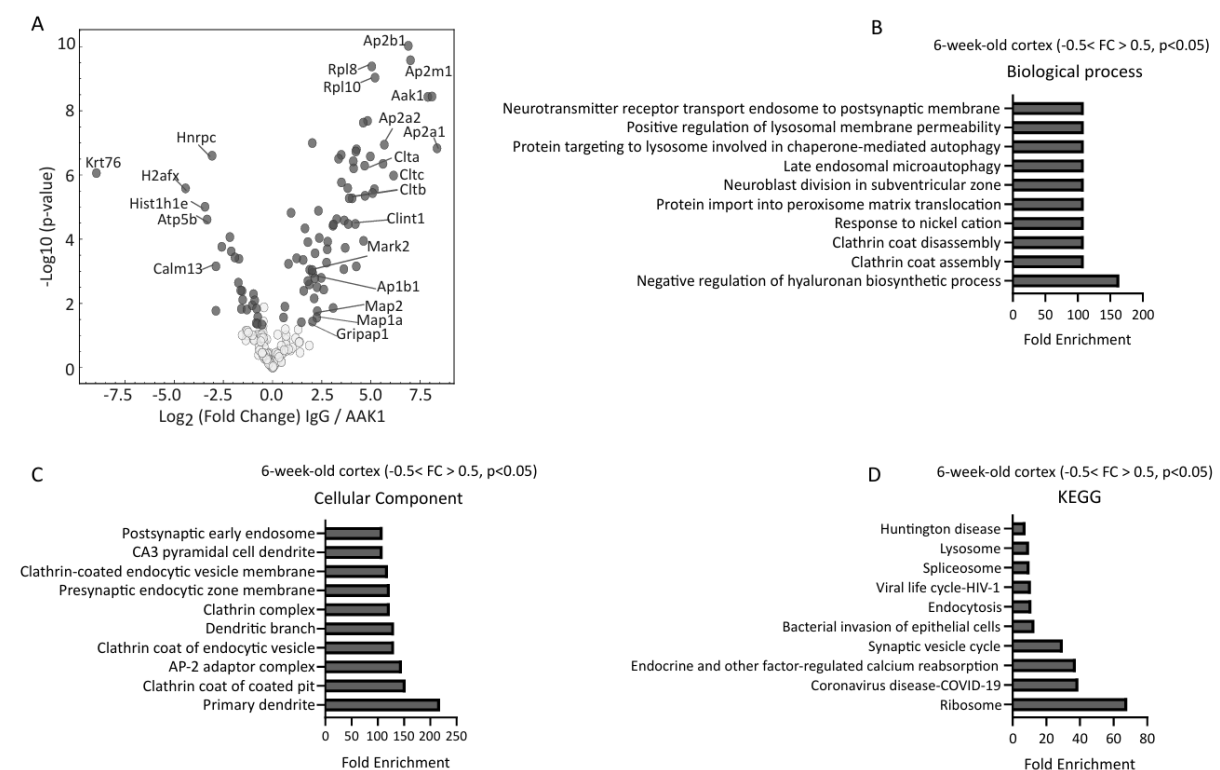


Figure 15: Identification of AAK1-associated proteins and enriched pathways in the cortex of 6-week-old mice. (A) Volcano plot showing proteins significantly enriched in AAK1IP compared to IgG controls, with notable proteins labeled in 6-week-old WT mice. Positive fold changes indicate proteins more associated with AAK1 IP than IgG. Significantly changed proteins highlighted in dark grey (N=5). $-0.5 < \text{Log}_2 \text{ fold change} > 0.5$ and $p\text{-value} < 0.05$ and $q\text{-value} < 0.05$. (B) GO biological processes of significantly changed proteins detected at 6 weeks of age. (C) GO cellular component analysis of significantly changed proteins.

significantly changed proteins detected at 6 weeks of age. (D) GO KEGG pathway analysis of significantly changed proteins detected at 6 weeks of age.

9. Proteomic and phosphoproteomic analysis reveals autophagy and trafficking pathways associated with AAK1 in the brain

Following the identification of AAK1 interactors by immunoprecipitation, we performed both proteomic (total 3317 protein detected and 1022 of them significantly dysregulated, p-value <0.05) and phosphoproteomic (total 9783 phosphosites detected and 5178 of them significantly dysregulated, p-value <0.05) analyses of cortex tissue from WT and AAK1 KO mice at 6 weeks of age. This allowed us to identify key changes in protein expression and phosphorylation states that may underlie the functional impacts of AAK1 depletion. The results revealed significant alterations in synaptic proteins, endocytic adaptors, and autophagy-related components, indicating potential disruption of synaptic vesicle trafficking and intracellular degradation pathways.

The total proteome analysis identified numerous key changes in proteins related to synaptic function, intracellular transport, and cellular metabolism. Pathway enrichment analysis of upregulated proteins in the AAK1 KO cortex (Fig. 16A-B) showed significant activation in autophagy, proteasome pathways, and long-term potentiation, suggesting that AAK1 may play a regulatory role in neuronal protein degradation and synaptic plasticity. These findings align well with our earlier immunoblot data, in which synaptic-related proteins such as AP-2 were significantly reduced in AAK1 KO conditions, hinting towards a loss of endocytic control affecting broader pathways related to protein turnover and degradation. Conversely, the downregulated pathways (Fig. 16C) showed significant enrichment for ribosomal protein synthesis, nucleotide metabolism, and notably, SNARE interactions in vesicular transport. This implies that AAK1 depletion impairs fundamental vesicular (might be synaptic, autophagic, endocytic) trafficking mechanisms, contributing to the observed hyperactive and motor-deficient behavioral phenotypes. The downregulation in ribosomal functions also suggests a potential reduction in global protein synthesis in neurons, possibly affecting their ability to respond to synaptic demand.

The phosphoproteome results (Fig. 16D-F) revealed changes in phosphorylation of multiple key synaptic proteins, including ATG9A and MARK2, both of which are critical in synaptic vesicle dynamics and autophagy regulation (Caiola et al 2024). The upregulated KEGG pathways (Fig. 16E) in the phosphoproteome data indicated increased activity in synaptic vesicle cycling and signaling pathways involving endocrine regulation, while the downregulated pathways included synaptic signaling, such as glutamatergic and GABAergic synapses,

pointing towards synaptic dysfunction in AAK1 KO neurons. The cellular component analysis (Fig. 16G, H) showed notable shifts in synaptic organization, particularly with an increase in components associated with dendritic structures and a decrease in components related to axonal architecture. The biological process enrichment (Fig. 16I, J) emphasized positive regulation of synaptic vesicle fusion and revealed deficits in neurotransmitter receptor trapping, both of which are essential for maintaining efficient synaptic transmission. Here also importantly, the identification kinesin-related pathways suggest a possible role for AAK1 in trafficking processes, potentially extending to synaptic function. Given that our proteomic analysis also revealed enrichment in endocytic and clathrin-coated vesicle pathways, it is plausible that AAK1 influences both endocytic and synaptic trafficking. Specifically, AAK1 could be involved in the regulation of synaptic vesicle recycling or receptor transport to and from synapses, processes that are vital for synaptic plasticity and transmission. This is also in line with downregulated “neurofibrillary tangles” (NFT) and upregulated “microtubule minus ends” in cellular components pathway analysis from phosphoproteomic dataset which will be discussed later (Fig. 16G, H).

These results collectively support the hypothesis that AAK1 plays a crucial role in maintaining synaptic integrity, likely by regulating synaptic vesicle endocytosis and protein trafficking. The observed alterations in pathways related to synaptic activity and plasticity upon AAK1 depletion are consistent with the endocytic impairments highlighted in earlier parts of our study. Furthermore, the specific reduction of synaptic components coupled with increased autophagy-related processes might suggest a compensatory mechanism in response to impaired endocytosis.

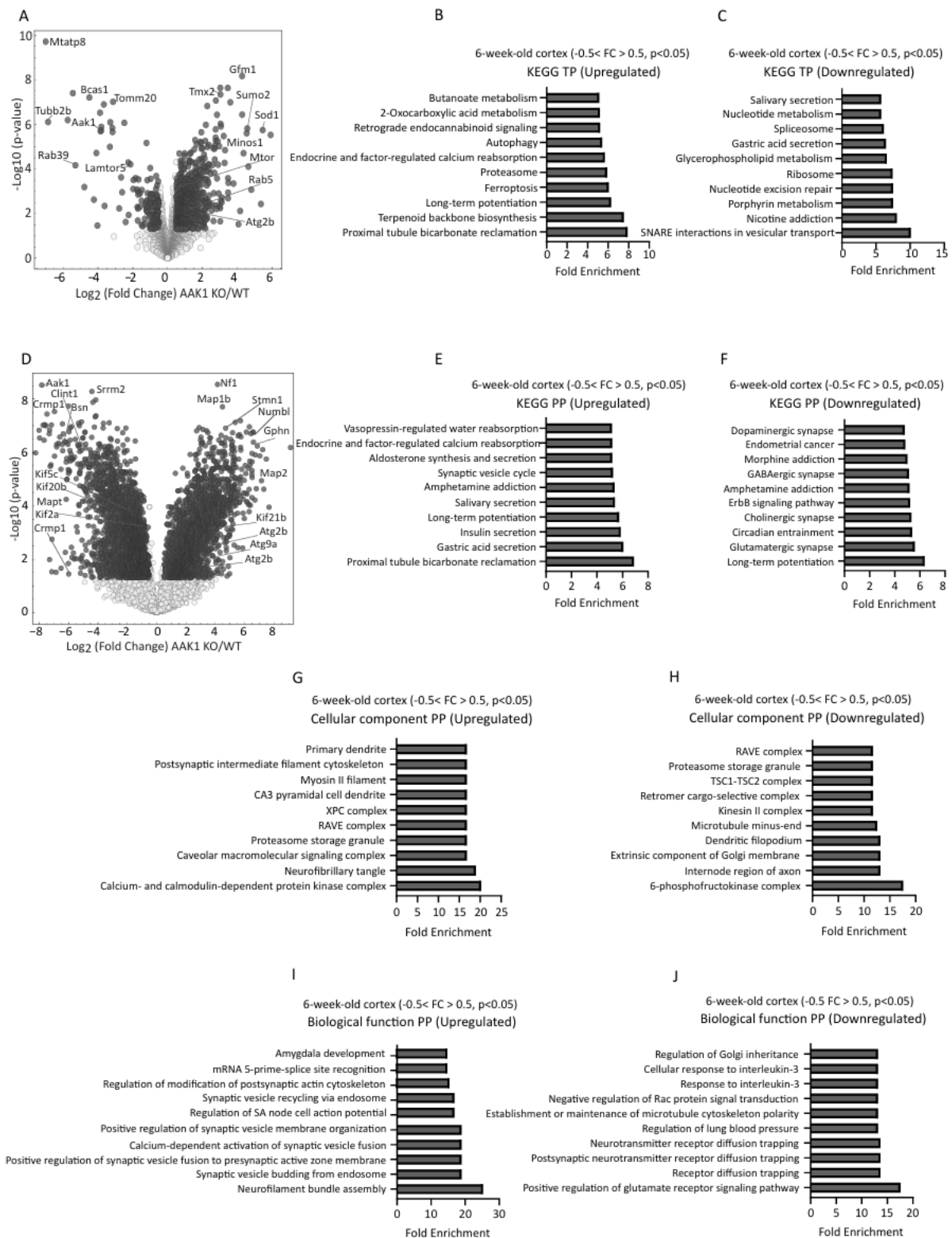


Figure 16: Comparative Analysis of Total and Phosphoproteome Pathway Enrichments in AAK1 KO Mouse Cortex. (A) Volcano plot shows differential expression of proteins between WT and AAK1 KO cortex, with notable proteins labeled in 6-week-old WT mice. Significantly changed proteins highlighted in dark grey (N=5). $-0.5 < \text{Log}_2 \text{fold change} > 0.5$ and $p\text{-value} < 0.05$. (B, C) KEGG pathway analysis of total proteome data (B) KEGG pathway enrichment analysis of upregulated proteins, filtered by fold change. (C) KEGG pathway enrichment analysis of downregulated proteins, also filtered by fold

change. (D) Volcano plot shows changes in phosphorylation levels across proteins in AAK1 KO cortex compared to WT. (E, F, G, H, I, J) Pathway enrichment analyses for upregulated and downregulated biological processes, cellular components, and KEGG pathways based on phosphoproteomic data. (E) Upregulated and (F) downregulated KEGG pathways of phosphoproteomic data. Cellular component analysis of (G) upregulated and, (H) downregulated phosphoproteomics data. Biological processes pathway analysis of (I) upregulated and (J) downregulated phosphoproteomic data.

10. AAK1 deficiency leads to age-dependent autophagic dysregulation and impaired autophagic flux

In addition to the identification of LC3-interacting region (LIR) motifs in AAK1 (Loi et al 2016), our proteomic analysis provided further support for AAK1's potential role in autophagy. The proteomics data revealed that AAK1 interacts with multiple components associated with autophagy and endocytic pathways highlighting its involvement in cellular trafficking mechanisms. This finding aligns with pathway enrichment analysis, which pointed to significant representation of autophagy-related pathways, including vesicle-mediated transport. Furthermore, phosphoproteomic analysis of AAK1 KO cortex identified phosphorylation sites on key autophagic regulators, suggesting that AAK1 may influence autophagy through phosphorylation-dependent mechanisms. These data (Fig. 16B, C, E, F, H, I) indicate that AAK1 might interface with autophagy machinery and potentially modulate protein trafficking and degradation processes. To investigate this hypothesis in the brain, we analyzed the expression of some autophagy markers in cortex from AAK1 KO mice at 6 and 12 weeks of age and assessed autophagic flux in primary neuronal cultures. Immunoblot analyses were conducted to evaluate key autophagy proteins, while autophagic flux experiments were designed to examine functional autophagy dynamics in the absence of AAK1.

Immunoblot analyses of autophagy-related markers, including LC3B (Fig. 17A), ATG5 (Fig. 17C), p62 (Fig. 17E), GABARAPL2 (Fig. 17G), and ATG9A (Fig. 17I), were performed in the cortex of 6-week-old KO mice. Quantification of these proteins (Fig. 17B, D, F, H, and J respectively) showed no significant differences between WT and KO groups, indicating that AAK1 deficiency does not appear to affect baseline levels of these autophagy markers at this age. In the 12-week-old cortex, a similar panel of autophagy markers was analyzed to assess any age-related changes in autophagy associated with AAK1 deficiency. Most autophagy markers, including LC3B (Fig. 17K), ATG5 (Fig. 17M), p62 (Fig. 17O), and GABARAPL2 (Fig. 17R), showed no significant differences between WT and KO mice (Fig. 17L, N, P, and S). However, a significant upregulation of ATG9A was observed in KO mice (Fig. 17T), as shown in Fig. 17U. ATG9A is a key component of the autophagic machinery, involved in vesicle trafficking to autophagosomes, and its upregulation in KO mice suggests that AAK1 may influence specific aspects of autophagy regulation, particularly in older animals.

To assess autophagic flux directly in neuronal culture, we used tamoxifen-inducible *CAG-Cre* system consists of Cre recombinase fused to a mutant form of the mouse estrogen receptor that does not bind to the natural ligand but is specifically activated by 4-hydroxytamoxifen (tamoxifen, Tmx). In the absence of tamoxifen, the Cre recombinase remains restricted to the cytoplasm; however, it translocates to the nucleus upon tamoxifen binding, allowing recombination to occur (Hayashi & McMahon 2002). Primary neuronal culture from tamoxifen inducible AAK1 KO pups (p0-p4) were subjected to basal conditions, nutrient deprivation (EBSS), and autophagy inhibition with BafA1, which blocks the fusion of autophagosomes with lysosomes, leading to autophagosome accumulation. In WT neurons, treatment with BafA1 significantly increased LC3B-II levels, confirming functional autophagic flux, as autophagosomes accumulated when their degradation was inhibited (Fig. 17Y). In contrast, AAK1 KO neurons showed a higher basal LC3B-II level compared to WT, suggesting an initial increase in autophagosome formation or impaired clearance. However, unlike in WT, BafA1 treatment did not lead to a significant increase in LC3B-II in KO neurons, indicating a potential disruption in autophagosome-lysosome fusion or impaired flux functionality. This lack of response to BafA1 in KO neurons suggests that autophagosomes may already be accumulating due to impaired clearance, and further inhibition does not exacerbate this effect. The combination of a higher basal LC3B-II levels and the unresponsive flux to BafA1 points toward a disruption in autophagic clearance rather than increased autophagosome formation alone. Notably, starvation with EBSS and treatment with EBSS + BafA1 did not induce an increase in LC3B-II levels in WT and KO neurons, which is line with literature (Kulkarni et al 2020), but WT neurons displayed a slight tendency for increased LC3B-II levels under these conditions. Together, these findings indicate that AAK1 deficiency may lead to an impairment in autophagosome processing, affecting overall autophagic flux and potentially contributing to cellular homeostasis disruptions.

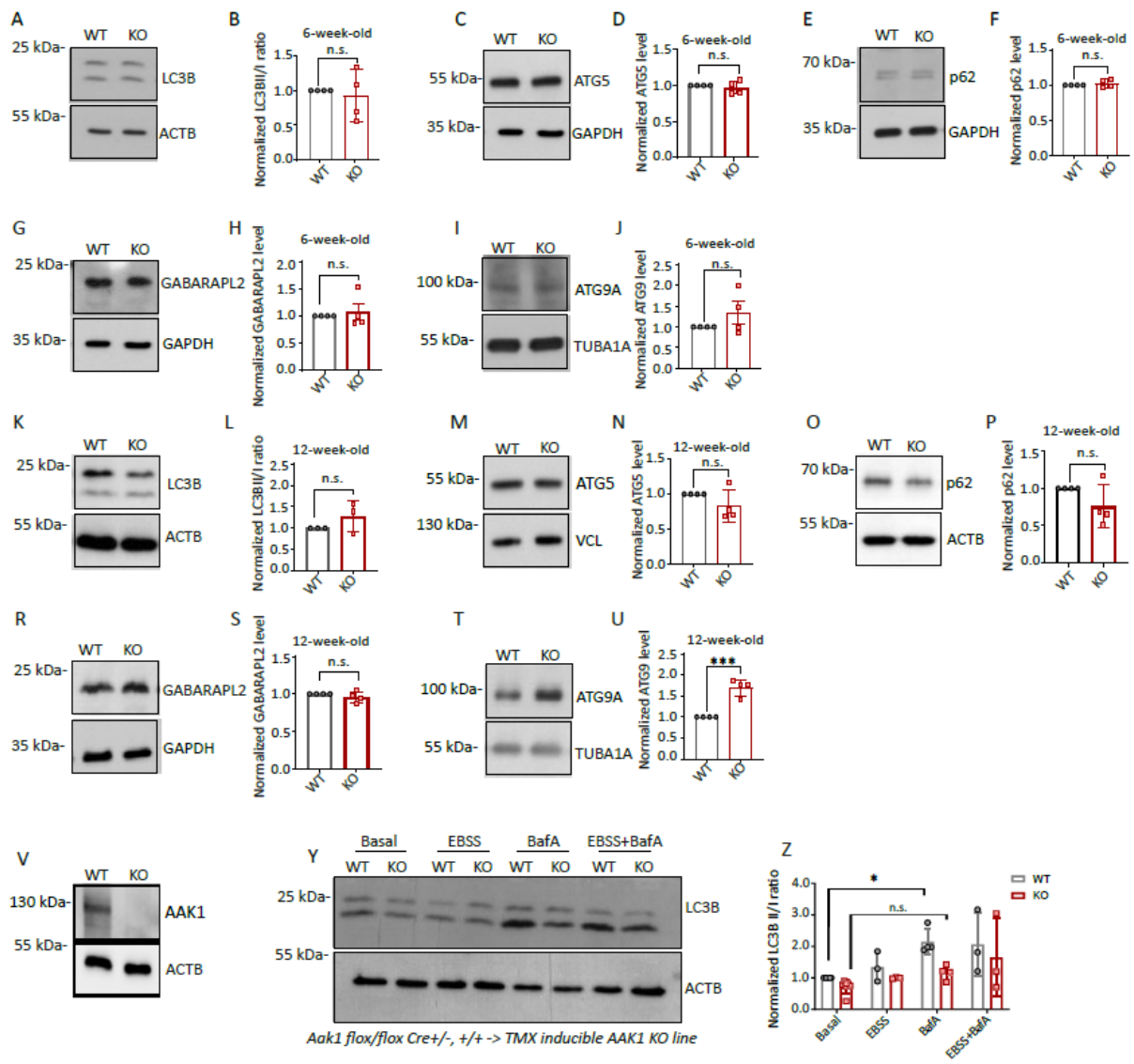


Figure 17: Effect of AAK1 depletion on autophagy in cortex and neurons. (A) Representative immunoblot of LC3B in cortex from 6-week-old WT and KO mice. ACTB was used as loading control for normalization of protein levels. (B) Quantification of LC3B expression level. Each dot represents one animal (N=4). One-tailed unpaired t-test was performed for comparison of WT and KO. (C) Representative immunoblot of ATG5 in cortex from 6-week-old WT and KO mice. GAPDH was used as loading control for normalization of protein levels. (D) Quantification of ATG5 expression level. Each dot represents one animal (N=4). One-tailed unpaired t-test was performed for comparison of WT and KO. (E) Representative immunoblot of p62 in cortex from 6-week-old WT and KO mice. GAPDH was used as loading control for normalization of protein levels. (F) Quantification of p62 expression level. Each dot represents one animal (N=4). One-tailed unpaired t-test was performed for comparison of WT and KO. (G) Representative immunoblot of GABARAPL2 in cortex from 6-week-old WT and KO mice. GAPDH was used as loading control for normalization of protein levels. (H) Quantification of GABARAPL2 expression level. Each dot represents one animal (N=4). One-tailed unpaired t-test was performed for comparison of WT and KO. (I) Representative immunoblot of ATG9A in cortex from 6-week-old WT and KO mice. TUBA1A was used as loading control for normalization of protein levels. (J) Quantification of ATG9A expression level. Each dot represents one animal (N=4). One-tailed unpaired t-test was performed for comparison of WT and KO. (K) Representative immunoblot of LC3B in cortex from 12-week-old WT and KO mice. ACTB was used as loading control for normalization of protein levels. (L) Quantification of LC3B expression level. Each dot represents one animal (N=3). One-tailed unpaired t-test was performed for comparison of WT and KO. (M) Representative immunoblot of ATG5

in cortex from 12-week-old WT and KO mice. VCL was used as loading control for normalization of protein levels. (N) Quantification of ATG5 expression level. Each dot represents one animal (N=4). One-tailed unpaired t-test was performed for comparison of WT and KO. (O) Representative immunoblot of p62 in cortex from 12-week-old WT and KO mice. ACTB was used as loading control for normalization of protein levels. (P) Quantification of p62 expression level. Each dot represents one animal (N=4). One-tailed unpaired t-test was performed for comparison of WT and KO. (R) Representative immunoblot of GABARAPL2 in cortex from 12-week-old WT and KO mice. GAPDH was used as loading control for normalization of protein levels. (S) Quantification of GABARAPL2 expression level. Each dot represents one animal (N=4). One-tailed unpaired t-test was performed for comparison of WT and KO. (T) Representative immunoblot of ATG9A in cortex from 12-week-old WT and KO mice. TUBA1A was used as loading control for normalization of protein levels. (U) Quantification of ATG9A expression level. Each dot represents one animal (N=4). One-tailed unpaired t-test was performed for comparison of WT and KO. (V) Representative immunoblot of AAK1 in primary neuronal culture from TMX inducible *Aak1 flox/flox, Cre+/-, Cre+/, Cre-/-* pups. ACTB was used as loading control. (Y) Representative immunoblot of LC3B in primary neuronal culture from TMX inducible *Aak1 flox/flox, Cre+/-, Cre+/, Cre-/-* pups. ACTB was used as loading control for normalization of protein levels. (Z) Quantification of LC3B expression level. Each dot represents one animal (Basal N=4, EBSS N=3, BafA1 N=4, EBSS+BafA1 N=3). Two-Way ANOVA with Holm-Sidak's multiple comparison test was performed. All Data are shown as mean \pm SEM. Significant differences are indicated by asterisks (* $p < 0.05$; ** $p < 0.01$; *** $p < 0.001$; **** $p < 0.0001$).

11. AAK1 depletion results in synaptic accumulation of ATG9A and changes in synaptic vesicular content

Given our interest in determining the effects of AAK1 depletion in the brain, we first performed immunostaining for ATG9A to examine where this autophagy-related protein accumulates in the AAK1 knockout brain. We also stained for VGLUT1 to determine whether ATG9A might be accumulating in synaptic regions. As shown in Fig. 18A and B, ATG9A exhibited increased colocalization with VGLUT1 in the cortex of AAK1 KO mice compared to WT controls. This colocalization was assessed using Manders' coefficient (M1) to quantify the overlap, and Pearson's correlation coefficient (r) to evaluate the correlation between ATG9A and VGLUT1 signals. The increased colocalization suggests that ATG9A accumulates specifically at synaptic sites in the absence of AAK1, potentially indicating impaired trafficking or increased autophagic activity within synaptic terminals.

To take a closer look at synaptic vesicle dynamics and better understand the consequences of AAK1 depletion and ATG9A accumulation, we employed transmission electron microscopy (TEM) to examine the synaptic ultrastructure in AAK1 KO mice (Fig. 18C). TEM analysis (Fig. 18D-F), allowed us to quantify the density of various vesicular structures, including clathrin-coated vesicles (CCVs), autophagosomes/autophagic vesicles (AVs), and synaptic vesicles (SVs). While the density of CCVs did not differ significantly between WT and KO groups, we observed a significant increase in the density of AVs and a reduction in synaptic vesicles (SVs) in the KO cortex.

The increased number of AVs in AAK1 KO animals may indicate either enhanced autophagic processes, potentially as a compensatory mechanism to clear accumulated material at the synapse, or an inefficient autophagic flux that leads to vesicle accumulation. Additionally, impaired microtubule-related transport might prevent AVs from undergoing retrograde movement to the cell soma for lysosomal fusion. On the other hand, the reduction in synaptic vesicles suggests an impairment in synaptic vesicle recycling or maintenance, which may directly contribute to deficits in synaptic transmission. This observation is particularly relevant when considered alongside the hyperactivity observed in behavioral tests and the motor deficits noted in the beam-walking assay. These motor phenotypes may be a consequence of impaired synaptic signaling resulting from synaptic vesicle depletion.

In summary, the accumulation of ATG9A at synaptic terminals and the subsequent reduction in synaptic vesicle density indicate that AAK1 plays a crucial role in maintaining proper vesicle trafficking and synaptic integrity. These findings link AAK1 to synaptic function, specifically through its involvement in synaptic vesicle recycling and autophagic processes, highlighting its potential importance in neuronal health and disease.

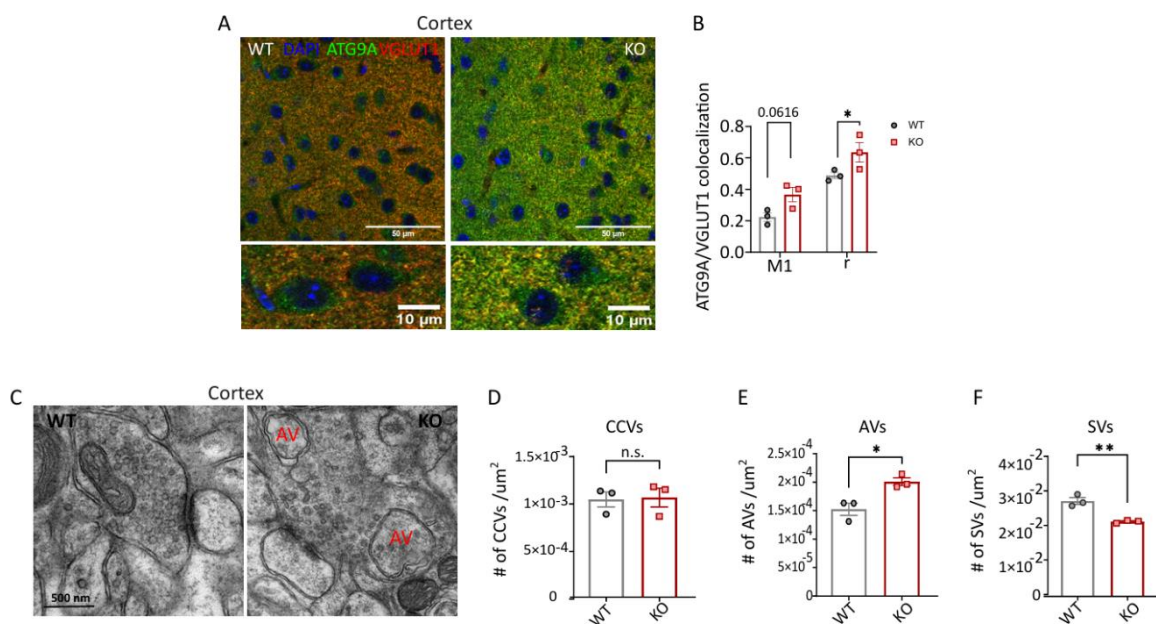


Figure 18: ATG9A accumulation and synaptic vesicular changes in AAK1 KO cortex. (A) Representative immunofluorescence images showing the colocalization of ATG9A (green) with VGLUT1 (red) in the cortex of 12-week-old WT and AAK1 KO mice. (B) Quantitative analysis of ATG9A and VGLUT1 colocalization in the cortex, using Manders' coefficient (M1) and Pearson's correlation coefficient (r). Each dot represents one animal (N=3). Multiple t-test was performed for comparison of WT and KO. (C) Representative EM images of synaptic regions in the cortex of WT and AAK1 KO mice, highlighting synaptic vesicles (SVs), clathrin-coated vesicles (CCVs), and autophagosomes (AVs). (D-F) Quantification of CCVs, AVs, and SVs per unit area. Each dot represents one animal (N=3). One-tailed unpaired t-test was performed for comparison of WT and KO. All Data are shown as mean \pm SEM. Significant differences are indicated by asterisks (* $p < 0.05$; ** $p < 0.01$; *** $p < 0.001$; **** $p < 0.0001$).

12. AAK1 depletion in cortical synaptosomes leads to dysregulation of autophagic flux

Here we investigated the synaptic localization of autophagic markers in AAK1-depleted synaptosomes, aiming to clarify AAK1's role in synaptic vesicular regulation. The schematic (Fig. 19A) outlines the workflow for isolating synaptosomes ensuring accurate separation of synaptic and cytoplasmic components. Afterwards synaptic enrichment validated by checking presence of PSD95 and SYT1 in the synaptosomal fraction (S) compared to cytoplasmic part (C) (Fig. 19B-E) via immunoblot, confirming successful isolation of synaptic structures from cortical slices. AAK1 KO synaptosomes exhibit significantly increased ATG9A levels, suggesting a buildup of autophagic components at synapses (Fig. 19F and G), while cytoplasmic ATG9A levels remain unchanged (Fig. 19H and I). This finding supports previous observations of synaptic ATG9A accumulation, potentially indicating disrupted autophagy or vesicular trafficking in AAK1-deficient neurons. Interestingly, LC3B levels show no significant differences in either synaptosomal or cytoplasmic fractions (Fig. 19J-M), this suggests that the increase in ATG9A might be a specific synaptic effect rather than indicative of a broader autophagic alteration. It is possible that the western blot analysis may not have been sensitive enough to detect subtle changes in LC3B levels that were evident in our EM data. To further understand synaptic autophagic flux, synaptosomes from WT and KO acute slices were subjected to conditions promoting autophagy by starvation (Artificial cerebrospinal fluid - ACSF) and treated with chloroquine (CQ) to block autophagic degradation. In WT synaptosomes, LC3B-II levels increase significantly under basal and basal+CQ conditions, indicating active autophagic flux. In contrast, AAK1 KO synaptosomes show reduced LC3B-II accumulation (Fig. 19O and P), suggesting impaired autophagic processing specifically at synapses. This synapse-specific autophagy impairment may underlie synaptic dysregulation observed in AAK1-deficient neurons.

These findings collectively reinforce the hypothesis that AAK1 is critical for maintaining synaptic autophagy and vesicle homeostasis, with its depletion leading to synaptic autophagy dysregulation. This synapse-specific autophagic disruption could play a role in the observed synaptic and behavioral deficits, linking AAK1 function to broader neurodegenerative and cognitive processes.

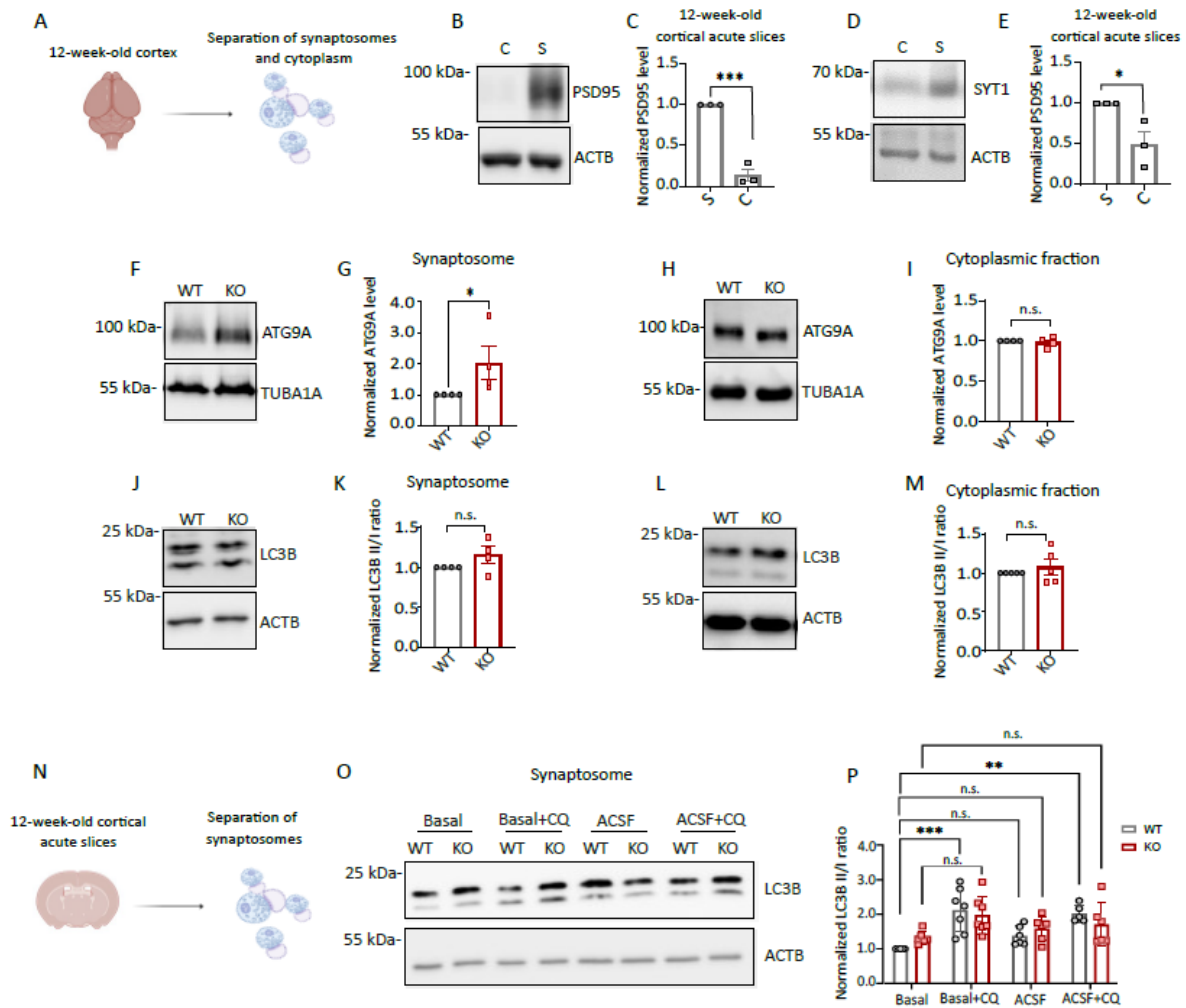


Figure 19: AAK1 depleted cortical synaptosomes shows dysregulation in autophagic flux. (A) Short schematic of experimental setup. WT mouse synaptosomes from cortex were used to validate synaptosome purification. (B) Representative immunoblot of PSD95 in cortical synaptosomes from 12-week-old WT mice. ACTB was used as loading control for normalization of protein levels. (C) Quantification of PSD95 expression level. Each dot represents one animal (N=3). One-tailed unpaired t-test was performed for comparison of synaptosome (S) and cytoplasmic fraction (C). (D) Representative immunoblot of SYT1 in cortical synaptosomes from 12-week-old WT mice. ACTB was used as loading control for normalization of protein levels. (E) Quantification of SYT1 expression level. Each dot represents one animal (N=3). One-tailed unpaired t-test was performed for comparison of synaptosome (S) and cytoplasmic fraction. (F) Representative immunoblot of ATG9A in cortical synaptosomes from 12-week-old WT and KO mice. TUBA1A was used as loading control for normalization of protein levels. (G) Quantification of ATG9A expression level. Each dot represents one animal (N=4). One-tailed unpaired t-test was performed for comparison of WT and KO synaptosomes. (H) Representative immunoblot of ATG9A in cytoplasmic fraction from 12-week-old WT and KO mice. TUBA1A was used as loading control for normalization of protein levels. (I) Quantification of ATG9A expression level. Each dot represents one animal (N=4). One-tailed unpaired t-test was performed for comparison of WT and KO cytoplasmic fractions. (J) Representative immunoblot of LC3B in cortical synaptosomes from 12-week-old WT and KO mice. ACTB was used as loading control for normalization of protein levels. (K) Quantification of LC3B expression level. Each dot represents one animal (N=4). One-tailed unpaired t-test was performed for comparison of WT and KO synaptosomes. (L) Representative immunoblot of LC3B in cytoplasmic fraction from 12-week-old WT and KO mice. ACTB was used as loading control for normalization of protein levels. (M) Quantification of LC3B expression level. Each dot represents one animal (N=4). One-tailed unpaired t-test was performed for comparison of WT and KO cytoplasmic fractions. (N) 12-week-old cortical acute slices. Separation of synaptosomes. (O) Synaptosome. Basal, Basal+CQ, ACSF, ACSF+CQ. WT, KO. 25 kDa, 55 kDa. LC3B, ACTB. (P) Normalized LC3B II/I ratio. Basal, Basal+CQ, ACSF, ACSF+CQ. WT, KO. n.s., **.

of WT and KO cytoplasmic fractions. (N) Schematic of experimental workflow for autophagy flux from acute slices. (O) Representative immunoblot of LC3B in cortical synaptosomes under different conditions from 12-week-old WT and KO mice. ACTB was used as loading control for normalization of protein levels. (P) Quantification of LC3B expression level. Each dot represents one animal (Basal N=5, Basal+CQ N=7, ACSF N=5, ACSF+CQ N=5). Two-Way ANOVA with Holm-Sidak's multiple comparison test was performed. All Data are shown as mean \pm SEM. Significant differences are indicated by asterisks (* $p < 0.05$; ** $p < 0.01$; *** $p < 0.001$; **** $p < 0.0001$).

13. Proteomics and phosphoproteomics from AAK1 KO cortical synaptosomes reveal significantly dysregulated vesicular and microtubule related pathways

Building on our prior findings indicating synaptic accumulation of ATG9A and altered synaptic vesicle numbers in AAK1-depleted mice, we aimed to further elucidate the molecular changes occurring within synapses. We performed proteomic (total 3216 protein detected and 1160 of them significantly dysregulated, p -value < 0.05) and phosphoproteomic (total 10111 phosphosites detected and 1425 of them significantly dysregulated, p -value < 0.05) analyses specifically in isolated cortical synaptosomes from AAK1 KO and WT mice to identify pathways involved in vesicular trafficking and potential microtubule-related mechanisms. The analyses revealed significant dysregulation in several key pathways, with a notable focus on synaptic vesicle dynamics and microtubule-associated processes.

In the total proteome (TP) data, KEGG pathway enrichment (Fig. 20B) highlights upregulated processes such as "Retrograde endocannabinoid signaling" and "Mitophagy," both of which are closely linked to vesicle trafficking and neuronal function. Especially, mitophagy might indicate compromised mitochondrial health, possibly due to impaired synaptic trafficking or altered microtubule dynamics, which are directly linked to proper mitochondrial distribution and turnover. Additionally, cellular component analysis (Fig. 20C) reveals an upregulation in "Endosome to plasma membrane transport vesicle" and "Cytoplasmic side of plasma membrane," supporting the evidence of vesicular dysregulation in AAK1-depleted synapses. These findings are consistent with our previous results of altered synaptic vesicle numbers, suggesting a broader disruption in endocytic and exocytic vesicle trafficking pathways.

For the phosphoproteomic (PP) data, KEGG analysis (Fig. 20F) indicates significant changes in synaptic pathways such as "GABAergic synapse" and "Long-term potentiation," both of which are critical to synaptic plasticity and depend on efficient vesicle dynamics. Cellular component enrichment (Fig. 20H) shows upregulation in "Dendritic branch," "Postsynaptic intermediate filament cytoskeleton," and "Cytoskeleton of presynaptic active zone." This suggests that microtubule and actin networks, which play vital roles in synaptic vesicle positioning and mobility, are significantly affected by AAK1 depletion. This could reinforce the

observed synaptic deficits, pointing toward a potential role of AAK1 in maintaining cytoskeletal integrity at the synapse.

The downregulated pathways in both datasets further point to synaptic dysregulation. For instance, "Synaptic vesicle cycle" (Fig. 20G) are significantly downregulated, implying impairments in the vesicle fusion and recycling processes that are crucial for effective neurotransmission. The downregulation of "Clathrin complex" (Fig. 20D), "Clathrin-coated endocytic vesicle", and "Clathrin-sculpted glutamate transport vesicle" (Fig. 20I) is especially relevant, given that AAK1 is known to regulate CME. This supports the notion that AAK1 depletion leads to impaired synaptic endocytosis, potentially explaining the reduced synaptic vesicle density we observed in earlier experiments.

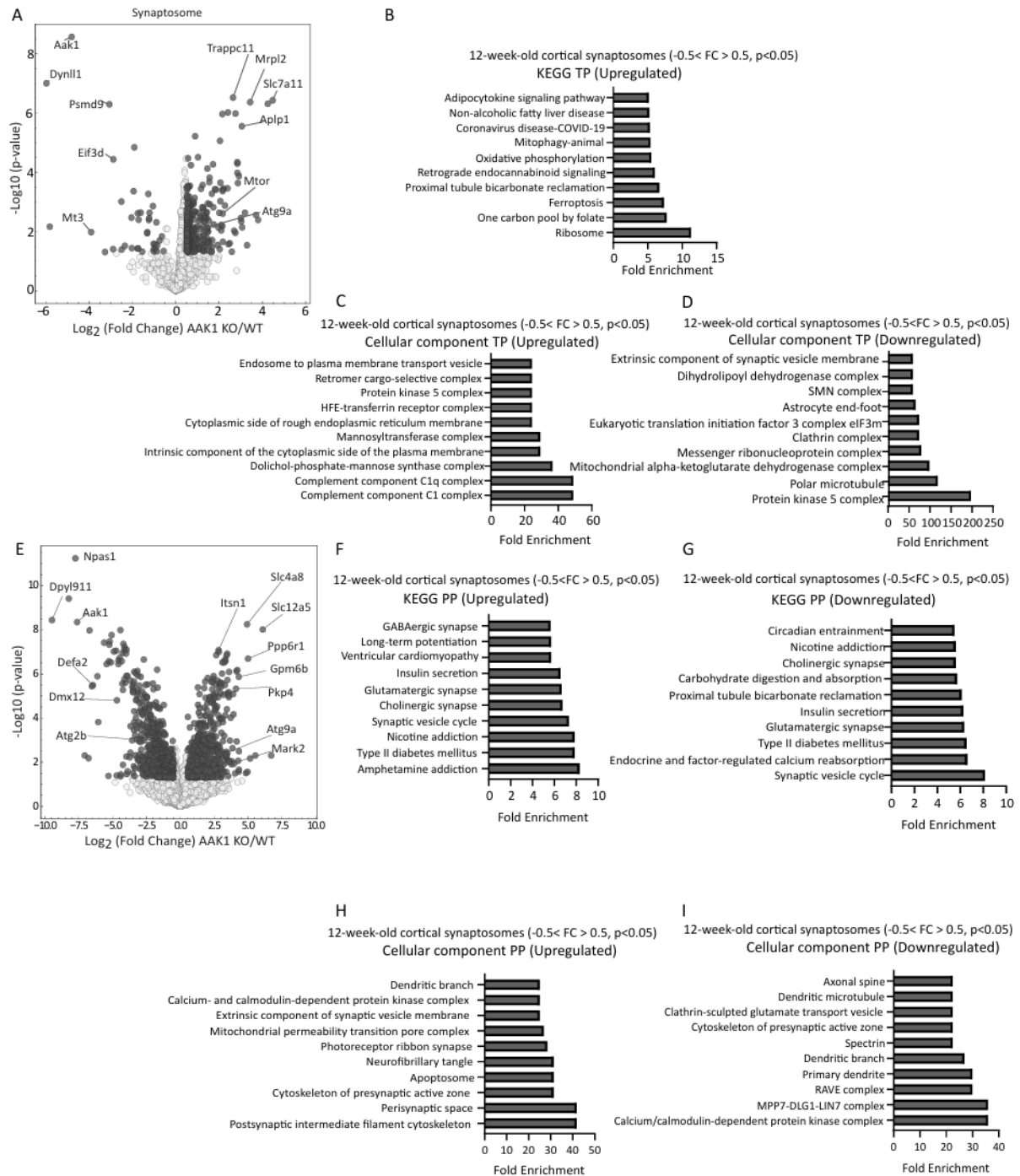


Figure 20: Comparative analysis of total and phosphoproteome pathway enrichments in AAK1 KO cortical synaptosomes. (A) Volcano plot shows differential expression of proteins between WT and AAK1 KO cortical synaptosomes at 12 weeks of age. Significantly changed proteins highlighted in dark grey (N=5). $-0.5 < \text{Log}_2 \text{fold change} > 0.5$ and $p\text{-value} < 0.05$. (B) KEGG pathway enrichment analysis of upregulated proteins. (C) Cellular component pathway enrichment analysis of upregulated and (D) downregulated proteins. (E) Volcano plot shows changes in phosphorylation levels across proteins in AAK1 KO cortical synaptosomes compared to WT. (F, G, H, I) Pathway enrichment analyses for upregulated and downregulated cellular components and KEGG pathways based on phosphoproteomic data. (F) Upregulated and (G) downregulated KEGG pathways of phosphoproteomic data. Cellular component analysis of (H) upregulated and, (I) downregulated phosphoproteomics data.

14. HEK cells plasma membrane-tagged TurboID approach reveals potential novel substrates of AAK1

To further explore the targets and substrates of AAK1, we utilized a stable HEK cell line expressing plasma membrane-targeted TurboID (*a generous gift from Jan Riemer Lab, cell line prepared by Sarah Gerlich*) (N-terminal Lyn11 tag – GCIKSKGKDSA (Inoue et al 2005)) to perform proximity labeling, both in the presence and absence of the AAK1 inhibitor, SGC-AAK1-1.

Figure 21A from (Cho et al 2020) illustrates the general workflow of the TurboID. Biotin, in combination with ATP, was utilized to generate reactive biotin intermediates that covalently attach to proximal proteins, effectively "tagging" them for isolation and analysis.

Figure 21B presents a volcano plot showing proteins enriched through TurboID labeling in HEK cells under basal conditions. Notably, proteins such as AP-2 μ , CLINT1, and MARK2 were significantly enriched in the dataset. These candidates are key regulators in CME and microtubule organization respectively. Figure 15C shows the differential protein abundance after treatment with an AAK1-specific inhibitor, SGC-AAK1-1, compared to the inactive control compound SGC-AAK1-1N. Firstly, the inhibition of AAK1 kinase activity resulted in a significant downregulation of AP-2 μ compared to the control condition. This result serves as an internal control to validate the efficacy of the inhibitor and demonstrates that the experimental approach worked effectively. Furthermore, proteins such as CLINT1, and MARK2 displayed significant changes, implicating these proteins as potential downstream targets of AAK1 or as directly influenced by its kinase activity. The marked changes in ATP5H, a subunit of ATP synthase, might reflect an AAK1-related influence on cellular energy metabolism. The enrichment of MARK2 is particularly noteworthy as it suggests a possible connection between AAK1 activity and microtubule dynamics, supporting the microtubule-related findings from earlier experiments.

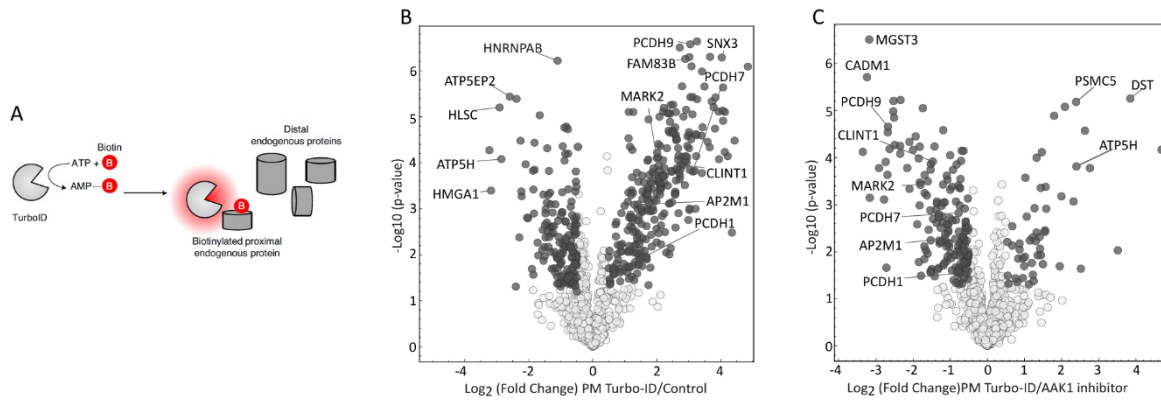


Figure 21: Investigation of AAK1 targets through TurboID proximity labeling and AAK1 inhibition in HEK cells. (A) General workflow of TurboID (B) Volcano plot showing differentially enriched proteins identified by TurboID in HEK cells, comparing biotinylated proteins with control conditions (no inhibitor treatment-basal condition). Significantly changed proteins highlighted in dark grey (N=4). $-0.5 < \text{Log}_2 \text{ fold change} > 0.5$ and $p\text{-value} < 0.05$. (C) Volcano plot showing differential protein abundance after AAK1 inhibition using SGC-AAK1-1 compared to control conditions (SGC-AAK1-1N). Significantly changed proteins highlighted in dark grey (N=4). $\text{Log}_2 \text{ fold change} > 0.5$ and $p\text{-value} < 0.05$.

15. AAK1 depleted primary neurons show decreased microtubule dynamics

To identify novel substrates of AAK1, we employed a multi-omics strategy that integrated phosphoproteomics, proteomics, TurboID proximity labeling in HEK cells, and immunoprecipitation (IP) datasets (Fig. 22A). With this combined data sets we narrowed down the potential substrates to MARK2 and CLINT1. Among these, we decide to focus on MARK2 which is a kinase involved in microtubule dynamics. Immunoblot analysis confirmed that the total protein level of MARK2 remained unchanged between WT and KO cortical synaptosomes (Fig. 22B and C), consistent with our previous proteomics results that indicated no significant difference in MARK2 abundance. Following this discovery, we aimed to explore how AAK1 depletion might influence microtubule dynamics. To achieve this, we utilized EB3-tdTomato tracking -a construct based on a +TIP protein that is associated with growing microtubule plus ends (Geraldo et al 2008, Nakagawa et al 2000) - to monitor microtubule plus-end dynamics in tamoxifen (TMX)-inducible AAK1 WT and KO primary neurons. Time-lapse imaging of EB3-positive microtubule comets demonstrated a significant reduction in EB3 puncta velocity in KO neurons compared to WT (Fig. 22D-F), as indicated by the decreased speed of EB3 puncta along the neurites. Representative kymographs further highlight the altered dynamic behavior in AAK1 KO neurons (Fig. 22E). These findings suggest that AAK1 depletion disrupts microtubule polymerization rates, likely mediated through impaired regulation of microtubule-associated proteins, such as MARK2.

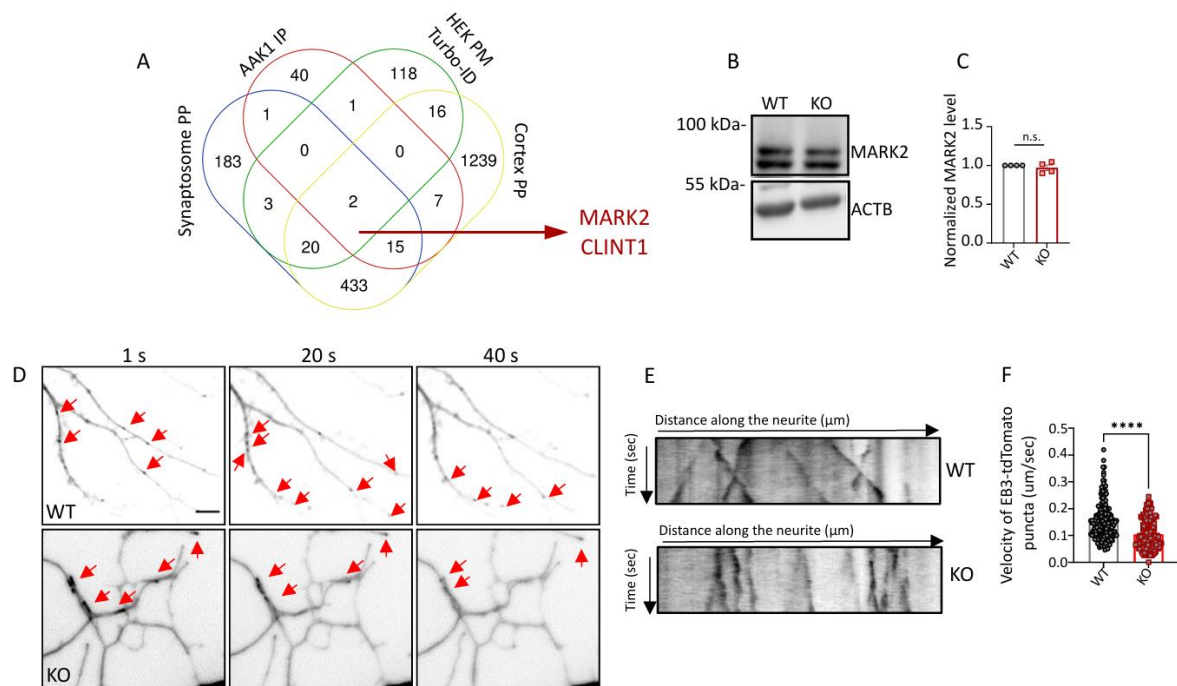


Figure 22: Microtubule dynamics in AAK1 KO neurons. (A) Venn diagram depicting the overlap among different phosphoproteomics and proteomics datasets: Synaptosome phosphoproteomics (PP), AAK1 IP, HEK Plasma Membrane (PM) Turbo-ID, and cortical phosphoproteomics. (B) Representative immunoblot of MARK2 in cortical synaptosomes from 12-week-old WT and AAK1 KO mice. ACTB was used as loading control for normalization of protein levels. (C) Quantification of MARK2 expression level. Each dot represents one animal (N=4). One-tailed unpaired t-test was performed for comparison of WT and AAK1 synaptosomes. (D) Representative images of EB3-tdTomato dynamics in primary AAK1 WT and KO cortical neurons at 1s, 20s, and 40s. Arrowheads indicate microtubule plus end movement. (E) Corresponding kymographs of (D) time-lapse images. Kymographs show decreased dynamics in AAK1 KO neurons. (F) Quantification of EB3-tdTomato puncta velocity in AAK1 WT and KO neurons, demonstrating a significant reduction in microtubule growth rates in AAK1 KO neurons. Each dot represents one comet from N=3 independent experiments. Two-tailed unpaired t-test was performed for EB3-tdTomato puncta comparison of WT and AAK1 KO neurons. All Data are shown as mean \pm SEM. Significant differences are indicated by asterisks (* $p < 0.05$; ** $p < 0.01$; *** $p < 0.001$; **** $p < 0.0001$).

16. AAK1 depletion impairs autophagosome trafficking in neurons

Since our results indicated less dynamic microtubules in KO neurons compared to WT, we sought to determine how AAK1 depletion affects autophagosome motility. Given that the proper transport of AVs depends on dynamic microtubule networks and the binding of motor proteins like dynein (Kimura, Noda & Yoshimori 2008) we performed live-imaging of LC3B-RFP in tamoxifen-induced AAK1 WT and KO neurons to assess the motility of autophagosomes. Time lapse imaging showed that LC3B-RFP puncta in WT neurons moved more dynamically compared to AAK1 KO neurons (Fig. 23A and B). Quantification of puncta velocity also revealed that LC3B-RFP puncta velocity (Fig. 23C) also reduced compared to WT neurons. Additionally, the density of LC3B-RFP puncta along the neurites was reduced in KO neurons, suggesting impaired autophagosome formation or transport (Fig. 23D). No significant

difference in the velocity of directionality of movement (anterograde vs. retrograde) was observed between WT and KO neurons (Fig.23E).

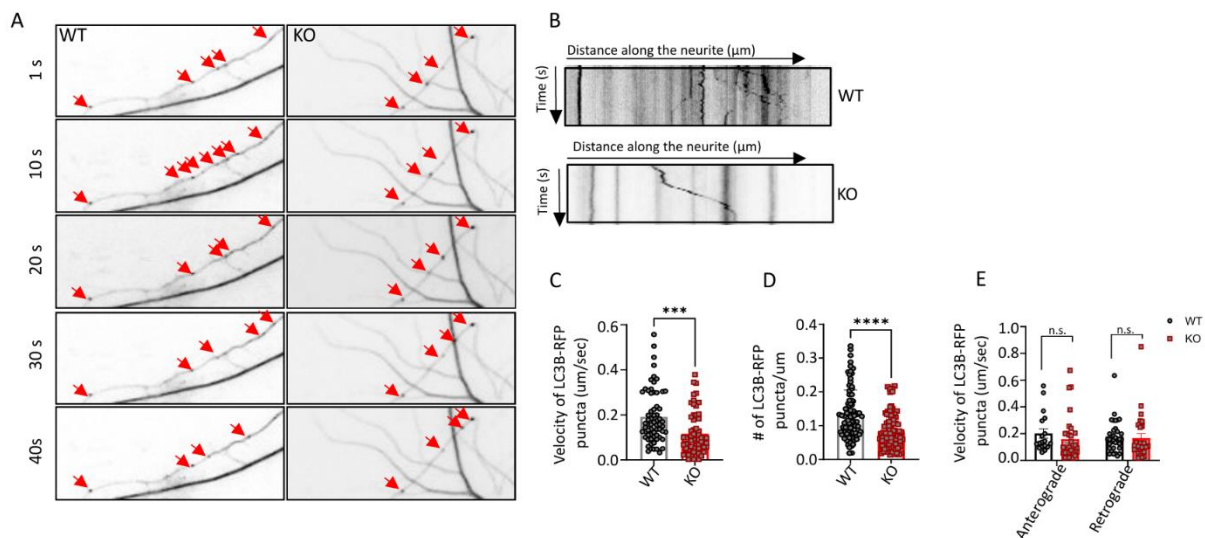


Figure 23: AAK1 KO neurons have impaired autophagosome trafficking. (A) Representative time lapse images of LC3B-RFP puncta (indicated with red arrow heads) in WT and TMX induced AAK1 KO neurons, recorded every 10 seconds for 40 seconds. (B) Corresponding kymographs of time lapse images. (C) Quantification of LC3B-RFP puncta velocity in AAK1 WT and KO neurons, demonstrating a significant reduction in velocity in AAK1 KO neurons. Each dot represents one LC3B puncta from N=3 independent experiments. Two-tailed unpaired t-test was performed for LC3B-RFP puncta comparison of WT and AAK1 KO neurons. (D) Quantification of number LC3B-RFP puncta/um in AAK1 WT and KO neurons, demonstrating a significant reduction in puncta number in AAK1 KO neurons compared to WT. Each dot represents one LC3B puncta from N=3 independent experiments. Two-tailed unpaired t-test was performed for LC3B-RFP puncta comparison of WT and AAK1 KO neurons. (E) No significant difference is observed in velocity of the directionality (anterograde vs. retrograde) between WT and KO neurons. Each dot represents one LC3B puncta from N=3 independent experiments. Multiple t-test was performed for LC3B-RFP puncta comparison of WT and AAK1 KO neurons. All Data are shown as mean \pm SEM. Significant differences are indicated by asterisks (* $p < 0.05$; ** $p < 0.01$; *** $p < 0.001$; **** $p < 0.0001$).

17. Inhibition of AAK1 kinase activity results in MARK2 relocalization in synapses

Since we did not observe any differences in total MARK2 levels within synaptosomes but found enrichment of MARK2 on the plasma membrane (PM) under basal conditions, as well as its downregulation upon treatment with the AAK1 inhibitor SGC-AAK1-1, we pursued to further investigate MARK2 localization in synapses. To do so, we isolated synaptosomes from acute brain slices treated with either AAK1 inhibitor or inactive control compound (Fig. 24A). Isolation of plasma membrane proteins from synaptosomes was validated by confirming the presence of E-cadherin (CDH1) in the PM fraction (Fig. 24B). Immunoblotting results showed that

inhibition AAK1 kinase effectively reduced phosphorylation of AP-2 μ (Fig. 24C), thus confirming the efficacy of the inhibition treatment. There was no observed change in total AP-2 μ (Fig. 24D). A dose-response experiment showed that 12.5 μ M SGC-AAK1-1 was sufficient to achieve stable inhibition of AAK1 kinase activity (Fig. 24E). Synaptosome fractionation from acute cortical slices revealed that MARK2 is present at the plasma membrane under basal conditions; however, AAK1 inhibition led to a substantial reduction of MARK2 in the plasma membrane (Fig. 24F and G). This shift was accompanied by a slight increase in the cytoplasmic fraction. These data suggest that AAK1 activity is necessary for localizing MARK2 at synaptic plasma membranes, possibly regulating microtubule interactions crucial for synaptic stability.

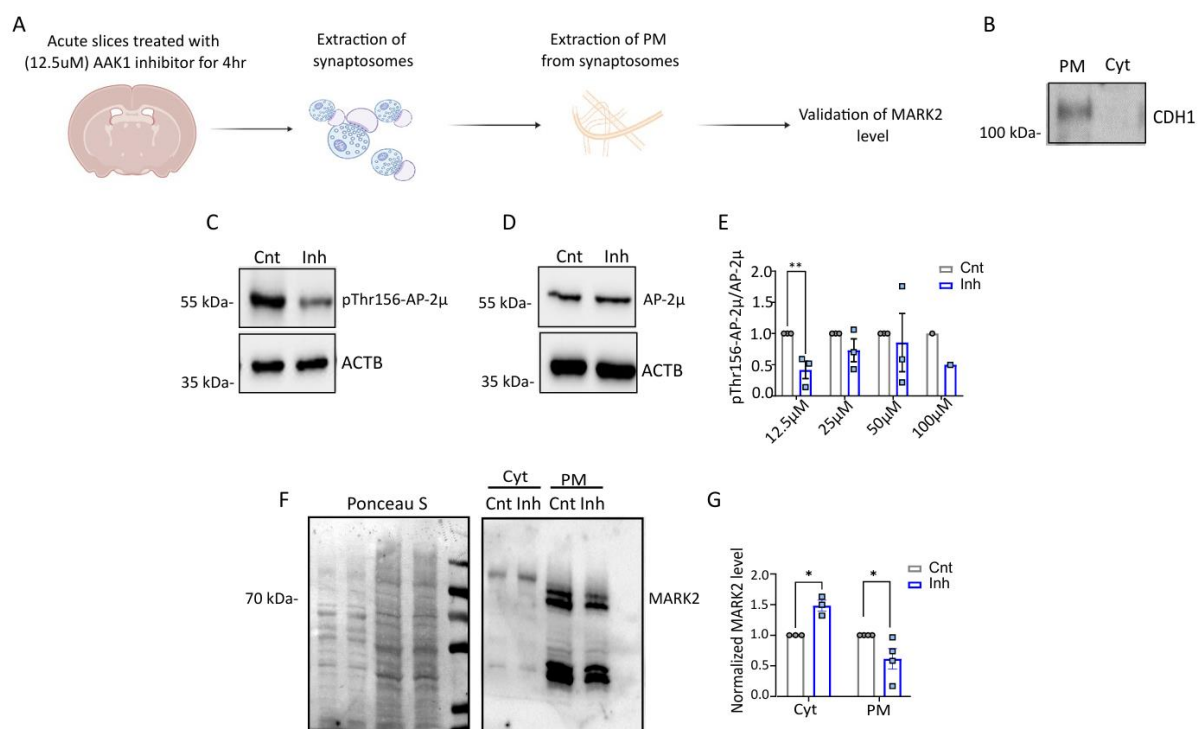
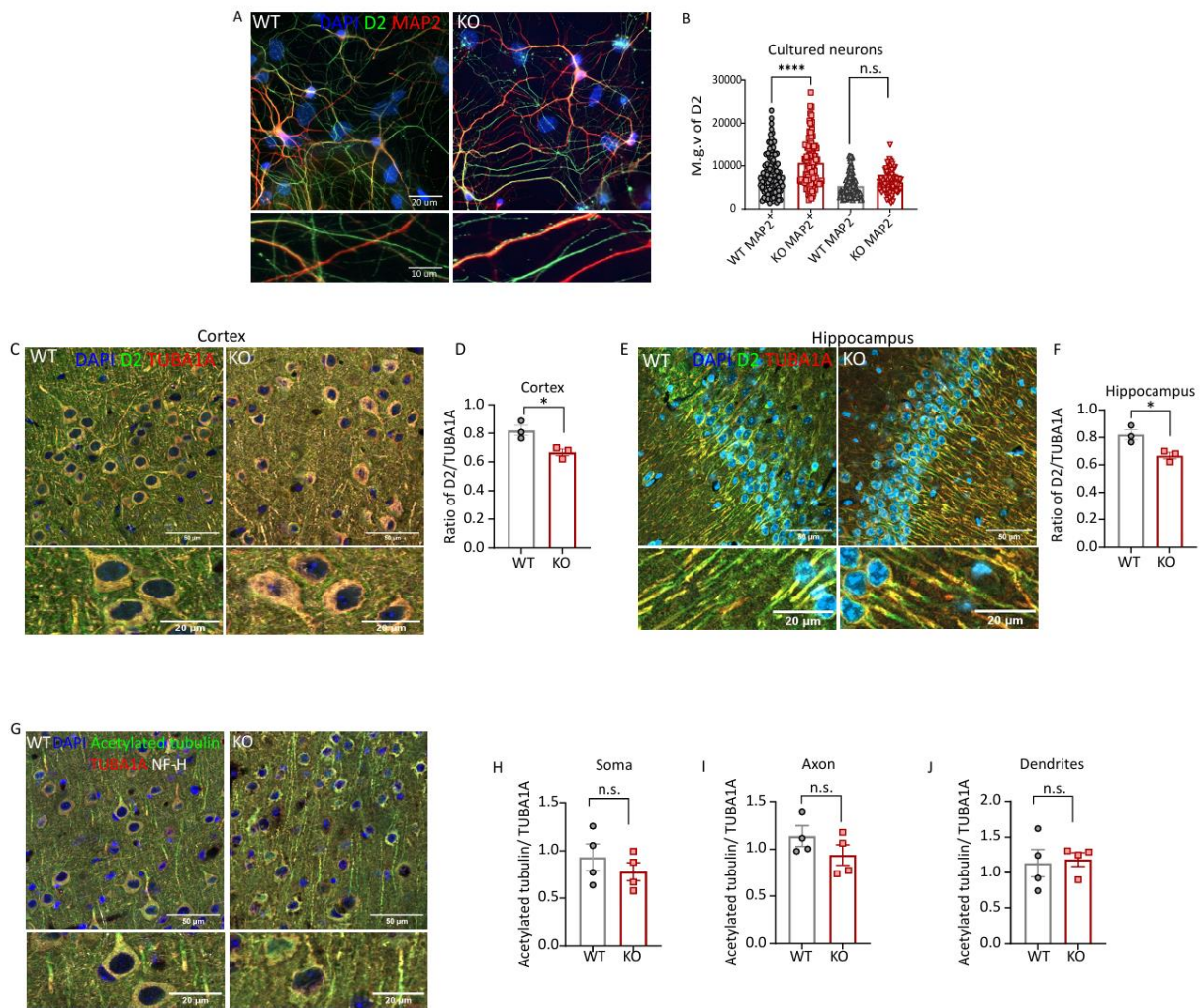


Figure 24: Inhibition of AAK1's kinase activity results in reduced MARK2 localization on PM (A) Short schematic of experimental setup. Acute slices treated with kinase inhibitor SGC-AAK1-1 or inactive control compound SGC-AAK1-1N for 4hr. Afterwards synaptosomes were isolated as mentioned above and this step followed by plasma membrane isolation. (B) Representative immunoblot of plasma membrane protein E cadherin (CDH1) as proof of principal. (C) Representative immunoblot of pThr¹⁵⁶- AP-2 μ in 12-week-old acute slices treated with SGC-AAK1-1 (Inh in WB) or SGC-AAK1-1N (Cnt in WB) (B). ACTB was used as loading control for normalization of protein levels. (D) Representative immunoblot of AP-2 μ in 12-week-old acute slices treated with SGC-AAK1-1 or SGC-AAK1-1N. ACTB was used as loading control for normalization of protein levels. (E) Quantification of pThr¹⁵⁶-AP-2 μ / AP-2 μ . Each dot represents one animal (N=3). Multiple t-test was performed for comparison of WT and AAK1 synaptosomes. (F) Representative Ponceau S stain and immunoblot of MARK2 from PM and cytosolic (Cyt) samples treated with SGC-AAK1-1 or SGC-AAK1-1N for 4hr. (G) Quantification of MARK2 level in PM and Cyt from 12-week-old cortical synaptosomes after treatment with SGC-AAK1-1 or SGC-AAK1-1N. Ponceau S was used as loading control for normalization of protein levels. Each dot represents one animal (N=3 for Cyt and N=4 for PM). Multiple t-test was performed for

comparison. All Data are shown as mean \pm SEM. Significant differences are indicated by asterisks (* $p < 0.05$; ** $p < 0.01$; *** $p < 0.001$; **** $p < 0.0001$).

18. AAK1 depletion results in changes in microtubule dynamics both in-vivo and in-vitro

To understand whether AAK1 depletion has any microtubule related manifestation in neurons, we performed immunostaining with delta-2 tubulin (D2) and acetylated tubulin in cultured primary neurons (DIV 14-16) and in brain sections of 12-week-old WT and AAK1 KO mice. In cultured neurons, we immunostained with D2 and MAP2 to examine the distribution and relative intensity of D2 between MAP2-positive (dendritic) and MAP2-negative (non-dendritic or axonal) regions (Fig. 25A) Interestingly, quantitative analysis of D2 levels showed a significant increase in D2 intensity in MAP2+ dendrites of KO neurons compared to WT, while no significant difference was observed in MAP2-negative processes (Fig. 25B). These findings suggest that AAK1 depletion results in an increased stabilization of microtubules in dendritic regions of cultured neurons. Contrary to the results in cultured neurons, D2 levels were significantly reduced in both the cortex and hippocampus of 12-week-old AAK1 KO brain sections when normalized to TUBA1A, a general microtubule marker (Fig. 25C–F). The discrepancy between cultured neurons and brain sections could be due to the differences in the developmental timing and microenvironmental context. To further assess microtubule stability, we examined acetylated tubulin levels in different compartments of the cortex using acetylated tubulin and TUBA1A co-staining (Fig. 25G). Acetylated tubulin is a marker of stable microtubules, typically present in less dynamic, mature microtubule networks (Janke & Chloë Bulinski 2011). Analysis of acetylated tubulin/TUBA1A ratios revealed no significant differences between WT and KO mice in the soma, axon, or dendritic compartments (Figure 25H–J), suggesting that AAK1 depletion may selectively impact more dynamic microtubules, such as those marked by delta-tubulin, rather than mature, stable microtubules.



V. Discussion

AAK1 is a kinase known for its well-established role in CME by phosphorylating AP-2, thereby enhancing efficiency of vesicle formation (Conner & Schmid 2002, Ricotta et al 2002). Apart from its canonical role in CME, various studies suggest that AAK1 likely has versatile biological functions extending beyond vesicular trafficking. Notably, AAK1 has been shown to control dendritic development in hippocampal neurons as a substrate of NDR1 and its depletion results in increased dendritic branching and length, underscoring its importance in neuronal morphogenesis (Ultanir et al 2012). Beyond neuronal development, AAK1 also appears to contribute to immune regulation by mediating the internalization of MHC class I molecules, an effect dependent on its recruitment by LC3B (Loi et al 2016). This finding positions AAK1 at the intersection of endocytic pathways and immune responses, further broadening its physiological relevance. Additionally, different studies have highlighted AAK1's potential role in disease physiology. AAK1 has been implicated in neurological disorders and neurodegenerative conditions, together with genetic studies identifying it as disease associated candidate gene (Fu et al 2018, Heaton et al 2020, Latourelle et al 2009, Liu et al 2021, Shi, Conner & Liu 2014). Despite these notable associations, the specific role of AAK1 in the brain—especially the consequences of its depletion *in vivo*—remains largely unexplored.

In this study, we sought to understand the role of AAK1 in the brain by progressively narrowing our focus from a broad, organ-level perspective down to synaptic organelles. Our aim was to elucidate AAK1's function – primarily through its depletion at the protein level- and to identify novel substrates within the brain. Our findings not only highlight AAK1's established role in synaptic regulation but also reveal its involvement in other essential processes, including microtubule dynamics and autophagosome trafficking, both of which are vital for neuronal function. To explore these aspects, we employed AAK1 KO mouse models alongside a comprehensive set of biochemical, proteomic, and imaging-based techniques. Through this multi-faceted approach, we demonstrated that AAK1 is crucial for regulating microtubule dynamics, autophagosome trafficking, and the localization of key substrates, such as MARK2, within synaptic compartments. These roles underscore AAK1's importance in maintaining synaptic stability and plasticity.

1. AAK1 expression in the brain shows regional and temporal diversity

In the analysis of WT mouse brains, we found that AAK1 protein expression varies significantly across different brain regions, with particularly high expression in the cortex compared to the hippocampus, striatum, cerebellum, hindbrain, and midbrain. The regional enrichment in the cortex suggests that AAK1 may play a more prominent role in cortical functions, which are

essential for cognition, sensory processing, and motor planning (Cadwell et al 2019, Rakic 2009).

Furthermore, the developmental analysis of AAK1 expression in the cortex revealed a temporal pattern. AAK1 levels were lowest in P7 mice, increased steadily until reaching a peak at 3 months, and subsequently declined by 12 months. This pattern suggests that AAK1 is particularly critical during the maturation phase of cortical synapses, coinciding with a peak in synaptic refinement and plasticity (Nazir et al 2018, Wong & Ghosh 2002). The decline in AAK1 levels by 12 months may reflect the reduction in synaptic plasticity or a shift towards synaptic maintenance instead of active remodeling, which aligns with age-related shifts in synaptic function (Ge et al 2007). Interestingly, AAK1's expression pattern closely parallels that of SYT1, which also peaks at 3 months of age. SYT1 is crucial for synaptic vesicle release and overall synaptic activity (Nazir et al 2018, Südhof 2013). These findings suggest that AAK1 might have context specific regulatory roles. It could be integral to synaptic development and maintenance, particularly within the cortex, with its peak expression at 3 months indicating a role in synaptic maturation and plasticity. Additionally, the age-dependent decline may point towards an evolving role for AAK1 in synaptic stability, with intriguing implications for further studies into neurodegenerative conditions, where synaptic dysfunction is a common feature (Henstridge, Tzioras & Paolicelli 2019).

2. AAK1 KO and cKO mice display hyperactivity, delayed growth and motor deficit

In our study, we generated a global AAK1 KO mouse model to dissect the role of AAK1 in the brain *in vivo*. AAK1 KO mice exhibited significant growth delays starting from early developmental stages, which was reflected by their reduced body weight compared to WT mice. Notably, this reduction in body weight was not due to weight loss over time, but rather a failure to gain weight at the same rate as WT mice, with this disparity becoming apparent around 2-3 weeks of age and persisting into adulthood for both males and females. Despite these differences in overall weight, there were no significant changes in body composition, such as lean mass, fat percentage, or bone growth, suggesting that the effect of AAK1 depletion was more specific to growth regulation rather than indicative of broader developmental abnormalities. These findings may suggest a systemic role for AAK1 in regulating overall metabolic or growth processes.

Further examination of brain morphology revealed differences between AAK1 KO and WT mice. At 3 weeks of age, the cortical area was significantly reduced in KO mice, suggesting impaired cortical development. This observation underscores the critical role of AAK1 in

ensuring proper cortical growth and maturation. Beyond its classical role in CME, AAK1 has also been implicated in other essential neurodevelopmental processes, including dendritic development and synaptic plasticity (Ultanir et al 2012). Interestingly, by 12 weeks, the cortical area had normalized, indicating some compensatory growth during maturation. However, the thickness of the corpus collosum remained reduced in KO mice at 12 weeks, suggesting long-term deficits in axonal growth. Given that the corpus collosum is crucial for communication between the brain's hemispheres, reduced thickness could potentially impair information processing and synchronization between cortical areas (Edwards et al 2020, Piscopo et al 2018).

While the overall gross morphology of the brain was not dramatically altered between WT and KO mice, there were subtle regional size differences observed at early stages. The reduced cortical and hippocampal areas at 3 weeks suggest that AAK1 is involved in neurodevelopmental processes specific to these brain regions during early postnatal development. These changes might also imply a temporal regulation where AAK1 activity is more crucial during specific windows of neuronal differentiation and growth, particularly in areas important for cognitive functions like memory and learning. Immunohistochemical analysis of cortical and hippocampal sections showed no major alterations in the distribution of neurons, astrocytes, or progenitor markers between WT and KO animals. This suggests that AAK1 deficiency may not drastically affect early neuronal differentiation or glial development but may instead influence other aspects of neuronal maturation or synaptic integration that could lead to the observed changes in brain structure. Additionally, the observed phenotypes in both brain and body weight could be attributed to impairments in CME. CME components are known to control mitotic progression independently of their classical roles in endocytosis, localizing to the centrosome or mitotic spindle to regulate spindle morphology and cytokinesis (Cambior-Perujo et al 2024, Lehtonen et al 2008, Olszewski et al 2014, Royle, Bright & Lagnado 2005). The reduction in body weight observed in AAK1 KO animals is also consistent with previous findings from AP-2 μ KO models, which indicate that impairments in the AP-2 complex can influence overall development (Kononenko et al 2017).

AP-2 is a well-known target of AAK1-mediated phosphorylation, playing a crucial role in CME (Conner & Schmid 2002). In AAK1 KO mice, AP-2 α and AP-2 μ levels were significantly downregulated at both 6-week and 12-week time points. This is consistent with AAK1's established role in stabilizing AP-2 components through phosphorylation (Conner & Schmid 2002, Ricotta et al 2002). Moreover, the level of CHC, a key endocytic protein, remained unchanged, indicating that the loss of AAK1 selectively affected AP-2 components rather than the entire CME machinery which is in line with a study showed that AP-2 subunits contribute independently to SV endocytosis (Gu et al 2013). Immunostaining of primary cultured neurons

from KO mice showed a substantial decrease in AP-2 α levels in MAP2-positive dendrites, and a decreased internalization of Tfn 488. This decreased endocytosis efficiency directly supports a critical role for AAK1 in CME, particularly in neurons where synaptic vesicle recycling relies on efficient endocytosis (Kononenko et al 2014, Slepnev & De Camilli 2000).

To understand whether neuronal function of AAK1 differs or results in different consequences we also created cKO AAK1 under *CaMKII α* promoter which is expressed primarily in excitatory neurons of the forebrain (Dragatsis & Zeitlin 2000). The growth curve indicates that AAK1 cKO mice exhibit lower body weights compared to their WT counterparts, similar to the global AAK1 KO phenotype. This reduction in body weight could be indicative of a systemic influence of AAK1 on metabolic processes or neuronal circuits that regulate growth and body weight. The femur length in cKO mice is slightly shorter, approaching significance. In the global KO model, the reduction in femur length was not significant. This suggests that the growth phenotype observed in the global KO may be partially due to non-neuronal effects, as the impact on femur length is exaggerated when AAK1 is knocked out specifically in neurons. It has been known that bone remodeling is a complex process regulated by various factors, including endocrine, paracrine, mechanical, and, more recently, neuronal influences. Interestingly, multiple neurodegenerative diseases, such as AD, PD, epilepsy, and autism spectrum disorders, have been associated with decreased bone marrow density (Ducy et al 2000, Kelly, Sidles & LaRue 2020, Takeda et al 2002). This suggests a potential link between neurological health and bone integrity. For future investigations, incorporating bone marrow density measurements alongside femur size assessments could provide a more comprehensive understanding of the phenotypic characteristics and help clarify how AAK1 impacts bone physiology.

AAK1 cKO mice have a significant reduction in lean mass and an increase in water percentage. Interestingly, there was no significant difference in fat content. In global KO mice we did not observe any significant change in MRI results. This might suggest that the neuronal function of AAK1 contributes to body composition, possibly via neuroendocrine signaling that influences lean body mass. Endocytosis, particularly CME, is critical for regulating receptor availability at the cell surface, which in turn influences signaling cascades that control cellular growth, proliferation, and differentiation (Puthenveedu & von Zastrow 2006, Sorkin & von Zastrow 2009). CME facilitates the internalization of receptor tyrosine kinases (RTKs) like the insulin receptor and epidermal growth factor receptor (EGFR) (Goh & Sorkin 2013, Gur G 2000, Sorkin & von Zastrow 2009, Yoneyama et al 2018). RTKs are central to many pathways that regulate growth and metabolism. When internalized through CME, these receptors can be either degraded or recycled, determining the strength and duration of their downstream signaling. AAK1's regulation of AP-2-dependent endocytosis thus allows precise control over RTK signaling, and disruptions in this mechanism could lead to altered cellular responses to

growth factors, contributing to metabolic changes (Goh & Sorkin 2013, Gur G 2000). Analysis of the cortex area and gross morphology did not reveal significant changes in the cKO compared to WT. This is in contrast with the global KO, where cortical thinning was observed, suggesting that cortical thinning may be largely driven by non-neuronal effects or requires AAK1 in both neurons and glial cells to manifest.

There is a marked reduction in AP-2 α levels in the cKO brain, similar to what was seen in the AAK1 KO model. Given that AP-2 α is a critical component of CME machinery, this decrease supports AAK1's role in regulating endocytosis within neurons. In contrast to AP-2 α , AP-2 μ and CHC levels are not significantly altered in the cKO compared to WT. This could indicate that AP-2 μ and CHC are regulated by AAK1 in non-neuronal cells, or that their regulation requires AAK1 activity across a broader cell population than just excitatory neurons. Given AAK1's known role in phosphorylating adaptor proteins to regulate CME, its neuron-specific deletion and the reduction in AP-2 α may indicate a direct effect on synaptic vesicle cycling, which is essential for neurotransmission (Asmerian et al 2024, Gu et al 2013).

In OF experiments both global and cKO mice showed clear differences in movement patterns between WT and KO mice. WT mice exhibit more uniform exploration of the arena, whereas global KO mice have erratic, disorganized movement. Both mouse lines exhibit hyperactivity, but it is much more pronounced in the global KO. This hyperactive behavior in the OF is consistent with increased exploratory drive and potential deficits in controlling impulsive movement, which are commonly observed in hyperactivity models (Lalonde & Strazielle 2009, Langford-Smith et al 2011, Radyushkin et al 2009). This neuron-specific effect is particularly significant, as it implies that AAK1 function in the brain is central to the regulation of locomotor activity and anxiety-like behavior. Important to emphasize before continuing, the less severe hyperactivity phenotype of cKO compared to the global KO suggests that AAK1 functions in both neuronal and non-neuronal cells might contribute to the regulation of movement and exploratory behavior. Hyperactive phenotype observed in AAK1 KO mice aligns well with characteristics of attention-deficit hyperactivity disorder (ADHD) and ASD (Martinez-Morga et al 2018, Waldren et al 2024), particularly in the way that ADHD is often linked to synaptic dysfunction (Dark, Homman-Ludiye & Bryson-Richardson 2018) and altered dopaminergic signaling (Schneider et al 2006). Given that AAK1 influences endocytic processes, including synaptic vesicle recycling, it's plausible that its loss may lead to altered synaptic transmission and hyperactive behavior. This is in line with literature where AAK1 was identified as one of the "hub genes" in a gene co-expression network analysis, showing high significance particularly in the context of major depressive disorders (MDD) and adult ADHD (de Jong et al 2016).

Additionally, a recent study highlighted that variants in MARK2 cause ASD, with Mark2-deficient mice exhibiting specific behavioral alterations, including social deficits, stereotyped behavior, and anxiety—key features of ASD found in individuals with these variants (Gong et al 2024). Given our findings of altered MARK2 phosphorylation and localization in the AAK1 KO model, it is possible that these changes contribute to the observed phenotype. This connection between AAK1 and MARK2 could imply an interplay affecting not only motor control but also behaviors related to ASD.

Studies on ASD often indicate changes in synaptic density, displaying hyperconnectivity or impaired synaptic pruning (Eltokhi et al 2020). In our AAK1 KO model, increased ATG9A accumulation and altered autophagic flux could indicate disruptions in synaptic maintenance processes and this may affect the synaptic density.

The beam walk motor coordination test is an excellent tool for assessing motor function, specifically focusing on balance and coordination. Here animals were subjected to beams in different thicknesses (25mm, 12mm and 5mm). As the thickness of the beam decreased, the number of slips increased drastically, especially on the 5 mm beam in both KO groups compared to WT littermates. However, for the other beams AAK1 cKO mice showed a similar, though milder trend when compared to the global KO mice. Interestingly, the less pronounced effect in the cKO mice compared to the global KO mice may suggest a compensatory mechanism in other cell types that helps maintain overall motor function or AAK1 function in multiple cell types may be required for precise motor coordination. Role of glial cells in synaptic plasticity and regulation might be worth to discuss in this context (Halassa & Haydon 2010, Henstridge, Tzioras & Paolicelli 2019). The AAK1 KO mice did not display any deficits in the rotarod test. In this context, it appears that in the beam walk test, which is more sensitive to subtle motor deficits and requires precise paw placement and posture control to traverse a narrow beam, the KO mice demonstrated a significantly increased number of foot slips compared to WT controls, indicating impaired motor coordination or a deficit in motor planning. This discrepancy between the rotarod and beam walk results suggests that while the core aspects of motor coordination remain intact (as evidenced by the rotarod), the AAK1 KO mice may have impairments in motor precision or planning, which are more apparent in tasks that require fine motor adjustments, such as the beam walk. These findings imply that AAK1 may play a role in regulating specific components of motor control, particularly those involving more precise, goal-directed movements that depend on the integration of sensory feedback, rather than general motor balance.

To sum up, these findings reveal that AAK1 depletion impairs motor coordination and balance, particularly under challenging conditions. As a complementary data to motor deficit phenotype,

we did not observe any anatomical changes in cerebellum or in Purkinje cells. However, slight p62 accumulation in cerebellum indicates some dysregulations or a link between AAK1 and autophagy. Interpretation of accumulated p62 is enigmatic while some papers showed that knock-down of it causes locomotor deficits and motor neuron axonal defects in ALS/FTLD (Lattante et al 2014) some others indicated accumulation of it accelerates the disease like in ALS (Gal et al 2007, Mitsui et al 2018).

3. AAK1 regulates autophagy

Our autophagic flux experiment indicated impaired autophagosome formation due to non responsive state of LC3B-II upon starvation and BafA1 and CQ treatment in neurons and synaptosomes respectively. This result may be related to AAK1's role in endocytosis, as it can modulate various protein trafficking processes, some of which overlap with autophagic machinery. Inhibition of CME causes defective autophagosome formation, which is associated with impaired uptake of plasma membrane into autophagic precursors and autophagosomes (Ravikumar et al 2010). Endocytic pathways and trafficking is often linked to autophagy (Bera et al 2020, Kononenko et al 2017, Overhoff, De Bruyckere & Kononenko 2021), particularly through the recycling of membrane components and regulation of signaling pathways that promote autophagy, including receptor tyrosine kinases and mTOR signaling (Birgisdottir & Johansen 2020, Tooze & Yoshimori 2010).

ATG9A is a critical regulator of autophagosome formation, and its function is essential for supplying membranes to the expanding phagophore, an essential precursor to autophagosomes (Yamamoto et al 2012). This upregulation of ATG9A could suggest a compensatory response to the impaired autophagic flux seen in the KO neurons and synaptosomes. When autophagy is inhibited, cells often upregulate essential autophagy proteins in an attempt to counterbalance the loss of functionality in the pathway (Matsunaga et al 2009). In this case, the increase in ATG9A in synapse might represent the cells attempting to increase autophagosome formation to counteract the impairment seen in autophagic flux, which could be particularly exacerbated as the mice mature. This might explain why an increase is observed at 12 weeks rather than 6 weeks of age, since 12-week-old mice are closer to a mature adult stage, where synaptic and metabolic demands are greater, thus necessitating effective autophagy (Nazir et al 2018, Südhof 2013).

The developmental expression pattern of AAK1 is another critical point that ties into the regulation of ATG9A and autophagy. Since AAK1 expression peaks around 12 weeks in the cortex, aligning with the observed increase in ATG9A levels in the KO mice. This could suggest that AAK1 may play a role in maintaining the homeostasis of ATG9A levels during this critical

developmental period. The loss of AAK1 appears to disrupt this balance, resulting in dysregulated autophagy, as reflected by the altered ATG9A expression levels.

ATG9A-containing vesicles are known to traffic from the plasma membrane to recycling endosomes, where they fuse with ATG16L1 vesicles to regulate autophagosome formation (Puri et al 2013). In this context, the increased colocalization of ATG9A with VGLUT1, along with the elevated number of autophagosomes observed in EM analysis, suggests a possible misdirection of ATG9A-containing vesicles toward synaptic regions, potentially due to impaired trafficking or regional accumulation due to the impairment in PM retrieval. Notably, our immunoblot analysis showed that ATG9A accumulation is present in the KO synaptosome fraction but not in the KO cytoplasmic fraction. This finding implies that the issue may not be related to anterograde trafficking but rather retrograde transport. It is likely that these vesicles become trapped within the synaptosome and are unable to effectively move back towards the soma. To investigate this possibility further, live imaging experiments focusing on the trafficking of ATG9A vesicles could be conducted to directly observe their dynamics. Additionally, synaptic vesicle purification could also provide valuable insights. It has been shown that ATG9A vesicles are enriched in synaptic regions and resemble SVs in their structure and composition, yet they have distinct biochemical properties. According to Binotti et al. (Binotti et al 2024), ATG9A-containing vesicles are enriched with proteins involved in CME, such as EPN1/Eps1, EPS15, and EPS15L1, as well as components of the AP-2 complex. Notably, these vesicles are depleted in V-ATPase, suggesting they do not acidify, which makes them biochemically distinct from other post-Golgi trafficking vesicles. Importantly, a study in *C. elegans* showed that ATG9-containing vesicles undergo exo-endocytosis at synapses in an activity-dependent manner (Yang et al 2022). These studies support the concept that ATG9A vesicles might represent a specialized pool in synapses, distinct from Golgi-derived ATG9 vesicles, and may undergo independent cycles of endo- and exocytosis regulated by synaptic activity. Thus, ATG9A vesicles at synapses could be differentially regulated compared to their Golgi counterparts, and this specialized role might be regulated through alternative endocytic mechanisms. AAK1 could potentially contribute to these processes by modulating the dynamics of ATG9A trafficking at the synapse. Another parallel and plausible explanation or idea to take into consideration is that these ATG9A vesicles accumulate abnormally at endocytic intermediates, as previously reported (Yang et al 2022). This suggests that the issue may lie in the recycling or maturation steps rather than in the initial trafficking. The correlation between these changes and the developmental peak of AAK1 expression emphasizes the role of AAK1 in regulating both synaptic maintenance and autophagic processes. Dysregulation of AAK1 could disrupt this balance, leading to impaired autophagic flux and improper synaptic vesicle recycling, ultimately contributing to synaptic dysfunction and reduced neuronal resilience. Future

experiments could further elucidate how AAK1 activity modulates ATG9A trafficking and whether restoring this balance could mitigate the synaptic deficits observed in AAK1 KO models.

Lastly, in our synaptosome proteomic analysis, we observed a striking prevalence of upregulated proteins compared to downregulated ones. This pattern could point to several underlying mechanisms. One possible interpretation is the accumulation of proteins within the synapse, which may reflect impaired protein trafficking. Such trafficking problems could result from disruptions in microtubule stability or motor protein function, which we observed in our D2 analysis, and could contribute to an altered distribution of proteins essential for synapse.

Another possibility is a deficit in protein degradation, which may be linked to impaired autophagic or proteasomal pathways. Given the increased number of Avs observed in AAK1 KO synapses, it is plausible that the upregulated proteins represent a backlog of material that is failing to be efficiently degraded. This impaired autophagic flux could lead to the accumulation of proteins that normally undergo synaptic recycling, thereby contributing to an imbalance in the synaptic proteome.

Lastly, the increased levels of proteins might also result from heightened protein synthesis, possibly as a compensatory response to synaptic dysfunction. It is conceivable that the cells are attempting to counterbalance deficits in synaptic proteins due to either loss of function or mislocalization. This hypothesis aligns with the increased levels of translation-associated pathways that we observed in the synaptosome proteomic data. While it is difficult to distinguish between these possibilities definitively, the combination of our biochemical and proteomic findings suggests that AAK1 plays a significant role in maintaining the equilibrium of synaptic protein turnover—by regulating both protein trafficking and degradation processes.

The notable imbalance in the proteome, with significantly more upregulated than downregulated proteins, highlights a broader dysregulation within synaptic compartments. This dysregulation may contribute to synaptic instability and functional decline, particularly in the context of impaired autophagosome trafficking and disrupted microtubule dynamics, both of which were evidenced by our data. The failure to maintain a homeostatic balance of proteins within synapses could ultimately contribute to the neurodegenerative phenotypes observed in AAK1 KO models, including synaptic vesicle loss and altered synaptic function.

4. AAK1 regulates microtubule dynamics and vesicular trafficking via MARK2 phosphorylation

OMICs data, live cell imaging and fractionation of subcellular organelles (synaptosome, cytosol, plasma membrane etc) showed that AAK1, through MARK2 phosphorylation might regulate trafficking dynamics which is critical to synaptic function. This connection could provide a new perspective on how AAK1 deficiency might lead to cellular or synaptic dysfunction, especially in the context of autophagy and neurodegeneration.

MARK2 is known to contain a conserved KA1 domain, which is a membrane-targeting domain involved in localizing the kinase to specific subcellular regions, including the plasma membrane (Moravcevic et al 2010). This study is, therefore, consistent with the idea that AAK1-mediated phosphorylation helps recruit or stabilize MARK2 at the membrane. The importance of MARK2 for microtubule stability and dynamics, particularly within neurons, has been extensively documented (Caiola et al 2024, Han et al 2024a, Mendoza et al 2024, Sapir et al 2008, Wu et al 2011). Its role in organizing the cytoskeleton by phosphorylating MAPs suggests that altering its localization could have downstream consequences on cytoskeletal and synaptic dynamics (Chin et al 2000, Drewes et al 1997, Sánchez, Díaz-Nido & Avila 2000).

The decrease in MARK2 localization to the plasma membrane upon AAK1 inhibition could indicate that AAK1 is necessary to promote the recruitment of MARK2 potentially through phosphorylation-dependent manner, perhaps to facilitate microtubule anchoring at the synapse and subsequent vesicular transport. This is in line with previous observations of microtubule regulation at synaptic terminals to ensure efficient endocytosis and recycling of synaptic vesicles (Parato & Bartolini 2021, Sakakibara et al 2013). Loss of AAK1 may impair MARK2 localization, reducing its ability to interact with and phosphorylate MAPs, ultimately affecting dendritic stability. This aligns with studies showing that deregulation of MARK2 can disrupt dendritic spine morphology and synaptic function (Hayashi et al 2011). Immunofluorescent-based analysis that we performed to understand the effect of mislocalization of MARK2 on microtubule and trafficking dynamics indicated reduction in D2 levels highlights a shift towards a more dynamic, less stable microtubule state in the dendritic compartment. Microtubule stability is critical for cellular transport and synaptic plasticity, and disruptions can impair neuronal connectivity (Conde & Cáceres 2009, Song & Brady 2014). Given that hippocampal and cortical regions are essential for memory and cognition, these findings could imply that AAK1 depletion disrupts neuronal function by compromising microtubule stability in key regions involved in learning and memory. In AD, increased level of D2 may serve as a compensatory response (Peris et al 2022, Vu et al 2017), whereas in AAK1 KO, the absence of this compensatory stabilization suggests an intrinsic vulnerability due to impaired MARK2 activity and localization. The lack of change in acetylated tubulin (even though we have a decreased trend in axon and soma it is not significant, likely to prevent a complete collapse of microtubule integrity) suggests that while the overall microtubule stability is disrupted, as indicated by delta-

tubulin levels, specific compartments retain their stability or compensate for the loss of delta-tubulin. Acetylation is associated with microtubule resilience (Portran et al 2017, Xu et al 2017) thus this data may represent compensatory mechanisms since reduction in acetylated tubulin (Hempfen & Brion 1996) and increased level of Histone deacetylases (HDACs) in AD mouse brain (Ding, Dolan & Johnson 2008, Govindarajan et al 2013) related to disease pathology.

In cultured neurons, we observed an increase in D2 tubulin in MAP2-positive neurites, which is indicative of less dynamic microtubules. This finding aligns well with the decreased velocity of both EB3 comets and LC3 puncta in AAK1 KO neurons, suggesting reduced microtubule dynamics. D2, which represents a detyrosinated form of tubulin, tends to accumulate on stable microtubules, indicating that microtubules in AAK1 KO neurons are shift towards a less dynamic state.

The discrepancy between the increased D2 levels in dendrites of cultured neurons versus decreased levels in brain sections could reflect the different microenvironments. In primary culture, neurons are isolated from their native environment, and they might not fully recapitulate the mature signaling environment that exists in a living brain. In the context of the in vivo brain, complex extracellular signaling and intercellular interactions tightly regulate microtubule dynamics. Elevated AAK1 levels in the mature brain might exert a more significant effect on MARK2-mediated pathways, resulting in fine-tuning of microtubule stability to facilitate mature synaptic function. Loss of AAK1 in the mature cortex could lead to dysregulation of these pathways and reduced D2 stabilization. Another thing, in the mature cortex (12-week-old), elevated AAK1 levels may exert a more nuanced regulation on microtubule stability through interactions with MARK2, leading to differential regulation of D2 that is compartment-specific. Loss of AAK1 might disrupts this regulation more dramatically in this age which is line with AAK1 abundancy in the brain over the time, resulting in lower levels of delta-tubulin and likely contributing to dendritic instability and synaptic dysfunction. As a part of microtubule related data it is worth to emphasize downregulated "neurofibrillary tangles" (NFT) and upregulated "microtubule minus ends" in cellular components pathway analysis from synaptosome phosphoproteomic dataset. NFTs are abnormal aggregates composed primarily of hyperphosphorylated tau protein, which have been widely characterized as a central hallmark of AD pathology (Grundke-Iqbal et al 1986). Their presence is typically associated with impaired synaptic function and neuronal loss (Colom-Cadena et al 2023, Jadhav et al 2015, Zhou et al 2017b). This upregulation might indicate a tendency for pathological tau accumulation in AAK1 KO synapses. Since AAK1 is linked to endocytic regulation, it is possible that impaired endocytosis or vesicular trafficking could exacerbate tau accumulation and its aggregation into tangles. Downregulation of "microtubule minus-end" in components might be indicative of impaired microtubule stability in the AAK1 KO condition. In healthy neurons or

under normal physiological conditions, tau protein stabilizes microtubules. However, hyperphosphorylation of tau reduces its ability to stabilize microtubules, leading to microtubule destabilization and fragmentation (Barbier et al 2019, Wang & Mandelkow 2016). This loss of stability at the microtubule minus-end may result in compromised microtubule function, leading to deficits in the retrograde and anterograde trafficking of synaptic components. The inability to properly stabilize microtubule minus-ends may also hinder the attachment and regulation of key motor proteins, such as dynein and kinesin, ultimately impairing the transport of synaptic vesicles and AVs. Together, the presence of upregulated NFTs and the downregulation of microtubule minus-end components highlight a critical intersection of impaired microtubule stability and pathological tau aggregation. This intersection is likely to exacerbate synaptic dysfunction in AAK1 KO model. Disrupted synaptic vesicle recycling and impaired trafficking of autophagic components could further contribute to the buildup of misfolded proteins and the formation of NFTs, leading to synaptic degeneration. This aligns with models of AD in which synaptic dysfunction is one of the earliest detectable features, occurring well before widespread neuronal loss (Selkoe 2002). The synaptic accumulation of hyperphosphorylated tau and subsequent formation of NFTs may therefore represent a key mechanism by which AAK1 loss leads to early synaptic vulnerability, potentially contributing to a cascade of neurodegenerative events.

This highlights a temporal and spatial regulation where AAK1 is critical for modulating microtubule stability, ensuring that cortical and hippocampal neurons/synapses maintain the proper balance of stable versus dynamic microtubules during development.

VI. Closing remarks

This study aimed to understand the role of AAK1 in the brain by shedding light on its localization, cell-type specific distribution and its novel substrates that may play a role in signaling and overall neuronal health. We demonstrated that the lack of AAK1 in both global and cKO mice resulted in a consistent phenotype characterized by hyperactivity, reduced body size and motor deficits. Although both models displayed similar deficits, the cKO mice showed relatively milder impairments, particularly in beam walk performance, suggesting that non-neuronal sources of AAK1 could modulate the severity of these phenotypes. One important takeaway is that AAK1 is predominantly expressed in neurons, as evidenced by the significant reduction in AAK1 levels observed in the cortex lysates of cKO mice, which targets CamKII α -positive excitatory neurons. The observed 80% reduction in AAK1 in the cortex suggests that its expression is primarily localized in CamKII α neurons. The remaining AAK1 expression, potentially accounting for 15-20%, might be found in inhibitory neurons or glial cells. This finding raises a fundamental question: what is the role of AAK1 in other cell types, and how might these cells contribute to the observed phenotypes or mechanisms? Future studies focusing on inhibitory neurons and glial cells may provide valuable insight into their contribution to AAK1-related functions. Our exploration of the synaptic and subcellular roles of AAK1 revealed several key functions that go beyond traditional CME pathways. The proteomics data led us to identify MARK2 as a promising novel substrate of AAK1, and further analyses indicated that AAK1 regulates MARK2 localization specifically at synaptic plasma membranes. This regulation appears to be vital for microtubule stability, synaptic plasticity, and autophagosome trafficking. We observed that in the absence of AAK1, MARK2 was less effectively localized to synaptic plasma membranes, which had a cascading effect on microtubule post-translational modifications, specifically impacting D2 levels. This dysregulation likely underlies the impairments in motor behavior and synaptic integrity that were observed in AAK1 KO models.

The observation of increased autophagosome accumulation, particularly in synaptic regions, along with reduced synaptic vesicle numbers, underscores a role for AAK1 in synaptic autophagy. The age-dependent expression of AAK1, which peaks at 12 weeks and coincides with a critical period of synaptic refinement, suggests that AAK1 might be particularly important for maintaining synaptic homeostasis during developmentally sensitive periods. The upregulation of ATG9A in KO animals provides further evidence that AAK1 may help coordinate autophagosome trafficking and vesicular dynamics, especially within the synaptic compartment. This aligns with the observed impaired autophagic flux in cultured neurons lacking AAK1, highlighting a broader role for AAK1 in autophagic regulation.

These findings bring forward several questions and future directions. First, what are the precise roles of AAK1 in non-neuronal cells such as astrocytes or microglia? Addressing this could help elucidate whether these cells contribute to the observed motor and behavioral phenotypes. Second, how does the dysregulation of autophagosome trafficking contribute to synaptic dysfunction and neurodegeneration in the long term? The interplay between AAK1, MARK2, and microtubule dynamics could be further explored to determine if pharmacological modulation of these pathways might ameliorate synaptic deficits in neurodegenerative disease models.

Finally, our work reveals that AAK1 is a key regulator of synaptic health, linking processes of endocytosis, autophagosome trafficking, and microtubule regulation. Further research into the diverse roles of AAK1 in specific brain regions, distinct neuronal populations, and different developmental stages will be essential in fully understanding its contributions to both normal brain function and disease.

VII. References

2023. 2023 Alzheimer's disease facts and figures. *Alzheimers Dement* 19: 1598-695
- Agajanian MJ, Walker MP, Axtman AD, Ruela-de-Sousa RR, Serafin DS, et al. 2019. WNT Activates the AAK1 Kinase to Promote Clathrin-Mediated Endocytosis of LRP6 and Establish a Negative Feedback Loop. *Cell Rep* 26: 79-93.e8
- Aidaralievá NJ, Kamino K, Kimura R, Yamamoto M, Morihara T, et al. 2008. Dynamin 2 gene is a novel susceptibility gene for late-onset Alzheimer disease in non-APOE-epsilon4 carriers. *J Hum Genet* 53: 296-302
- Alberts B JA, Lewis J, et al. 2002. Molecular Biology of the Cell. 4th edition. *Garland Science*
- Alsaqati M, Thomas RS, Kidd EJ. 2018. Proteins Involved in Endocytosis Are Upregulated by Ageing in the Normal Human Brain: Implications for the Development of Alzheimer's Disease. *J Gerontol A Biol Sci Med Sci* 73: 289-98
- Alsaqati M, Thomas RS, Kidd EJ. 2023. Upregulation of endocytic protein expression in the Alzheimer's disease male human brain. *Aging Brain* 4: 100084
- Aman Y, Schmauck-Medina T, Hansen M, Morimoto RI, Simon AK, et al. 2021. Autophagy in healthy aging and disease. *Nature Aging* 1: 634-50
- Anjur-Dietrich MI, Hererra VG, Farhadifar R, Wu H, Merta H, et al. 2023. Clustering of cortical dynein regulates the mechanics of spindle orientation in human mitotic cells. *bioRxiv*
- Ashford TP, Porter KR. 1962. Cytoplasmic components in hepatic cell lysosomes. *J Cell Biol* 12: 198-202
- Asmerian H, Alberts J, Sanetra AM, Diaz AJ, Silm K. 2024. Role of adaptor protein complexes in generating functionally distinct synaptic vesicle pools. *J Physiol*
- Avinoam O, Schorb M, Beese CJ, Briggs JA, Kaksonen M. 2015. ENDOCYTOSIS. Endocytic sites mature by continuous bending and remodeling of the clathrin coat. *Science* 348: 1369-72
- Axe EL, Walker SA, Manifava M, Chandra P, Roderick HL, et al. 2008. Autophagosome formation from membrane compartments enriched in phosphatidylinositol 3-phosphate and dynamically connected to the endoplasmic reticulum. *Journal of Cell Biology* 182: 685-701
- Baba M, Takeshige K, Baba N, Ohsumi Y. 1994. Ultrastructural analysis of the autophagic process in yeast: detection of autophagosomes and their characterization. *J Cell Biol* 124: 903-13
- Barbier P, Zejneli O, Martinho M, Lasorsa A, Belle V, et al. 2019. Role of Tau as a Microtubule-Associated Protein: Structural and Functional Aspects. *Front Aging Neurosci* 11: 204
- Barouch W, Prasad K, Greene LE, Eisenberg E. 1994. ATPase activity associated with the uncoating of clathrin baskets by Hsp70. *J Biol Chem* 269: 28563-8
- Bates GP, Dorsey R, Gusella JF, Hayden MR, Kay C, et al. 2015. Huntington disease. In *Nat Rev Dis Primers*, pp. 15005
- Bera S, Cambor-Perujo S, Calleja Barca E, Negrete-Hurtado A, Racho J, et al. 2020. AP2 reduces amyloidogenesis by promoting BACE1 trafficking and degradation in neurons. *EMBO reports* 21: e47954
- Biernat J, Wu YZ, Timm T, Zheng-Fischhöfer Q, Mandelkow E, Meijer L, Mandelkow EM. 2002. Protein kinase MARK/PAR-1 is required for neurite outgrowth and establishment of neuronal polarity. *Mol Biol Cell* 13: 4013-28
- Binotti B, Ninov M, Cepeda AP, Ganzella M, Matti U, et al. 2024. ATG9 resides on a unique population of small vesicles in presynaptic nerve terminals. *Autophagy* 20: 883-901
- Birgisdottir ÅB, Johansen T. 2020. Autophagy and endocytosis – interconnections and interdependencies. *Journal of Cell Science* 133
- Blakely RD, Edwards RH. 2012. Vesicular and plasma membrane transporters for neurotransmitters. *Cold Spring Harb Perspect Biol* 4

- Borgonovo JE, Troncoso M, Lucas JJ, Sosa MA. 2013. Mutant huntingtin affects endocytosis in striatal cells by altering the binding of AP-2 to membranes. *Experimental Neurology* 241: 75-83
- Braun AR, Sevcsik E, Chin P, Rhoades E, Tristram-Nagle S, Sachs JN. 2012. α -Synuclein induces both positive mean curvature and negative Gaussian curvature in membranes. *J Am Chem Soc* 134: 2613-20
- Brodsky FM, Hill BL, Acton SL, Nätthke I, Wong DH, Ponnambalam S, Parham P. 1991. Clathrin light chains: arrays of protein motifs that regulate coated-vesicle dynamics. *Trends Biochem Sci* 16: 208-13
- Bulinski JC, Borisy GG. 1979. Self-assembly of microtubules in extracts of cultured HeLa cells and the identification of HeLa microtubule-associated proteins. *Proceedings of the National Academy of Sciences* 76: 293-97
- Burré J. 2015. The Synaptic Function of α -Synuclein. *J Parkinsons Dis* 5: 699-713
- Burré J, Sharma M, Tsetsenis T, Buchman V, Etherton MR, Südhof TC. 2010. Alpha-synuclein promotes SNARE-complex assembly in vivo and in vitro. *Science* 329: 1663-7
- Busch DJ, Oliphint PA, Walsh RB, Banks SM, Woods WS, George JM, Morgan JR. 2014. Acute increase of α -synuclein inhibits synaptic vesicle recycling evoked during intense stimulation. *Mol Biol Cell* 25: 3926-41
- Cadwell CR, Bhaduri A, Mostajo-Radji MA, Keefe MG, Nowakowski TJ. 2019. Development and Arealization of the Cerebral Cortex. *Neuron* 103: 980-1004
- Caiola HO, Wu Q, Li J, Wang XF, Soni S, et al. 2024. Neuronal connectivity, behavioral, and transcriptional alterations associated with the loss of MARK2. *Faseb j* 38: e70124
- Caire MJ, Reddy V, Varacallo M. 2024. Physiology, Synapse In *StatPearls*. Treasure Island (FL): StatPearls Publishing
- Copyright © 2024, StatPearls Publishing LLC.
- Cambor-Perujo S, Ozer Yildiz E, Küpper H, Overhoff M, Rastogi S, Bazzi H, Kononenko NL. 2024. The AP-2 complex interacts with γ -TuRC and regulates the proliferative capacity of neural progenitors. *Life Science Alliance* 7: e202302029
- Cao M, Milosevic I, Giovedi S, De Camilli P. 2014. Upregulation of Parkin in endophilin mutant mice. *J Neurosci* 34: 16544-9
- Cao Y, Xiao Y, Ravid R, Guan ZZ. 2010. Changed clathrin regulatory proteins in the brains of Alzheimer's disease patients and animal models. *J Alzheimers Dis* 22: 329-42
- Carlsson AE, Bayly PV. 2014. Force generation by endocytic actin patches in budding yeast. *Biophys J* 106: 1596-606
- Cason SE, Holzbaur ELF. 2022. Selective motor activation in organelle transport along axons. *Nature Reviews Molecular Cell Biology* 23: 699-714
- Chanaday NL, Cousin MA, Milosevic I, Watanabe S, Morgan JR. 2019a. The Synaptic Vesicle Cycle Revisited: New Insights into the Modes and Mechanisms. *J Neurosci* 39: 8209-16
- Chanaday NL, Cousin MA, Milosevic I, Watanabe S, Morgan JR. 2019b. The Synaptic Vesicle Cycle Revisited: New Insights into the Modes and Mechanisms. *The Journal of Neuroscience* 39: 8209-16
- Chen J, Zhao H, Liu M, Chen L. 2024. A new perspective on the autophagic and non-autophagic functions of the GABARAP protein family: a potential therapeutic target for human diseases. *Molecular and Cellular Biochemistry* 479: 1415-41
- Cheong H, Nair U, Geng J, Klionsky DJ. 2008. The Atg1 Kinase Complex Is Involved in the Regulation of Protein Recruitment to Initiate Sequestering Vesicle Formation for Nonspecific Autophagy in *Saccharomyces cerevisiae*. *Molecular Biology of the Cell* 19: 668-81
- Chin JY, Knowles RB, Schneider A, Drewes G, Mandelkow EM, Hyman BT. 2000. Microtubule-affinity regulating kinase (MARK) is tightly associated with neurofibrillary tangles in

- Alzheimer brain: a fluorescence resonance energy transfer study. *J Neuropathol Exp Neurol* 59: 966-71
- Cho KF, Branon TC, Udeshi ND, Myers SA, Carr SA, Ting AY. 2020. Proximity labeling in mammalian cells with TurboID and split-TurboID. *Nature Protocols* 15: 3971-99
- Chudobová J, Zempel H. 2023. Microtubule affinity regulating kinase (MARK/Par1) isoforms differentially regulate Alzheimer-like TAU missorting and A β -mediated synapse pathology. *Neural Regeneration Research* 18: 335-36
- Cocucci E, Aguet F, Boulant S, Kirchhausen T. 2012. The first five seconds in the life of a clathrin-coated pit. *Cell* 150: 495-507
- Collins BM, McCoy AJ, Kent HM, Evans PR, Owen DJ. 2002. Molecular architecture and functional model of the endocytic AP2 complex. *Cell* 109: 523-35
- Colom-Cadena M, Davies C, Sirisi S, Lee J-E, Simzer EM, et al. 2023. Synaptic oligomeric tau in Alzheimer's disease; A potential culprit in the spread of tau pathology through the brain. *Neuron* 111: 2170-83.e6
- Conde C, Cáceres A. 2009. Microtubule assembly, organization and dynamics in axons and dendrites. *Nature Reviews Neuroscience* 10: 319-32
- Conner SD, Schmid SL. 2002. Identification of an adaptor-associated kinase, AAK1, as a regulator of clathrin-mediated endocytosis. *J Cell Biol* 156: 921-9
- Conner SD, Schröter T, Schmid SL. 2003. AAK1-mediated micro2 phosphorylation is stimulated by assembled clathrin. *Traffic* 4: 885-90
- Dark C, Homman-Ludiye J, Bryson-Richardson RJ. 2018. The role of ADHD associated genes in neurodevelopment. *Developmental Biology* 438: 69-83
- De Jesús-Cortés HJ, Noguera-Ortiz CJ, Gearing M, Arnold SE, Vega IE. 2012. Amphiphysin-1 protein level changes associated with tau-mediated neurodegeneration. *Neuroreport* 23: 942-6
- de Jong S, Newhouse SJ, Patel H, Lee S, Dempster D, et al. 2016. Immune signatures and disorder-specific patterns in a cross-disorder gene expression analysis. *Br J Psychiatry* 209: 202-8
- de Lau LM, Breteler MM. 2006. Epidemiology of Parkinson's disease. *Lancet Neurol* 5: 525-35
- Denenberg VH. 1969. Open-field behavior in the rat: what does it mean? *Ann N Y Acad Sci* 159: 852-9
- Denker A, Rizzoli SO. 2010. Synaptic vesicle pools: an update. In *Front Synaptic Neurosci*, pp. 135
- Dice JF. 1990. Peptide sequences that target cytosolic proteins for lysosomal proteolysis. *Trends Biochem Sci* 15: 305-9
- Ding H, Dolan PJ, Johnson GV. 2008. Histone deacetylase 6 interacts with the microtubule-associated protein tau. *J Neurochem* 106: 2119-30
- Dooley HC, Razi M, Polson HE, Girardin SE, Wilson MI, Tooze SA. 2014. WIPI2 links LC3 conjugation with PI3P, autophagosome formation, and pathogen clearance by recruiting Atg12-5-16L1. *Mol Cell* 55: 238-52
- Dragatsis I, Zeitlin S. 2000. CaMKIIalpha-Cre transgene expression and recombination patterns in the mouse brain. *Genesis* 26: 133-5
- Drewes G, Ebnet A, Preuss U, Mandelkow E-M, Mandelkow E. 1997. MARK, a Novel Family of Protein Kinases That Phosphorylate Microtubule-Associated Proteins and Trigger Microtubule Disruption. *Cell* 89: 297-308
- Ducy P, Amling M, Takeda S, Priemel M, Schilling AF, et al. 2000. Leptin inhibits bone formation through a hypothalamic relay: a central control of bone mass. *Cell* 100: 197-207
- Ebnet A, Drewes G, Mandelkow EM, Mandelkow E. 1999. Phosphorylation of MAP2c and MAP4 by MARK kinases leads to the destabilization of microtubules in cells. *Cell Motil Cytoskeleton* 44: 209-24

- Eckermann K, Mocanu MM, Khlistunova I, Biernat J, Nissen A, et al. 2007. The beta-propensity of Tau determines aggregation and synaptic loss in inducible mouse models of tauopathy. *J Biol Chem* 282: 31755-65
- Edwards TJ, Fenlon LR, Dean RJ, Bunt J, Sherr EH, Richards LJ. 2020. Altered structural connectivity networks in a mouse model of complete and partial dysgenesis of the corpus callosum. *NeuroImage* 217: 116868
- Eltokhi A, Janmaat IE, Genedi M, Haarman BCM, Sommer IEC. 2020. Dysregulation of synaptic pruning as a possible link between intestinal microbiota dysbiosis and neuropsychiatric disorders. *Journal of Neuroscience Research* 98: 1335-69
- Farsi Z, Gowrisankaran S, Kronic M, Rammner B, Woehler A, et al. 2018. Clathrin coat controls synaptic vesicle acidification by blocking vacuolar ATPase activity. *Elife* 7
- Farsi Z, Jahn R, Woehler A. 2017. Proton electrochemical gradient: Driving and regulating neurotransmitter uptake. *Bioessays* 39
- Fu X, Ke M, Yu W, Wang X, Xiao Q, Gu M, Lü Y. 2018. Periodic Variation of AAK1 in an A β (1-42)-Induced Mouse Model of Alzheimer's Disease. *J Mol Neurosci* 65: 179-89
- Furuya N, Yu J, Byfield M, Patingre S, Levine B. 2005. The evolutionarily conserved domain of Beclin 1 is required for Vps34 binding, autophagy and tumor suppressor function. *Autophagy* 1: 46-52
- Gal J, Ström A-L, Kilty R, Zhang F, Zhu H. 2007. p62 Accumulates and Enhances Aggregate Formation in Model Systems of Familial Amyotrophic Lateral Sclerosis*. *Journal of Biological Chemistry* 282: 11068-77
- Ganapathy AS, Saha K, Suchanec E, Singh V, Verma A, et al. 2022. AP2M1 mediates autophagy-induced CLDN2 (claudin 2) degradation through endocytosis and interaction with LC3 and reduces intestinal epithelial tight junction permeability. *Autophagy* 18: 2086-103
- Ge L, Schekman R. 2014. The ER-Golgi intermediate compartment feeds the phagophore membrane. *Autophagy* 10: 170-72
- Ge S, Yang CH, Hsu KS, Ming GL, Song H. 2007. A critical period for enhanced synaptic plasticity in newly generated neurons of the adult brain. *Neuron* 54: 559-66
- George A, Zand DJ, Hufnagel RB, Sharma R, Sergeev YV, et al. 2016. Biallelic Mutations in MITF Cause Coloboma, Osteopetrosis, Microphthalmia, Macrocephaly, Albinism, and Deafness. *Am J Hum Genet* 99: 1388-94
- Geraldo S, Khanzada UK, Parsons M, Chilton JK, Gordon-Weeks PR. 2008. Targeting of the F-actin-binding protein drebrin by the microtubule plus-tip protein EB3 is required for neuriteogenesis. *Nature Cell Biology* 10: 1181-89
- Giansanti M, Theinert T, Boeing SK, Haas D, Schlegel P-G, et al. 2023. Exploiting autophagy balance in T and NK cells as a new strategy to implement adoptive cell therapies. *Molecular Cancer* 22: 201
- Goh LK, Sorkin A. 2013. Endocytosis of receptor tyrosine kinases. *Cold Spring Harb Perspect Biol* 5: a017459
- Gong HS, Guo Y, Tian C, Xie WL, Shi Q, et al. 2012. Reduction of protein kinase MARK4 in the brains of experimental scrapie rodents and human prion disease correlates with deposits of PrP(Sc). *Int J Mol Med* 30: 569-78
- Gong M, Li J, Qin Z, Machado Bressan Wilke MV, Liu Y, et al. 2024. MARK2 variants cause autism spectrum disorder via the downregulation of WNT/ β -catenin signaling pathway. *The American Journal of Human Genetics*
- Govindarajan N, Rao P, Burkhardt S, Sananbenesi F, Schlüter OM, et al. 2013. Reducing HDAC6 ameliorates cognitive deficits in a mouse model for Alzheimer's disease. *EMBO Mol Med* 5: 52-63
- Grundke-Iqbal I, Iqbal K, Tung YC, Quinlan M, Wisniewski HM, Binder LI. 1986. Abnormal phosphorylation of the microtubule-associated protein tau (tau) in Alzheimer cytoskeletal pathology. *Proceedings of the National Academy of Sciences* 83: 4913-17

- Gu M, Liu Q, Watanabe S, Sun L, Hollopeter G, Grant BD, Jorgensen EM. 2013. AP2 hemicomplexes contribute independently to synaptic vesicle endocytosis. *Elife* 2: e00190
- Guo J, Ge J-l, Hao M, Sun Z-c, Wu X-s, et al. 2015. A Three-Pool Model Dissecting Readily Releasable Pool Replenishment at the Calyx of Held. *Scientific Reports* 5: 9517
- Gupta-Rossi N, Ortica S, Meas-Yedid V, Heuss S, Moretti J, Olivo-Marin JC, Israël A. 2011. The adaptor-associated kinase 1, AAK1, is a positive regulator of the Notch pathway. *J Biol Chem* 286: 18720-30
- Gur G ZY, Yarden Y. . 2000. Endocytosis of Receptor Tyrosine Kinases: Implications for Signal Transduction by Growth Factors
- Halassa MM, Haydon PG. 2010. Integrated brain circuits: astrocytic networks modulate neuronal activity and behavior. *Annu Rev Physiol* 72: 335-55
- Han Y, Li M, Zhao B, Wang H, Liu Y, et al. 2024a. MARK2 phosphorylates KIF13A at a 14-3-3 binding site to polarize vesicular transport of transferrin receptor within dendrites. *Proc Natl Acad Sci U S A* 121: e2316266121
- Han Y, Li M, Zhao B, Wang H, Liu Y, et al. 2024b. MARK2 phosphorylates KIF13A at a 14-3-3 binding site to polarize vesicular transport of transferrin receptor within dendrites. *Proceedings of the National Academy of Sciences* 121: e2316266121
- Hara T, Nakamura K, Matsui M, Yamamoto A, Nakahara Y, et al. 2006. Suppression of basal autophagy in neural cells causes neurodegenerative disease in mice. *Nature* 441: 885-89
- Hardy J, Allsop D. 1991. Amyloid deposition as the central event in the aetiology of Alzheimer's disease. *Trends Pharmacol Sci* 12: 383-8
- Harjes P, Wanker EE. 2003. The hunt for huntingtin function: interaction partners tell many different stories. *Trends in biochemical sciences* 28: 425-33
- Hasegawa J, Iwamoto R, Otomo T, Nezu A, Hamasaki M, Yoshimori T. 2016. Autophagosome-lysosome fusion in neurons requires INPP5E, a protein associated with Joubert syndrome. *Embo j* 35: 1853-67
- Haucke V, Kozlov MM. 2018. Membrane remodeling in clathrin-mediated endocytosis. *J Cell Sci* 131
- Hawkins WD, Klionsky DJ. 2020. A separation that's for the best: coming together at the PAS. *Cell Research* 30: 372-73
- Hayashi K, Suzuki A, Hirai S, Kurihara Y, Hoogenraad CC, Ohno S. 2011. Maintenance of dendritic spine morphology by partitioning-defective 1b through regulation of microtubule growth. *J Neurosci* 31: 12094-103
- Hayashi S, McMahon AP. 2002. Efficient recombination in diverse tissues by a tamoxifen-inducible form of Cre: a tool for temporally regulated gene activation/inactivation in the mouse. *Dev Biol* 244: 305-18
- Heaton GR, Landeck N, Mamais A, Nalls MA, Nixon-Abell J, et al. 2020. Sequential screening nominates the Parkinson's disease associated kinase LRRK2 as a regulator of Clathrin-mediated endocytosis. *Neurobiology of Disease* 141: 104948
- Heidary Arash E, Shibani A, Song S, Attisano L. 2017. MARK4 inhibits Hippo signaling to promote proliferation and migration of breast cancer cells. *EMBO reports* 18: 420-36
- Hemelaar J, Lelyveld VS, Kessler BM, Ploegh HL. 2003. A single protease, Apg4B, is specific for the autophagy-related ubiquitin-like proteins GATE-16, MAP1-LC3, GABARAP, and Apg8L. *J Biol Chem* 278: 51841-50
- Hempfen B, Brion JP. 1996. Reduction of acetylated alpha-tubulin immunoreactivity in neurofibrillary tangle-bearing neurons in Alzheimer's disease. *J Neuropathol Exp Neurol* 55: 964-72
- Henderson DM, Conner SD. 2007. A novel AAK1 splice variant functions at multiple steps of the endocytic pathway. *Mol Biol Cell* 18: 2698-706
- Henne WM, Boucrot E, Meinecke M, Evergren E, Vallis Y, Mittal R, McMahon HT. 2010. FCHO proteins are nucleators of clathrin-mediated endocytosis. *Science* 328: 1281-4

- Henstridge CM, Tzioras M, Paolicelli RC. 2019. Glial Contribution to Excitatory and Inhibitory Synapse Loss in Neurodegeneration. *Front Cell Neurosci* 13: 63
- Heuser JE, Reese TS. 1973. Evidence for recycling of synaptic vesicle membrane during transmitter release at the frog neuromuscular junction. *J Cell Biol* 57: 315-44
- Hinrichsen L, Harborth J, Andrees L, Weber K, Ungewickell EJ. 2003. Effect of clathrin heavy chain- and alpha-adaptin-specific small inhibitory RNAs on endocytic accessory proteins and receptor trafficking in HeLa cells. *J Biol Chem* 278: 45160-70
- Hirst J, Barlow LD, Francisco GC, Sahlender DA, Seaman MN, Dacks JB, Robinson MS. 2011. The fifth adaptor protein complex. *PLoS Biol* 9: e1001170
- Hirst J, Irving C, Borner GH. 2013. Adaptor protein complexes AP-4 and AP-5: new players in endosomal trafficking and progressive spastic paraplegia. *Traffic* 14: 153-64
- Hirst J, Itzhak DN, Antrobus R, Borner GHH, Robinson MS. 2018. Role of the AP-5 adaptor protein complex in late endosome-to-Golgi retrieval. *PLoS Biology* 16: e2004411
- Hirst J, Robinson MS. 1998. Clathrin and adaptors. *Biochim Biophys Acta* 1404: 173-93
- Hirst J, Schlacht A, Norcott JP, Traynor D, Bloomfield G, et al. 2014. Characterization of TSET, an ancient and widespread membrane trafficking complex. *eLife* 3: e02866
- Holderith N, Lorincz A, Katona G, Rózsa B, Kulik A, Watanabe M, Nusser Z. 2012. Release probability of hippocampal glutamatergic terminals scales with the size of the active zone. In *Nat Neurosci*, pp. 988-97
- Hollopeter G, Lange JJ, Zhang Y, Vu TN, Gu M, et al. 2014. The membrane-associated proteins FCHO and SGIP are allosteric activators of the AP2 clathrin adaptor complex. *Elife* 3
- Höning S, Ricotta D, Krauss M, Späte K, Spolaore B, et al. 2005. Phosphatidylinositol-(4,5)-bisphosphate regulates sorting signal recognition by the clathrin-associated adaptor complex AP2. *Mol Cell* 18: 519-31
- Hopkins CR, Miller K, Beardmore JM. 1985. Receptor-mediated endocytosis of transferrin and epidermal growth factor receptors: a comparison of constitutive and ligand-induced uptake. *J Cell Sci Suppl* 3: 173-86
- Ichimura Y, Kirisako T, Takao T, Satomi Y, Shimonishi Y, et al. 2000. A ubiquitin-like system mediates protein lipidation. *Nature* 408: 488-92
- Inoue T, Heo WD, Grimley JS, Wandless TJ, Meyer T. 2005. An inducible translocation strategy to rapidly activate and inhibit small GTPase signaling pathways. *Nature Methods* 2: 415-18
- Itakura E, Kishi C, Inoue K, Mizushima N. 2008. Beclin 1 forms two distinct phosphatidylinositol 3-kinase complexes with mammalian Atg14 and UVRAG. *Mol Biol Cell* 19: 5360-72
- Itakura E, Mizushima N. 2010. Characterization of autophagosome formation site by a hierarchical analysis of mammalian Atg proteins. *Autophagy* 6: 764-76
- Jackson LP, Kelly BT, McCoy AJ, Gaffry T, James LC, et al. 2010. A large-scale conformational change couples membrane recruitment to cargo binding in the AP2 clathrin adaptor complex. *Cell* 141: 1220-9
- Jadhav S, Cubinkova V, Zimova I, Brezovakova V, Madari A, Cigankova V, Zilka N. 2015. Tau-mediated synaptic damage in Alzheimer's disease. *Transl Neurosci* 6: 214-26
- Jahn R, Fasshauer D. 2012. Molecular machines governing exocytosis of synaptic vesicles. *Nature* 490: 201-07
- Janke C, Chloë Bulinski J. 2011. Post-translational regulation of the microtubule cytoskeleton: mechanisms and functions. *Nature Reviews Molecular Cell Biology* 12: 773-86
- Jatana N, Ascher DB, Pires DEV, Gokhale RS, Thukral L. 2020. Human LC3 and GABARAP subfamily members achieve functional specificity via specific structural modulations. *Autophagy* 16: 239-55
- Jaye S, Sandau US, Saugstad JA. 2024. Clathrin mediated endocytosis in Alzheimer's disease: cell type specific involvement in amyloid beta pathology. *Front Aging Neurosci* 16: 1378576

- Jiang P, Nishimura T, Sakamaki Y, Itakura E, Hatta T, Natsume T, Mizushima N. 2014. The HOPS complex mediates autophagosome-lysosome fusion through interaction with syntaxin 17. *Mol Biol Cell* 25: 1327-37
- Jordens I, Fernandez-Borja M, Marsman M, Dusseljee S, Janssen L, et al. 2001. The Rab7 effector protein RILP controls lysosomal transport by inducing the recruitment of dynein-dynactin motors. *Curr Biol* 11: 1680-5
- Kabeya Y, Mizushima N, Ueno T, Yamamoto A, Kirisako T, et al. 2000. LC3, a mammalian homologue of yeast Apg8p, is localized in autophagosome membranes after processing. *Embo j* 19: 5720-8
- Kadlecova Z, Spielman SJ, Loerke D, Mohanakrishnan A, Reed DK, Schmid SL. 2017. Regulation of clathrin-mediated endocytosis by hierarchical allosteric activation of AP2. *J Cell Biol* 216: 167-79
- Kaksonen M, Roux A. 2018. Mechanisms of clathrin-mediated endocytosis. *Nat Rev Mol Cell Biol* 19: 313-26
- Kaushik S, Cuervo AM. 2012. Chaperone-mediated autophagy: a unique way to enter the lysosome world. *Trends Cell Biol* 22: 407-17
- Kawamata T, Kamada Y, Kabeya Y, Sekito T, Ohsumi Y. 2008. Organization of the Pre-autophagosomal Structure Responsible for Autophagosome Formation. *Molecular Biology of the Cell* 19: 2039-50
- Kelly-Castro EC, Shear R, Dindigal AH, Bhagwat M, Zhang H. 2024. MARK1 regulates dendritic spine morphogenesis and cognitive functions in vivo. *Exp Neurol* 376: 114752
- Kelly RR, Sidles SJ, LaRue AC. 2020. Effects of Neurological Disorders on Bone Health. *Frontiers in Psychology* 11
- Kennedy MB. 2013. Synaptic Signaling in Learning and Memory. *Cold Spring Harb Perspect Biol* 8: a016824
- Kim J, Dalton VM, Eggerton KP, Scott SV, Klionsky DJ. 1999. Apg7p/Cvt2p is required for the cytoplasm-to-vacuole targeting, macroautophagy, and peroxisome degradation pathways. *Mol Biol Cell* 10: 1337-51
- Kimura S, Noda T, Yoshimori T. 2008. Dynein-dependent movement of autophagosomes mediates efficient encounters with lysosomes. *Cell Struct Funct* 33: 109-22
- Köchl R, Hu XW, Chan EYW, Tooze SA. 2006. Microtubules Facilitate Autophagosome Formation and Fusion of Autophagosomes with Endosomes. *Traffic* 7: 129-45
- Komatsu M, Waguri S, Chiba T, Murata S, Iwata J-i, et al. 2006. Loss of autophagy in the central nervous system causes neurodegeneration in mice. *Nature* 441: 880-84
- Komatsu M, Waguri S, Ueno T, Iwata J, Murata S, et al. 2005. Impairment of starvation-induced and constitutive autophagy in Atg7-deficient mice. *J Cell Biol* 169: 425-34
- Kononenko NL, Claßen GA, Kuijpers M, Puchkov D, Maritzen T, et al. 2017. Retrograde transport of TrkB-containing autophagosomes via the adaptor AP-2 mediates neuronal complexity and prevents neurodegeneration. *Nature Communications* 8: 14819
- Kononenko Natalia L, Haucke V. 2015. Molecular Mechanisms of Presynaptic Membrane Retrieval and Synaptic Vesicle Reformation. *Neuron* 85: 484-96
- Kononenko NL, Puchkov D, Classen GA, Walter AM, Pechstein A, et al. 2014. Clathrin/AP-2 mediate synaptic vesicle reformation from endosome-like vacuoles but are not essential for membrane retrieval at central synapses. *Neuron* 82: 981-8
- Kostich W, Hamman BD, Li YW, Naidu S, Dandapani K, et al. 2016. Inhibition of AAK1 Kinase as a Novel Therapeutic Approach to Treat Neuropathic Pain. *J Pharmacol Exp Ther* 358: 371-86
- KOTANI S, MUROFUSHI H, MAEKAWA S, SATO C, SAKAI H. 1986. Characterization of microtubule-associated proteins isolated from bovine adrenal gland. *European Journal of Biochemistry* 156: 23-29

- Kuai L, Ong SE, Madison JM, Wang X, Duvall JR, et al. 2011. AAK1 identified as an inhibitor of neuregulin-1/ErbB4-dependent neurotrophic factor signaling using integrative chemical genomics and proteomics. *Chem Biol* 18: 891-906
- Kulkarni A, Dong A, Kulkarni VV, Chen J, Laxton O, Anand A, Maday S. 2020. Differential regulation of autophagy during metabolic stress in astrocytes and neurons. *Autophagy* 16: 1651-67
- Kuma A, Mizushima N, Ishihara N, Ohsumi Y. 2002. Formation of the approximately 350-kDa Apg12-Apg5-Apg16 multimeric complex, mediated by Apg16 oligomerization, is essential for autophagy in yeast. *J Biol Chem* 277: 18619-25
- Lalonde R, Strazielle C. 2009. The relation between open-field and emergence tests in a hyperactive mouse model. *Neuropharmacology* 57: 722-4
- Langemeyer L, Fröhlich F, Ungermann C. 2018. Rab GTPase Function in Endosome and Lysosome Biogenesis. *Trends Cell Biol* 28: 957-70
- Langford-Smith A, Malinowska M, Langford-Smith KJ, Wegrzyn G, Jones S, et al. 2011. Hyperactive behaviour in the mouse model of mucopolysaccharidosis IIIB in the open field and home cage environments. *Genes Brain Behav* 10: 673-82
- Latourelle JC, Pankratz N, Dumitriu A, Wilk JB, Goldwurm S, et al. 2009. Genomewide association study for onset age in Parkinson disease. *BMC Med Genet* 10: 98
- Lattante S, de Calbiac H, Le Ber I, Brice A, Ciura S, Kabashi E. 2014. Sqstm1 knock-down causes a locomotor phenotype ameliorated by rapamycin in a zebrafish model of ALS/FTLD. *Human Molecular Genetics* 24: 1682-90
- Lee HJ, Suk JE, Bae EJ, Lee JH, Paik SR, Lee SJ. 2008. Assembly-dependent endocytosis and clearance of extracellular alpha-synuclein. *Int J Biochem Cell Biol* 40: 1835-49
- Lehtonen S, Shah M, Nielsen R, Iino N, Ryan JJ, Zhou H, Farquhar MG. 2008. The Endocytic Adaptor Protein ARH Associates with Motor and Centrosomal Proteins and Is Involved in Centrosome Assembly and Cytokinesis. *Molecular Biology of the Cell* 19: 2949-61
- Leng K, Li E, Eser R, Piergies A, Sit R, et al. 2021. Molecular characterization of selectively vulnerable neurons in Alzheimer's disease. *Nat Neurosci* 24: 276-87
- Liu D, Zuo X, Zhang P, Zhao R, Lai D, et al. 2021. The Novel Regulatory Role of lncRNA-miRNA-mRNA Axis in Amyotrophic Lateral Sclerosis: An Integrated Bioinformatics Analysis. *Comput Math Methods Med* 2021: 5526179
- Loi M, Müller A, Steinbach K, Niven J, Barreira da Silva R, et al. 2016. Macroautophagy Proteins Control MHC Class I Levels on Dendritic Cells and Shape Anti-viral CD8⁺ Cell Responses. *Cell Reports* 15: 1076-87
- Lund H, Gustafsson E, Svensson A, Nilsson M, Berg M, Sunnemark D, von Euler G. 2014. MARK4 and MARK3 associate with early tau phosphorylation in Alzheimer's disease granulovacuolar degeneration bodies. *Acta Neuropathol Commun* 2: 22
- Machino H, Kaneko S, Komatsu M, Ikawa N, Asada K, et al. 2022. The metabolic stress-activated checkpoint LKB1-MARK3 axis acts as a tumor suppressor in high-grade serous ovarian carcinoma. *Commun Biol* 5: 39
- Maeda S, Otomo C, Otomo T. 2019. The autophagic membrane tether ATG2A transfers lipids between membranes. *Elife* 8
- Manning G, Whyte DB, Martinez R, Hunter T, Sudarsanam S. 2002. The protein kinase complement of the human genome. *Science* 298: 1912-34
- Mao D, Lin G, Tepe B, Zuo Z, Tan KL, et al. 2019. VAMP associated proteins are required for autophagic and lysosomal degradation by promoting a PtdIns4P-mediated endosomal pathway. *Autophagy* 15: 1214-33
- Mari M, Griffith J, Rieter E, Krishnappa L, Klionsky DJ, Reggiori F. 2010. An Atg9-containing compartment that functions in the early steps of autophagosome biogenesis. *J Cell Biol* 190: 1005-22

- Martinez-Morga M, Quesada-Rico MP, Bueno C, Martinez S. 2018. [Neurobiological bases of autistic spectrum disorder and attention deficit hyperactivity disorder: neural differentiation and synaptogenesis]. *Rev Neurol* 66: S97-s102
- Marx A, Nugoor C, Panneerselvam S, Mandelkow E. 2010. Structure and function of polarity-inducing kinase family MARK/Par-1 within the branch of AMPK/Snf1-related kinases. *Faseb j* 24: 1637-48
- Matsunaga K, Saitoh T, Tabata K, Omori H, Satoh T, et al. 2009. Two Beclin 1-binding proteins, Atg14L and Rubicon, reciprocally regulate autophagy at different stages. *Nature Cell Biology* 11: 385-96
- Maussion G, Carayol J, Lepagnol-Bestel A-M, Tores F, Loe-Mie Y, et al. 2008. Convergent evidence identifying MAP/microtubule affinity-regulating kinase 1 (MARK1) as a susceptibility gene for autism. *Human Molecular Genetics* 17: 2541-51
- Maycox PR, Link E, Reetz A, Morris SA, Jahn R. 1992. Clathrin-coated vesicles in nervous tissue are involved primarily in synaptic vesicle recycling. *J Cell Biol* 118: 1379-88
- McAdam RL, Morton A, Gordon SL, Alterman JF, Khvorova A, Cousin MA, Smillie KJ. 2020. Loss of huntingtin function slows synaptic vesicle endocytosis in striatal neurons from the *htt*^{Q140/Q140} mouse model of Huntington's disease. *Neurobiology of disease* 134: 104637
- McMahon HT, Boucrot E. 2011. Molecular mechanism and physiological functions of clathrin-mediated endocytosis. *Nat Rev Mol Cell Biol* 12: 517-33
- McNally FJ, Vale RD. 1993. Identification of katanin, an ATPase that severs and disassembles stable microtubules. *Cell* 75: 419-29
- Medeiros AT, Soll LG, Tessari I, Bubacco L, Morgan JR. 2017. α -Synuclein Dimers Impair Vesicle Fission during Clathrin-Mediated Synaptic Vesicle Recycling. *Front Cell Neurosci* 11: 388
- Mendoza CS, Plowinske CR, Montgomery AC, Quinones GB, Banker G, Bentley M. 2024. Kinesin Regulation in the Proximal Axon is Essential for Dendrite-selective Transport. *Mol Biol Cell* 35: ar81
- Metchnikoff E. 1884. Classics in infectious diseases. Concerning the relationship between phagocytes and anthrax bacilli. By Elie Metchnikoff. 1884. *Rev Infect Dis* 6: 761-70
- Mettlen M, Chen PH, Srinivasan S, Danuser G, Schmid SL. 2018. Regulation of Clathrin-Mediated Endocytosis. *Annu Rev Biochem* 87: 871-96
- Mettlen M, Stoeber M, Loerke D, Antonescu CN, Danuser G, Schmid SL. 2009. Endocytic accessory proteins are functionally distinguished by their differential effects on the maturation of clathrin-coated pits. *Mol Biol Cell* 20: 3251-60
- Mitsui S, Otomo A, Nozaki M, Ono S, Sato K, et al. 2018. Systemic overexpression of SQSTM1/p62 accelerates disease onset in a SOD1H46R-expressing ALS mouse model. *Molecular Brain* 11: 30
- Mizushima N, Noda T, Yoshimori T, Tanaka Y, Ishii T, et al. 1998. A protein conjugation system essential for autophagy. *Nature* 395: 395-8
- Mocanu MM, Nissen A, Eckermann K, Khlistunova I, Biernat J, et al. 2008. The potential for beta-structure in the repeat domain of tau protein determines aggregation, synaptic decay, neuronal loss, and coassembly with endogenous Tau in inducible mouse models of tauopathy. *J Neurosci* 28: 737-48
- Mohan N, Sorokina EM, Verdeny IV, Alvarez AS, Lakadamyali M. 2018. Detyrosinated microtubules spatially constrain lysosomes facilitating lysosome-autophagosome fusion. *Journal of Cell Biology* 218: 632-43
- Moravcevic K, Mendrola JM, Schmitz KR, Wang YH, Slochower D, Janmey PA, Lemmon MA. 2010. Kinase associated-1 domains drive MARK/PAR1 kinases to membrane targets by binding acidic phospholipids. *Cell* 143: 966-77
- Morgan JR, Prasad K, Hao W, Augustine GJ, Lafer EM. 2000. A conserved clathrin assembly motif essential for synaptic vesicle endocytosis. *J Neurosci* 20: 8667-76

- Morgan JR, Prasad K, Jin S, Augustine GJ, Lafer EM. 2001. Uncoating of clathrin-coated vesicles in presynaptic terminals: roles for Hsc70 and auxilin. *Neuron* 32: 289-300
- Morgan JR, Zhao X, Womack M, Prasad K, Augustine GJ, Lafer EM. 1999. A role for the clathrin assembly domain of AP180 in synaptic vesicle endocytosis. *J Neurosci* 19: 10201-12
- Moroni RF, De Biasi S, Colapietro P, Larizza L, Beghini A. 2006. Distinct expression pattern of microtubule-associated protein/microtubule affinity-regulating kinase 4 in differentiated neurons. *Neuroscience* 143: 83-94
- Morris SA, Schmid SL. 1995. Synaptic vesicle recycling. The Ferrari of endocytosis? *Curr Biol* 5: 113-5
- Nakagawa H, Koyama K, Murata Y, Morito M, Akiyama T, Nakamura Y. 2000. EB3, a novel member of the EB1 family preferentially expressed in the central nervous system, binds to a CNS-specific APC homologue. *Oncogene* 19: 210-6
- Nakamura Y, Takeda M, Yoshimi K, Hattori H, Hariguchi S, et al. 1994. Involvement of clathrin light chains in the pathology of Alzheimer's disease. *Acta Neuropathol* 87: 23-31
- Naudi-Fabra S, Elena-Real CA, Vedel IM, Tengo M, Motzny K, et al. 2024. An extended interaction site determines binding between AP180 and AP2 in clathrin mediated endocytosis. *Nat Commun* 15: 5884
- Nazir FH, Becker B, Brinkmalm A, Höglund K, Sandelius Å, et al. 2018. Expression and secretion of synaptic proteins during stem cell differentiation to cortical neurons. *Neurochem Int* 121: 38-49
- Negrete-Hurtado A, Overhoff M, Bera S, De Bruyckere E, Schätzmüller K, et al. 2020. Autophagy lipidation machinery regulates axonal microtubule dynamics but is dispensable for survival of mammalian neurons. *Nat Commun* 11: 1535
- Newmyer SL, Christensen A, Sever S. 2003. Auxilin-dynamin interactions link the uncoating ATPase chaperone machinery with vesicle formation. *Dev Cell* 4: 929-40
- Nishida K, Matsumura K, Tamura M, Nakamichi T, Shimamori K, et al. 2023. Effects of three microtubule-associated proteins (MAP2, MAP4, and Tau) on microtubules' physical properties and neurite morphology. *Scientific Reports* 13: 8870
- Noda T, Ohsumi Y. 1998. Tor, a phosphatidylinositol kinase homologue, controls autophagy in yeast. *J Biol Chem* 273: 3963-6
- Oba T, Saito T, Asada A, Shimizu S, Iijima KM, Ando K. 2020. Microtubule affinity-regulating kinase 4 with an Alzheimer's disease-related mutation promotes tau accumulation and exacerbates neurodegeneration. *J Biol Chem* 295: 17138-47
- Ohno H, Stewart J, Fournier MC, Bosshart H, Rhee I, et al. 1995. Interaction of tyrosine-based sorting signals with clathrin-associated proteins. *Science* 269: 1872-5
- Olszewski MB, Chandris P, Park B-C, Eisenberg E, Greene LE. 2014. Disruption of Clathrin-Mediated Trafficking Causes Centrosome Overduplication and Senescence. *Traffic* 15: 60-77
- Olusanya O, Andrews PD, Swedlow JR, Smythe E. 2001. Phosphorylation of threonine 156 of the mu2 subunit of the AP2 complex is essential for endocytosis in vitro and in vivo. *Curr Biol* 11: 896-900
- Osawa T, Kotani T, Kawaoka T, Hirata E, Suzuki K, et al. 2019. Atg2 mediates direct lipid transfer between membranes for autophagosome formation. *Nat Struct Mol Biol* 26: 281-88
- Overhoff M, De Bruyckere E, Kononenko NL. 2021. Mechanisms of neuronal survival safeguarded by endocytosis and autophagy. *Journal of Neurochemistry* 157: 263-96
- Parato J, Bartolini F. 2021. The microtubule cytoskeleton at the synapse. *Neurosci Lett* 753: 135850
- Peris L, Parato J, Qu X, Soleilhac JM, Lanté F, et al. 2022. Tubulin tyrosination regulates synaptic function and is disrupted in Alzheimer's disease. *Brain* 145: 2486-506
- Peter BJ, Kent HM, Mills IG, Vallis Y, Butler PJ, Evans PR, McMahon HT. 2004. BAR domains as sensors of membrane curvature: the amphiphysin BAR structure. *Science* 303: 495-9

- Piscopo DM, Weible AP, Rothbart MK, Posner MI, Niell CM. 2018. Changes in white matter in mice resulting from low-frequency brain stimulation. *Proceedings of the National Academy of Sciences* 115: E6339-E46
- Portran D, Schaedel L, Xu Z, Théry M, Nachury Maxence V. 2017. Tubulin acetylation protects long-lived microtubules against mechanical ageing. *Nature Cell Biology* 19: 391-98
- Posor Y, Eichhorn-Gruenig M, Puchkov D, Schöneberg J, Ullrich A, et al. 2013. Spatiotemporal control of endocytosis by phosphatidylinositol-3,4-bisphosphate. *Nature* 499: 233-7
- Prichard KL, O'Brien NS, Murcia SR, Baker JR, McCluskey A. 2021. Role of Clathrin and Dynamin in Clathrin Mediated Endocytosis/Synaptic Vesicle Recycling and Implications in Neurological Diseases. In *Front Cell Neurosci*, pp. 754110
- Pu J, Schindler C, Jia R, Jarnik M, Backlund P, Bonifacino JS. 2015. BORC, a multisubunit complex that regulates lysosome positioning. *Dev Cell* 33: 176-88
- Puri C, Renna M, Bento Carla F, Moreau K, Rubinsztein David C. 2013. Diverse Autophagosome Membrane Sources Coalesce in Recycling Endosomes. *Cell* 154: 1285-99
- Puthenveedu MA, von Zastrow M. 2006. Cargo regulates clathrin-coated pit dynamics. *Cell* 127: 113-24
- Radyushkin K, Hammerschmidt K, Boretius S, Varoqueaux F, El-Kordi A, et al. 2009. Neuroligin-3-deficient mice: model of a monogenic heritable form of autism with an olfactory deficit. *Genes, Brain and Behavior* 8: 416-25
- Rakic P. 2009. Evolution of the neocortex: a perspective from developmental biology. *Nature Reviews Neuroscience* 10: 724-35
- Ravikumar B, Acevedo-Arozena A, Imarisio S, Berger Z, Vacher C, et al. 2005. Dynein mutations impair autophagic clearance of aggregate-prone proteins. *Nat Genet* 37: 771-6
- Ravikumar B, Moreau K, Jahreiss L, Puri C, Rubinsztein DC. 2010. Plasma membrane contributes to the formation of pre-autophagosomal structures. *Nat Cell Biol* 12: 747-57
- Ricotta D, Conner SD, Schmid SL, von Figura K, Honing S. 2002. Phosphorylation of the AP2 mu subunit by AAK1 mediates high affinity binding to membrane protein sorting signals. *J Cell Biol* 156: 791-5
- Ringstad N, Gad H, Löw P, Di Paolo G, Brodin L, Shupliakov O, De Camilli P. 1999. Endophilin/SH3p4 is required for the transition from early to late stages in clathrin-mediated synaptic vesicle endocytosis. *Neuron* 24: 143-54
- Ritter B, Murphy S, Dokainish H, Girard M, Gudheti MV, et al. 2013. NECAP 1 regulates AP-2 interactions to control vesicle size, number, and cargo during clathrin-mediated endocytosis. *PLoS Biol* 11: e1001670
- Robinson MS. 2015. Forty Years of Clathrin-coated Vesicles. *Traffic* 16: 1210-38
- Robinson PJ, Liu JP, Powell KA, Fykse EM, Südhof TC. 1994. Phosphorylation of dynamin I and synaptic-vesicle recycling. *Trends Neurosci* 17: 348-53
- Roth TF, Porter KR. 1964. YOLK PROTEIN UPTAKE IN THE OOCYTE OF THE MOSQUITO AEDES AEGYPTI. L. *J Cell Biol* 20: 313-32
- Roux A, Uyhazi K, Frost A, De Camilli P. 2006. GTP-dependent twisting of dynamin implicates constriction and tension in membrane fission. *Nature* 441: 528-31
- Royle SJ, Bright NA, Lagnado L. 2005. Clathrin is required for the function of the mitotic spindle. *Nature* 434: 1152-57
- Rubinsztein DC, Ravikumar B, Acevedo-Arozena A, Imarisio S, O'Kane CJ, Brown SD. 2005. Dyneins, autophagy, aggregation and neurodegeneration. *Autophagy* 1: 177-8
- Sakakibara A, Ando R, Sapir T, Tanaka T. 2013. Microtubule dynamics in neuronal morphogenesis. *Open Biol* 3: 130061
- Samra S, Sharma M, Vaseghi-Shanjani M, Del Bel KL, Byres L, et al. 2024. Gain-of-function MARK4 variant associates with pediatric neurodevelopmental disorder and dysmorphism. *HGG Adv* 5: 100259

- Sánchez C, Díaz-Nido J, Avila J. 2000. Phosphorylation of microtubule-associated protein 2 (MAP2) and its relevance for the regulation of the neuronal cytoskeleton function. *Prog Neurobiol* 61: 133-68
- Sapir T, Shmueli A, Levy T, Timm T, Elbaum M, Mandelkowitz EM, Reiner O. 2008. Antagonistic effects of doublecortin and MARK2/Par-1 in the developing cerebral cortex. *J Neurosci* 28: 13008-13
- Scarmato P, Kirchhausen T. 1990. Analysis of clathrin light chain-heavy chain interactions using truncated mutants of rat liver light chain LCB3. *The Journal of biological chemistry* 265: 3661-68
- Schlossman DM, Schmid SL, Braell WA, Rothman JE. 1984. An enzyme that removes clathrin coats: purification of an uncoating ATPase. *J Cell Biol* 99: 723-33
- Schmid EM, McMahon HT. 2007. Integrating molecular and network biology to decode endocytosis. *Nature* 448: 883-8
- Schmid SL, Sorkin A, Zerial M. 2014. Endocytosis: Past, present, and future. *Cold Spring Harb Perspect Biol* 6: a022509
- Schneider M, Retz W, Coogan A, Thome J, Rösler M. 2006. Anatomical and functional brain imaging in adult attention-deficit/hyperactivity disorder (ADHD)—A neurological view. *European Archives of Psychiatry and Clinical Neuroscience* 256: i32-i41
- Schöneberg J, Lehmann M, Ullrich A, Posor Y, Lo WT, et al. 2017. Lipid-mediated PX-BAR domain recruitment couples local membrane constriction to endocytic vesicle fission. *Nat Commun* 8: 15873
- Schork NJ, Elman JA. 2023. Pathway-Specific Polygenic Risk Scores Correlate with Clinical Status and Alzheimer's Disease-Related Biomarkers. *J Alzheimers Dis* 95: 915-29
- Schubert KO, Föcking M, Prehn JHM, Cotter DR. 2012. Hypothesis review: are clathrin-mediated endocytosis and clathrin-dependent membrane and protein trafficking core pathophysiological processes in schizophrenia and bipolar disorder? *Molecular Psychiatry* 17: 669-81
- Schwarz T, Sohn C, Kaiser B, Jensen ED, Mansky KC. 2010. The 19S proteasomal lid subunit POH1 enhances the transcriptional activation by Mitf in osteoclasts. *J Cell Biochem* 109: 967-74
- Selkoe DJ. 2002. Alzheimer's disease is a synaptic failure. *Science* 298: 789-91
- Shi B, Conner SD, Liu J. 2014. Dysfunction of Endocytic Kinase AAK1 in ALS. *International Journal of Molecular Sciences* 15: 22918-32
- Shintani T, Mizushima N, Ogawa Y, Matsuura A, Noda T, Ohsumi Y. 1999. Apg10p, a novel protein-conjugating enzyme essential for autophagy in yeast. *Embo j* 18: 5234-41
- Silm K, Yang J, Marcott PF, Asensio CS, Eriksen J, et al. 2019. Synaptic Vesicle Recycling Pathway Determines Neurotransmitter Content and Release Properties. *Neuron* 102: 786-800.e5
- Silva AJ, Paylor R, Wehner JM, Tonegawa S. 1992. Impaired spatial learning in alpha-calmodulin kinase II mutant mice. *Science* 257: 206-11
- Singh M, Jadhav HR, Bhatt T. 2017. Dynamin Functions and Ligands: Classical Mechanisms Behind. *Mol Pharmacol* 91: 123-34
- Skarnes WC, Rosen B, West AP, Koutsourakis M, Bushell W, et al. 2011. A conditional knockout resource for the genome-wide study of mouse gene function. *Nature* 474: 337-42
- Slepnev VI, De Camilli P. 2000. Accessory factors in clathrin-dependent synaptic vesicle endocytosis. *Nat Rev Neurosci* 1: 161-72
- Sloboda RD, Dentler WL, Rosenbaum JL. 1976. Microtubule-associated proteins and the stimulation of tubulin assembly in vitro. *Biochemistry* 15: 4497-505
- Smythe E, Ayscough KR. 2003. The Ark1/Prk1 family of protein kinases. Regulators of endocytosis and the actin skeleton. *EMBO Rep* 4: 246-51
- Song MS, Baker GB, Todd KG, Kar S. 2011. Inhibition of β -amyloid1-42 internalization attenuates neuronal death by stabilizing the endosomal-lysosomal system in rat cortical cultured neurons. *Neuroscience* 178: 181-8

- Song Y, Brady ST. 2014. Stabilization of neuronal connections and the axonal cytoskeleton. *BioArchitecture* 4: 22-24
- Sorkin A, von Zastrow M. 2009. Endocytosis and signalling: intertwining molecular networks. *Nat Rev Mol Cell Biol* 10: 609-22
- Sorrell FJ, Szklarz M, Abdul Azeez KR, Elkins JM, Knapp S. 2016. Family-wide Structural Analysis of Human Numb-Associated Protein Kinases. *Structure* 24: 401-11
- Sossi V, de la Fuente-Fernández R, Holden JE, Schulzer M, Ruth TJ, Stoessl J. 2004. Changes of dopamine turnover in the progression of Parkinson's disease as measured by positron emission tomography: their relation to disease-compensatory mechanisms. *J Cereb Blood Flow Metab* 24: 869-76
- Spillantini MG, Crowther RA, Jakes R, Hasegawa M, Goedert M. 1998. alpha-Synuclein in filamentous inclusions of Lewy bodies from Parkinson's disease and dementia with lewy bodies. *Proc Natl Acad Sci U S A* 95: 6469-73
- Srinivasan S, Gal J, Bachstetter A, Nelson PT. 2022. Alpha adaptins show isoform-specific association with neurofibrillary tangles in Alzheimer's disease. *Neuropathol Appl Neurobiol* 48: e12776
- Stanford SC. 2007. The Open Field Test: reinventing the wheel. *J Psychopharmacol* 21: 134-5
- Stenmark H. 2009. Rab GTPases as coordinators of vesicle traffic. *Nature Reviews Molecular Cell Biology* 10: 513-25
- Sudhof TC. 2004. The synaptic vesicle cycle. *Annu Rev Neurosci* 27: 509-47
- Südhof TC. 2013. Neurotransmitter release: the last millisecond in the life of a synaptic vesicle. *Neuron* 80: 675-90
- Sun TQ, Lu B, Feng JJ, Reinhard C, Jan YN, Fantl WJ, Williams LT. 2001. PAR-1 is a Dishevelled-associated kinase and a positive regulator of Wnt signalling. *Nat Cell Biol* 3: 628-36
- Takeda S, Elefteriou F, Lévassieur R, Liu X, Zhao L, et al. 2002. Leptin regulates bone formation via the sympathetic nervous system. *Cell* 111: 305-17
- Takei K, Slepnev VI, Haucke V, De Camilli P. 1999. Functional partnership between amphiphysin and dynamin in clathrin-mediated endocytosis. *Nature Cell Biology* 1: 33-39
- Takehige K, Baba M, Tsuboi S, Noda T, Ohsumi Y. 1992. Autophagy in yeast demonstrated with proteinase-deficient mutants and conditions for its induction. *J Cell Biol* 119: 301-11
- Tanida I, Tanida-Miyake E, Ueno T, Kominami E. 2001. The human homolog of *Saccharomyces cerevisiae* Apg7p is a Protein-activating enzyme for multiple substrates including human Apg12p, GATE-16, GABARAP, and MAP-LC3. *J Biol Chem* 276: 1701-6
- Terlecky SR, Chiang HL, Olson TS, Dice JF. 1992. Protein and peptide binding and stimulation of in vitro lysosomal proteolysis by the 73-kDa heat shock cognate protein. *J Biol Chem* 267: 9202-9
- Tesi N, van der Lee SJ, Hulsman M, Jansen IE, Stringa N, et al. 2020. Immune response and endocytosis pathways are associated with the resilience against Alzheimer's disease. *Transl Psychiatry* 10: 332
- Thomas RS, Lelos MJ, Good MA, Kidd EJ. 2011. Clathrin-mediated endocytic proteins are upregulated in the cortex of the Tg2576 mouse model of Alzheimer's disease-like amyloid pathology. *Biochem Biophys Res Commun* 415: 656-61
- Tian X, Teng J, Chen J. 2021. New insights regarding SNARE proteins in autophagosome-lysosome fusion. *Autophagy* 17: 2680-88
- Timm T, Marx A, Panneerselvam S, Mandelkow E, Mandelkow EM. 2008. Structure and regulation of MARK, a kinase involved in abnormal phosphorylation of Tau protein. *BMC Neurosci* 9 Suppl 2: S9
- Tirnauer JS, Bierer BE. 2000. Eb1 Proteins Regulate Microtubule Dynamics, Cell Polarity, and Chromosome Stability. *Journal of Cell Biology* 149: 761-66
- Tooze SA, Yoshimori T. 2010. The origin of the autophagosomal membrane. *Nature Cell Biology* 12: 831-35

- Traub LM. 2009. Tickets to ride: selecting cargo for clathrin-regulated internalization. *Nat Rev Mol Cell Biol* 10: 583-96
- Traub LM, Bonifacino JS. 2013. Cargo recognition in clathrin-mediated endocytosis. *Cold Spring Harb Perspect Biol* 5: a016790
- Trowbridge IS, Collawn JF, Hopkins CR. 1993. Signal-dependent membrane protein trafficking in the endocytic pathway. *Annu Rev Cell Biol* 9: 129-61
- Trushina E, Singh RD, Dyer RB, Cao S, Shah VH, et al. 2006. Mutant huntingtin inhibits clathrin-independent endocytosis and causes accumulation of cholesterol in vitro and in vivo. *Hum Mol Genet* 15: 3578-91
- Tsuyoshi I, Yuzuru I. 2015. Regulation of vesicular trafficking by Parkinson's disease-associated genes. *AIMS Molecular Science* 2: 461-75
- Tyanova S, Temu T, Cox J. 2016. The MaxQuant computational platform for mass spectrometry-based shotgun proteomics. *Nature Protocols* 11: 2301-19
- Tyanova S, Temu T, Sinitcyn P, Carlson A, Hein MY, et al. 2016. The Perseus computational platform for comprehensive analysis of (prote)omics data. *Nature Methods* 13: 731-40
- Ultanir SK, Hertz NT, Li G, Ge WP, Burlingame AL, et al. 2012. Chemical genetic identification of NDR1/2 kinase substrates AAK1 and Rabin8 Uncovers their roles in dendrite arborization and spine development. *Neuron* 73: 1127-42
- Ungewickell E. 1985. The 70-kd mammalian heat shock proteins are structurally and functionally related to the uncoating protein that releases clathrin triskelia from coated vesicles. *Embo j* 4: 3385-91
- Valverde DP, Yu S, Boggavarapu V, Kumar N, Lees JA, et al. 2019. ATG2 transports lipids to promote autophagosome biogenesis. *J Cell Biol* 218: 1787-98
- Vidyadhara DJ, Lee JE, Chandra SS. 2019. Role of the endolysosomal system in Parkinson's disease. *J Neurochem* 150: 487-506
- Vu HT, Akatsu H, Hashizume Y, Setou M, Ikegami K. 2017. Increase in α -tubulin modifications in the neuronal processes of hippocampal neurons in both kainic acid-induced epileptic seizure and Alzheimer's disease. *Sci Rep* 7: 40205
- Waldren LH, Leung FYN, Hargitai LD, Burgoyne AP, Licalalde VRT, Livingston LA, Shah P. 2024. Unpacking the overlap between Autism and ADHD in adults: A multi-method approach. *Cortex* 173: 120-37
- Wang L, Diao J. 2022. VAMP8 phosphorylation regulates lysosome dynamics during autophagy. *Autophagy Reports* 1: 79-82
- Wang Y, Mandelkow E. 2016. Tau in physiology and pathology. *Nature Reviews Neuroscience* 17: 22-35
- Weidberg H, Shvets E, Shpilka T, Shimron F, Shinder V, Elazar Z. 2010. LC3 and GATE-16/GABARAP subfamilies are both essential yet act differently in autophagosome biogenesis. *Embo j* 29: 1792-802
- Wen L, Lu YS, Zhu XH, Li XM, Woo RS, et al. 2010. Neuregulin 1 regulates pyramidal neuron activity via ErbB4 in parvalbumin-positive interneurons. *Proc Natl Acad Sci U S A* 107: 1211-6
- Wijdeven RH, Janssen H, Nahidiazar L, Janssen L, Jalink K, Berlin I, Neefjes J. 2016. Cholesterol and ORP1L-mediated ER contact sites control autophagosome transport and fusion with the endocytic pathway. *Nat Commun* 7: 11808
- Wong ROL, Ghosh A. 2002. Activity-dependent regulation of dendritic growth and patterning. *Nature Reviews Neuroscience* 3: 803-12
- Wu M, Huang B, Graham M, Raimondi A, Heuser JE, Zhuang X, De Camilli P. 2010. Coupling between clathrin-dependent endocytic budding and F-BAR-dependent tubulation in a cell-free system. *Nat Cell Biol* 12: 902-8
- Wu PR, Tsai PI, Chen GC, Chou HJ, Huang YP, et al. 2011. DAPK activates MARK1/2 to regulate microtubule assembly, neuronal differentiation, and tau toxicity. *Cell Death & Differentiation* 18: 1507-20

- Xin X, Wang Y, Zhang L, Zhang D, Sha L, et al. 2023. Development and therapeutic potential of adaptor-associated kinase 1 inhibitors in human multifaceted diseases. *Eur J Med Chem* 248: 115102
- Xiong Y, Neifert S, Karuppagounder SS, Liu Q, Stankowski JN, et al. 2018. Robust kinase- and age-dependent dopaminergic and norepinephrine neurodegeneration in LRRK2 G2019S transgenic mice. *Proc Natl Acad Sci U S A* 115: 1635-40
- Xu Z, Schaedel L, Portran D, Aguilar A, Gaillard J, et al. 2017. Microtubules acquire resistance from mechanical breakage through intraluminal acetylation. *Science* 356: 328-32
- Yadati T, Houben T, Bitorina A, Shiri-Sverdlov R. 2020. The Ins and Outs of Cathepsins: Physiological Function and Role in Disease Management. *Cells* 9: 1679
- Yamamoto H, Kakuta S, Watanabe TM, Kitamura A, Sekito T, et al. 2012. Atg9 vesicles are an important membrane source during early steps of autophagosome formation. *J Cell Biol* 198: 219-33
- Yang S, Park D, Manning L, Hill SE, Cao M, et al. 2022. Presynaptic autophagy is coupled to the synaptic vesicle cycle via ATG-9. *Neuron* 110: 824-40.e10
- Yang WK, Peng YH, Li H, Lin HC, Lin YC, et al. 2011. Nak regulates localization of clathrin sites in higher-order dendrites to promote local dendrite growth. *Neuron* 72: 285-99
- Yao PJ, Morsch R, Callahan LM, Coleman PD. 1999. Changes in synaptic expression of clathrin assembly protein AP180 in Alzheimer's disease analysed by immunohistochemistry. *Neuroscience* 94: 389-94
- Yao PJ, Weimer JM, O'Herron TM, Coleman PD. 2000. Clathrin assembly protein AP-2 is detected in both neurons and glia, and its reduction is prominent in layer II of frontal cortex in Alzheimer's disease. *Neurobiol Aging* 21: 921-9
- Yoneyama Y, Lanzerstorfer P, Niwa H, Umehara T, Shibano T, et al. 2018. IRS-1 acts as an endocytic regulator of IGF-I receptor to facilitate sustained IGF signaling. *eLife* 7: e32893
- Yoshimura Y, Terabayashi T, Miki H. 2010. Par1b/MARK2 phosphorylates kinesin-like motor protein GAKIN/KIF13B to regulate axon formation. *Mol Cell Biol* 30: 2206-19
- Young AR, Chan EY, Hu XW, Köchl R, Crawshaw SG, et al. 2006. Starvation and ULK1-dependent cycling of mammalian Atg9 between the TGN and endosomes. *J Cell Sci* 119: 3888-900
- Yu A, Shibata Y, Shah B, Calamini B, Lo DC, Morimoto RI. 2014a. Protein aggregation can inhibit clathrin-mediated endocytosis by chaperone competition. *Proc Natl Acad Sci U S A* 111: E1481-90
- Yu A, Shibata Y, Shah B, Calamini B, Lo DC, Morimoto RI. 2014b. Protein aggregation can inhibit clathrin-mediated endocytosis by chaperone competition. *Proceedings of the National Academy of Sciences of the United States of America* 111: E1481-90
- Zeng H, Chattarji S, Barbarosie M, Rondi-Reig L, Philpot BD, et al. 2001. Forebrain-specific calcineurin knockout selectively impairs bidirectional synaptic plasticity and working/episodic-like memory. *Cell* 107: 617-29
- Zhang Q, Mesner LD, Calabrese GM, Dirckx N, Li Z, et al. 2021. Genomic variants within chromosome 14q32.32 regulate bone mass through MARK3 signaling in osteoblasts. *J Clin Invest* 131
- Zhou C, Ma K, Gao R, Mu C, Chen L, et al. 2017a. Regulation of mATG9 trafficking by Src- and ULK1-mediated phosphorylation in basal and starvation-induced autophagy. *Cell Res* 27: 184-201
- Zhou L, McInnes J, Wierda K, Holt M, Herrmann AG, et al. 2017b. Tau association with synaptic vesicles causes presynaptic dysfunction. *Nature Communications* 8: 15295
- Zou L, Tian Y, Zhang Z. 2021. Dysfunction of Synaptic Vesicle Endocytosis in Parkinson's Disease. *Front Integr Neurosci* 15: 619160

VIII. Acknowledgments

First and foremost, I would like to express my sincere thanks to Prof. Dr. Natalia Kononenko for giving me the opportunity to carry out my PhD thesis in her group. Her guidance, scientific expertise, and invaluable advice have been instrumental throughout my project.

I am also deeply grateful to my TAC committee members, Prof. Dr. Marcus Krüger and Prof. Dr. Thorsten Hoppe, for their insightful contributions and constructive feedback. I would also like to extend my special thanks to my thesis committee members, Prof. Dr. Marcus Krüger and Prof. Dr. Jan Riemer, for their continued support and guidance.

My heartfelt thanks go to my former and current RTG2550-Reloc coordinators, Susanne Vorhagen and Alexander Rüter, as well as the program coordinator Prof. Dr. Jan Riemer for their unwavering support throughout this journey. I am also grateful to Theresa Bock and Sarah Gerlich from the RTG team for their help with protocols. It has been a privilege to be part of this incredible program.

I would also like to express my appreciation to all the members of the Kononenko lab for their assistance and camaraderie. Special thanks to Lotte Ickert, Marianna Tolve, Janine Tutas, and Veronika Fritz. I will always cherish the joyful moments we shared. Having great colleagues is a privilege, but having great friends is priceless.

Lastly, I want to express my deepest gratitude to my family and especially to my beloved husband. Thank you for always being there for me, for your endless love and encouragement.

Erklärung zur Dissertation

gemäß der Promotionsordnung vom 12. März 2020

Diese Erklärung muss in der Dissertation enthalten sein.

(This version must be included in the doctoral thesis)

„Hiermit versichere ich an Eides statt, dass ich die vorliegende Dissertation selbstständig und ohne die Benutzung anderer als der angegebenen Hilfsmittel und Literatur angefertigt habe. Alle Stellen, die wörtlich oder sinngemäß aus veröffentlichten und nicht veröffentlichten Werken dem Wortlaut oder dem Sinn nach entnommen wurden, sind als solche kenntlich gemacht. Ich versichere an Eides statt, dass diese Dissertation noch keiner anderen Fakultät oder Universität zur Prüfung vorgelegen hat; dass sie - abgesehen von unten angegebenen Teilpublikationen und eingebundenen Artikeln und Manuskripten - noch nicht veröffentlicht worden ist sowie, dass ich eine Veröffentlichung der Dissertation vor Abschluss der Promotion nicht ohne Genehmigung des Promotionsausschusses vornehmen werde. Die Bestimmungen dieser Ordnung sind mir bekannt. Darüber hinaus erkläre ich hiermit, dass ich die Ordnung zur Sicherung guter wissenschaftlicher Praxis und zum Umgang mit wissenschaftlichem Fehlverhalten der Universität zu Köln gelesen und sie bei der Durchführung der Dissertation zugrundeliegenden Arbeiten und der schriftlich verfassten Dissertation beachtet habe und verpflichte mich hiermit, die dort genannten Vorgaben bei allen wissenschaftlichen Tätigkeiten zu beachten und umzusetzen. Ich versichere, dass die eingereichte elektronische Fassung der eingereichten Druckfassung vollständig entspricht.“

Teilpublikationen:

Datum, Name und Unterschrift

01.12.2024, Ebru ÖZER YILDIZ

